

MICROCOPY RESOLUTION TEST CHART
NATIONAL BUREAU OF STANDARDS-1963-A

1. Report No. 19 FAA-EM 80-16- VOL-2 AD-A094 152	2. Government Accession No. AD-A094 152	3. Recipient's Catalog No.
4. Title and Subtitle Interim Report on the Conflict Monitoring Analysis of Parallel Route Spacing in the High Altitude CONUS Airspace - Volume II		5. Report Date July 1980
6. Author(s) Arthur P. Smith, III		7. Performing Organization Code 12
8. Performing Organization Name and Address The MITRE Corporation Metrek Division 1320 Dolley Madison Boulevard McLean, Virginia 22102		9. Performing Organization Report No. MTR-79W00235 - Volume II
10. Sponsoring Agency Name and Address Office of Systems Engineering Management Federal Aviation Administration Department of Transportation Washington, D.C. 20591		11. Work Unit No. (TRIS)
12. Supplementary Notes		12. Contract or Grant No. DOT-FAR0WA-4370
13. Abstract <p>The work reported in this document was undertaken as part of the examination of the soundness of the current standards for the spacing between parallel aircraft routes and the enhancement of analytical methods to evaluate future standards. This interim report describes work completed to date on the Conflict Monitoring Parallel Route Spacing Analysis. This analysis assesses the potential for collision and the controller workload associated with aircraft flying on same direction parallel routes. To assess the potential for collision the analysis considers a conflict alert function similar to that employed in the National Airspace System. The conflict alert function detects pairs of aircraft which are projected to violate the radar separation standard within a given time period. In the analysis the event of a conflict alert is followed by a probabilistic delay and a resolution maneuver characterized by a randomly chosen horizontal turn rate. The controller intervention rate is estimated by using a simulation. Actual aircraft tracks were sampled from the FAA data base which supports this activity. These tracks are initiated on the routes based on randomly chosen sector entry times which reflect the level of route loading. For both the potential for collision and the intervention rate, trial results based on a subset of the FAA data are given. Further analysis is required to investigate opposite direction and transitioning traffic. In conjunction with this work, the reliability of the surveillance and control systems has to be addressed as well as other performance measures.</p>		13. Type of Report and Period Covered INTERIM report
17. Key Words Collision Risk Methodology Safety Controller Intervention Rate VOR Route Spacing Aircraft Separation	18. Distribution Statement Unlimited Availability. Document may be released to the National Technical Information Service, Springfield, Virginia, 22161 for sale to the public	
19. Security Classification of this report Unclassified	20. Security Classification of this page Unclassified	21. No. of Pages 22. Price

4

ACKNOWLEDGEMENTS

The author wishes to thank those who have contributed to the review of this document. In particular, thanks go to Dr. Nancy Kirkendall for offering suggestions along the way and then reviewing the results. Gratitude is also expressed to Dr. Joseph Matney for his guidance and review. And special thanks to Miss Louise Jasinski who did a superb job of producing this document as well as the many previous drafts. The author, of course, assumes full responsibility for any remaining errors.

TABLE OF CONTENTS

1. INTRODUCTION	1-1
APPENDIX A: THE CONFLICT REGION BOUNDARY	A-1
APPENDIX B: COMPUTATION OF THE PROBABILITY OF HORIZONTAL OVERLAP	B-1
B1. INTRODUCTION	B-1
B2. DELAY TIME	B-1
B2.1 Delay Due to Detection	B-1
B2.2 Delay Due to the Controller, the Communication Link, and the Pilot	B-5
B2.3 Total Delay	B-6
B3. TURN RATE	B-6
B4. HORIZONTAL OVERLAP REGION	B-8
B5. COMPUTATION OF THE PROBABILITY OF HORIZONTAL OVERLAP	B-27
APPENDIX C: PROBABILITY OF OBSERVING AN AIRCRAFT PAIR WITHIN THE CONFLICT REGION	C-1
C1. INTRODUCTION	C-1
C2. THE CONFLICT REGION	C-1
C3. THE TRACKER PERFORMANCE	C-3
C3.1 The Tracker Simulation	C-3
C3.2 The NAS Tracker	C-4
C3.3 Simulation Results	C-6
C4. INTEGRATION OF A BIVARIATE NORMAL DISTRIBUTION OVER A POLYGON	C-10
APPENDIX D: THE FAST FINITE FOURIER TRANSFORM	D-1
D1. INTRODUCTION	D-1
D2. PROPERTIES OF THE FINITE TRANSFORM	D-1
D3. THE DOUBLING ALGORITHM	D-3
D4. FEATURES	D-6
D5. THE COMPUTER PROGRAM	D-9
APPENDIX E: PROBABILITY OF ALONTRACK SEPARATION	E-1
E1. INTRODUCTION	E-1
E2. DISTRIBUTION OF ALONGTRACK SEPARATION	E-1
E3. RELATIONSHIP BETWEEN $P_{\Delta x}$ AND P_x	E-3
E4. ESTIMATING P_x	E-4

Accession For	
NTIS GRA&I <input checked="" type="checkbox"/>	<input type="checkbox"/>
DTIC TAB <input type="checkbox"/>	<input type="checkbox"/>
Unannounced <input type="checkbox"/>	<input type="checkbox"/>
Justification _____	
By _____	
Distribution/ _____	
Availability Codes	
Dist	Avail and/or Special
A	

TABLE OF CONTENTS
(Concl'd)

	<u>Page</u>
APPENDIX F: CALCULATION OF THE JOINT CLOSING SPEED-SEPARATION HISTOGRAM FROM SINGLE AIRCRAFT DATA	F-1
APPENDIX G: INTERVENTION RATE SIMULATION	G-1
G1. INTRODUCTION	G-1
G2. THE INPUT	G-1
G3. THE SIMULATION FLOW	G-1
G4. THE OUTPUT	G-5
G5. THE ANALYSIS OF THE OUTPUT	G-5
APPENDIX H: THE NAS CONFLICT ALERT	H-1
APPENDIX I: GLOSSARY	I-1
APPENDIX J: REFERENCES	J-1

LIST OF ILLUSTRATIONS

	<u>Page</u>
TABLE C-1: NAS TRACKER PARAMETERS	C-5
TABLE C-2: NAS TRACKER SIMULATION RESULTS	C-7
TABLE D-1: THE FAST FINITE FOURIER TRANSFORM COMPUTER PROGRAM	D-10
TABLE H-1: HORIZONTAL CONFLICT ALERT PARAMETERS	H-3
FIGURE A-1: CONFLICT GEOMETRY	A-2
FIGURE A-2: THE CONFLICT REGION	A-5
FIGURE A-3: MAX/MIN REGION FOR DISCRIMINANT IN EQUATION A-3	A-7
FIGURE A-4: ENVELOPE OF CONFLICT REGION BOUNDARIES FOR $x= 0.0$ NMI	A-9
FIGURE A-5: ENVELOPE OF CONFLICT REGION BOUNDARIES FOR $x=+3.0$ NMI	A-10
FIGURE A-6: ENVELOPE OF CONFLICT REGION BOUNDARIES FOR $x= +5.0$ NMI	A-11
FIGURE A-7: DISTRIBUTION OF EARLY (-) OR LATE (+) DETECTIONS ($x=0$ NMI)	A-12
FIGURE A-8: DISTRIBUTION OF EARLY (-) OR LATE (+) DETECTIONS ($x=+3$ NMI)	A-13
FIGURE A-9: DISTRIBUTION OF EARLY (-) OR LATE (+) DETECTION ($x=+5$ NMI)	A-14
FIGURE A-10: ENVELOPE OF CONFLICT REGION BOUNDARIES FOR $x=+6.5$ NMI	A-15
FIGURE B-1: PROGRESSION OF A PAIR OF AIRCRAFT ACROSS THE CONFLICT REGION BOUNDARY	B-2
FIGURE B-2: CROSSTRACK SEPARATIONS DURING THE DETECTION PROCESS	B-4

LIST OF ILLUSTRATIONS
(cont'd)

	<u>Page</u>
FIGURE B-3: DELAY DISTRIBUTION	B-7
FIGURE B-4: PROBABILITY DENSITY FUNCTION OF THE BANK ANGLE	B-9
FIGURE B-5: PROBABILITY DENSITY FUNCTION OF THE TURN RATE	B-10
FIGURE B-6: COLLISION GEOMETRY	B-12
FIGURE B-7: REGIONS WHERE AIRCRAFT WILL OVERLAP	B-17
FIGURE B-8: SELECTED COMBINATIONS OF ALONGTRACK SEPARATION AND CROSSTRACK CLOSING SPEEDS	B-18
FIGURE B-9: OVERLAP REGIONS FOR VARIOUS COMBINATIONS OF ALONGTRACK SEPARATION, CROSSTRACK CLOSING SPEED	B-19
FIGURE B-10: THE ENVELOPE OF HORIZONTAL OVERLAP REGIONS FOR A GIVEN CELL ON THE CONFLICT REGION BOUNDARY	B-20
FIGURE B-11: STRAIGHT LINE OVERLAP REGION	B-23
FIGURE B-12: GENERAL FORM OF HORIZONTAL OVERLAP REGION	B-25
FIGURE B-13: VARIATIONS ON THE FORM OF THE HORIZONTAL OVERLAP REGION	B-26
FIGURE B-14: CONFLICT BOUNDARY SURFACE	B-28
FIGURE B-15: HORIZONTAL OVERLAP REGION FOR CONFLICT BOUNDARY CELL i	B-30
FIGURE C-1: THE CONFLICT REGION	C-2
FIGURE C-2: MARGINAL DISTRIBUTION OF POSITION ERROR	C-8
FIGURE C-3: MARGINAL DISTRIBUTION OF VELOCITY ERROR	C-9
FIGURE C-4: TRACKER OUTPUT ERRORS SUPERIMPOSED ON THE CONFLICT REGION	C-11

LIST OF ILLUSTRATIONS
(concl'd)

	<u>Page</u>
FIGURE C-5: THE TRANSFORMED TRACKER OUTPUT ERRORS AND CONFLICT REGION	C-13
FIGURE C-6: GEOMETRY FOR INTEGRATION OVER A TRIANGULAR REGION IN $u-v$ SPACE	C-14
FIGURE C-7: THE PARTITIONED TRANSFORMED CONFLICT REGION (ORIGIN INCLUDED)	C-17
FIGURE C-8: THE PARTITIONED TRANSFORMED CONFLICT REGION (ORIGIN EXCLUDED)	C-18
FIGURE E-1: INTERAIRCRAFT SPACING GEOMETRY	E-2
FIGURE G-1: INTERVENTION RATE SIMULATION FLOW	G-2
FIGURE H-1: HORIZONTAL CONFLICT ALERT FILTERS USED IN SIMULATION	H-2

1. INTRODUCTION

In November 1976, the FAA Associate Administrator for Air Traffic and Airway Facilities requested assistance from the Associate Administrator for Engineering and Development in certain analytical activities relating to air traffic separation.⁽¹⁾ In part, that request asked for an examination of the soundness of the current standards for the horizontal separation of aircraft in the continental U.S. The request also called for an enhancement of analytical methods for the operational evaluation of future standards.

The response to that request is a program within the FAA's Office of Systems Engineering Management (AEM-100) to study VOR-defined air route separation. This study's initial goal is to develop an understanding of the relationship of safe route spacing to system performance on the high altitude CONUS en route airways. The system consists of both the airborne and ground elements of navigation and air traffic control. After the safety/performance relationship is better understood, improved specifications of navigation and control system performance needed to support specific route spacings can be developed.

The FAA's VOR-defined air route separation program is based on a data collection followed by modelling and analytical activities. The precursor to the data collection was a mini data collection in 1975 done by MITRE with support from ANA-220 at NAFEC.⁽²⁾ From this experience, MITRE wrote the specifications for the main data collection.^(2,3) The main data collection was planned and conducted by NAFEC (ANA-220) from September 1977 to April 1978.⁽⁴⁾ At the present time, NAFEC is reducing the data and compiling the data base.

Concurrent with the data collection, there are several analyses being performed which address the relationship of navigation and ATC system performance to safety of operations on the VOR route system. These analyses address the potential for collision between aircraft assigned to different routes under various conditions. NAFEC's analysis addresses the potential for collision between aircraft assigned to parallel routes under the assumption that there is no radar being used to separate the aircraft.⁽⁵⁾ There is also an effort at Princeton University to address the potential for collision of aircraft on intersecting routes where no radar coverage is available.⁽⁶⁾

The first volume of this report describes MITRE's Conflict Monitoring Analysis. This analysis addresses the potential for collision and the controller intervention rate for aircraft assigned to same direction parallel routes when the controller monitors aircraft movements with radar surveillance. The appendices in this volume present the details of the analysis performed to estimate the probability of horizontal overlap and controller intervention rate.

Appendix A describes the conflict region boundary. This boundary demarcates those pairs of aircraft which are projected to be in conflict from those pairs of aircraft which are not projected to be in conflict. Appendix B describes the estimation of the probability of horizontal overlap given that the aircraft pair is on the conflict region boundary. In order to make this estimate, one needs to be able to find the probability of being observed within the conflict region when there are uncertainties in the position and velocity estimates from the tracker. The estimation of this probability is given in Appendix C. It is also necessary to be able to numerically convolve probability distributions in this analysis. The Fast Fourier Transform is used to do this. This procedure is described in Appendix D. As part of the probability of horizontal overlap estimation one needs to estimate the probability of alongtrack separation. This estimate is developed in Appendix E.

In all of the analyses mentioned above one needs the probability that an aircraft pair has a particular crosstrack separation and crosstrack closing speed. Since the data is taken on single aircraft, a procedure is required to convert the single aircraft data into aircraft pair data. This procedure is described in Appendix F.

The controller intervention rate due to conflict alerts was estimated by simulation. The simulation is described in Appendix G. The NAS Conflict Alert function which was emulated in the simulation is described in Appendix H.

A list of all the variables and symbols used in both this volume and Volume I can be found in the glossary in Appendix I. The references for this volume are found in Appendix J.

APPENDIX A

THE CONFLICT REGION BOUNDARY

This appendix will develop the concept of the conflict region boundary. As indicated in Section 3 of Volume I, the conflict region boundary in the analysis is a straight line on the crosstrack separation, crosstrack closing speed plane. The equation for this line and the assumptions that were made in constructing the line will be developed in this appendix.

The situation is the following: A pair of aircraft are flying the same direction on two parallel routes. They are assumed to have the same forward speed but each aircraft can have different alongtrack and crosstrack component speeds. The aircraft are positioned on their respective routes as shown in Figure A-1. The aircraft are projected ahead along straight line paths for a time T_L . If within that time they are separated by less than a distance D , then the aircraft pair is said to be in potential conflict.

The sign conventions for the deviations and velocities are as follows: Crosstrack deviations and crosstrack velocities for the individual aircraft are measured with respect to the route centerlines of the respective routes and are positive in the direction toward the other route. In Figure A-1, Y_i and V_{yi} are the crosstrack deviation and velocity, respectively, for an aircraft on route i . The crosstrack separation between a pair of aircraft is denoted as y and is positive when the sum of the crosstrack deviations is less than the spacing between the routes. Alongtrack displacement between the aircraft, x , is measured with respect to the aircraft on route 1. The alongtrack displacement x , is positive when the aircraft on route 2 is ahead of the aircraft on route 1. With these conventions, the distance between the aircraft (d) as a function of time (t) (assuming rectilinear motion) is

$$d = \sqrt{\left\{x + (v_{x2} - v_{x1}) t\right\}^2 + \left\{y - (v_{y2} + v_{y1}) t\right\}^2} \quad (\text{A-1})$$

If we let

$$\dot{x} = v_{x2} - v_{x1} \quad (\text{alongtrack closing speed})$$

$$\dot{y} = v_{y2} + v_{y1} \quad (\text{crosstrack closing speed})$$

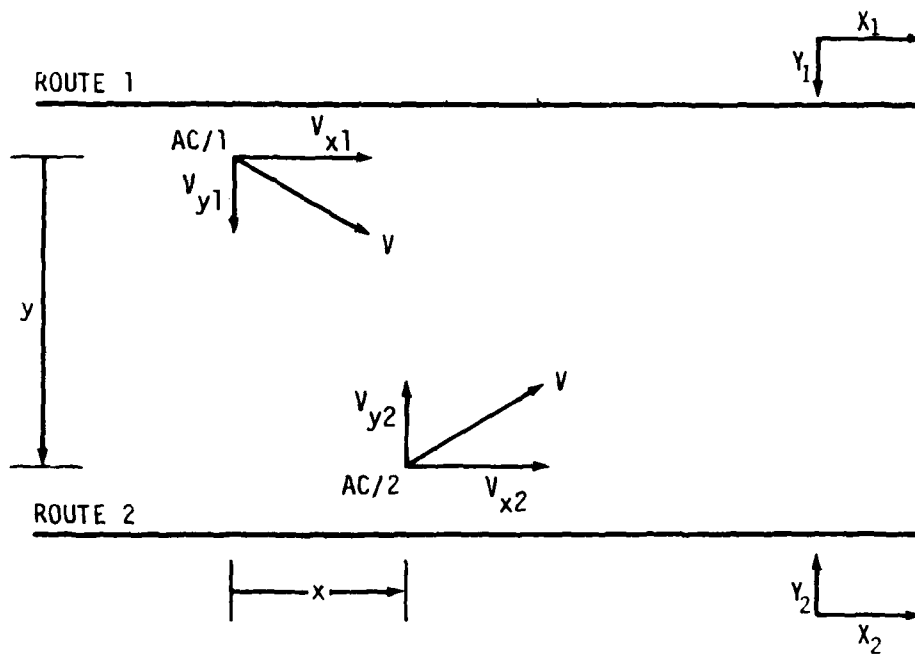


**FIGURE A-1
CONFLICT GEOMETRY**

and solve (A-1) for y then

$$y = \dot{y}t + \sqrt{d^2 - x^2 - t^2 \dot{x}^2 - 2tx\dot{x}} \quad (A-2)$$

The objective in this analysis is to arrive at a relationship between the crosstrack separation of an aircraft pair and the conditions under which a potential conflict would exist. Thus, one would want to know when the aircraft pair first enters into potential conflict. This can be determined by letting d equal the threshold distance for a potential conflict, D, and t equal the look-ahead time, TL. Hence, one finds the crosstrack separation, y, at which the threshold separation, D, will be achieved at time TL in the future.

It is assumed at this point that prior to entering into potential conflict the aircraft are oriented with respect to each other in the same way that their respective routes are oriented and they are closing in the crosstrack direction. In other words, with reference to the sign convention used in Figure A-1, the crosstrack separation and the crosstrack closing speed are both positive prior to entering into potential conflict. With this assumption, the plus sign in front of the radical in equation A-2 is chosen.

Making the substitutions into equation A-2 we can define the conflict region boundary as:

$$y = \dot{y} TL + \sqrt{D^2 - x^2 - TL^2 \dot{x}^2 - 2TL x \dot{x}} \quad (A-3)$$

Given TL, D, x, and \dot{x} one could plot the conflict region boundary on the \dot{y} , y plane. However, \dot{x} in general can take on many values for a given value of \dot{y} . In fact, if the maximum crosstrack speed of an aircraft is $v_{y\max}$, then the range of alongtrack closing speeds (\dot{x}) for a given crosstrack closing speed (\dot{y}) is

$$\sqrt{v^2 - v_{y\max}^2} - \sqrt{v^2 - (v_{y\max} - \dot{y})^2} \leq \dot{x} \leq \sqrt{v^2 - (v_{y\max} - \dot{y})^2} + \sqrt{v^2 - v_{y\max}^2}$$

(A-4)

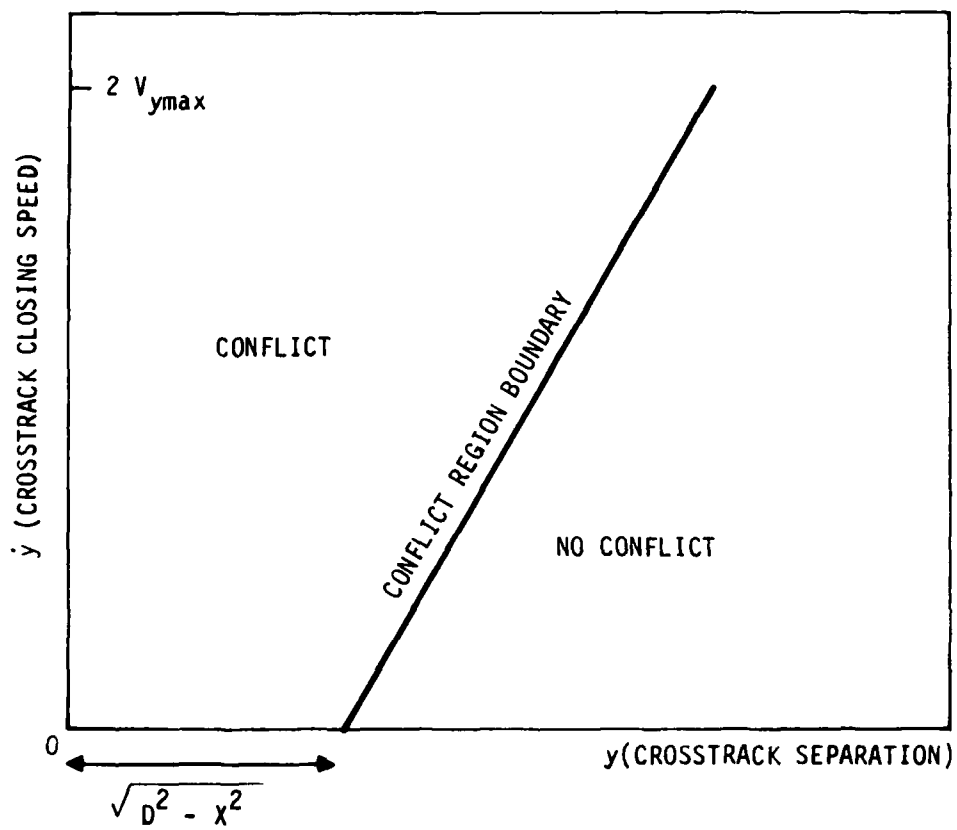
where V is the forward speed of the two aircraft. It should be remembered that the x dimension is measured with respect to the position of the aircraft on route 1.

If it is assumed that the distributions of crosstrack speed for single aircraft on the two routes are the same and the aircraft all have equal speed, then the expected alongtrack closing speed ($E(\dot{x})$) over all values of \dot{y} will be zero. To get a first order look at the conflict boundary we substitute $\dot{x}=0$ into (A-3) to arrive at

$$y = \dot{y} T_L + \sqrt{D^2 - x^2} \quad (A-5)$$

The conflict region based on (A-5) is shown in Figure A-2. Recall that the line in Figure A-2 defines the point at which the threshold separation, D , is projected to be violated at a time T_L in the future. Since the aircraft pair is closer together for smaller values of y , the region to the left of the line in Figure A-2 represents combinations of y and \dot{y} where the threshold separation is violated prior to time T_L . Note also that the y -intercept of this curve is $\sqrt{D^2 - x^2}$, which depends on the initial alongtrack separation x . At the point $\dot{y}=0$ the horizontal separation will be $\sqrt{D^2 - x^2}$. In other words, if the aircraft were not closing on each other ($\dot{y}=0, \dot{x}=0$) but their horizontal separation were less than $\sqrt{D^2 - x^2}$ then the aircraft pair would be in potential conflict. The maximum value for \dot{y} is $2 V_{y\max}$ since each aircraft could be flying away from its route centerline with no more than the maximum crosstrack speed $V_{y\max}$.

When proximity is discussed in the Conflict Monitoring Analysis, its meaning is based on the allowable range of x values. One thing which should be noted about equation (A-5) is that there is a limited range for x . If $|x| > D$, then the square root in equation (A-5) gives an imaginary number. This means that if $\dot{x}=0$ and the aircraft are separated alongtrack by more than D then there can be no potential conflict. In other words, if the aircraft are not closing in the alongtrack direction ($\dot{x}=0$), then no matter how close they are in the crosstrack direction they will always be separated by more than the distance D . Aircraft which are spaced alongtrack greater than a distance D are not proximate because they cannot be in potential conflict and hence the analysis indicates that they cannot collide.



GIVEN X (THE ALONGTRACK SEPARATION)

FIGURE A-2
THE CONFLICT REGION

The expression for the conflict region boundary given in equation (A-5) and illustrated in Figure A-2 was used in the Conflict Monitoring Analysis. Recall that it was derived from equation (A-3) by replacing \dot{x} by its expected value. Equation (A-5) was used because it is simpler than (A-3) (being a straight line) and it is a reasonable approximation to the conflict region boundaries with $\dot{x} \neq 0$.

To see how good an approximation equation (A-5) is we shall go back and investigate equation (A-3). From equation (A-3) it is apparent that for a given value of \dot{y} , the value of y will be a minimum when

$$z = D^2 - (x + TL \dot{x})^2 \quad (A-6)$$

is a minimum greater than or equal to zero. The value of y will be a maximum when z is a maximum. However, it is necessary from (A-4) that

$$\dot{x}_1 < \dot{x} < \dot{x}_2 \quad (A-7)$$

where

$$\dot{x}_1 = \sqrt{v^2 - v_{y\max}^2} - \sqrt{v^2 - (\dot{y} - v_{y\max})^2}$$

and

$$\dot{x}_2 = \sqrt{v^2 - (\dot{y} - v_{y\max})^2} - \sqrt{v^2 - v_{y\max}^2}$$

If we let $M = x + TL \dot{x}$, then equation (A-6) is a parabola as shown in Figure A-3. The value of M must be between the values of M_1 and M_2 to satisfy equation (A-2). If either M_1 or M_2 is outside the range $-D \leq M \leq D$ then the minimum z is zero. If both M_1 and M_2 are inside the range $-D \leq M \leq D$ then z is the minimum of $D^2 - M_1^2$ and $D^2 - M_2^2$. The maximum z is the maximum of $D^2 - M_1^2$ and $D^2 - M_2^2$ if M_1 and M_2 are both on the same side of the origin. If M_1 and M_2 are on opposite sides of the origin the maximum z is D^2 .

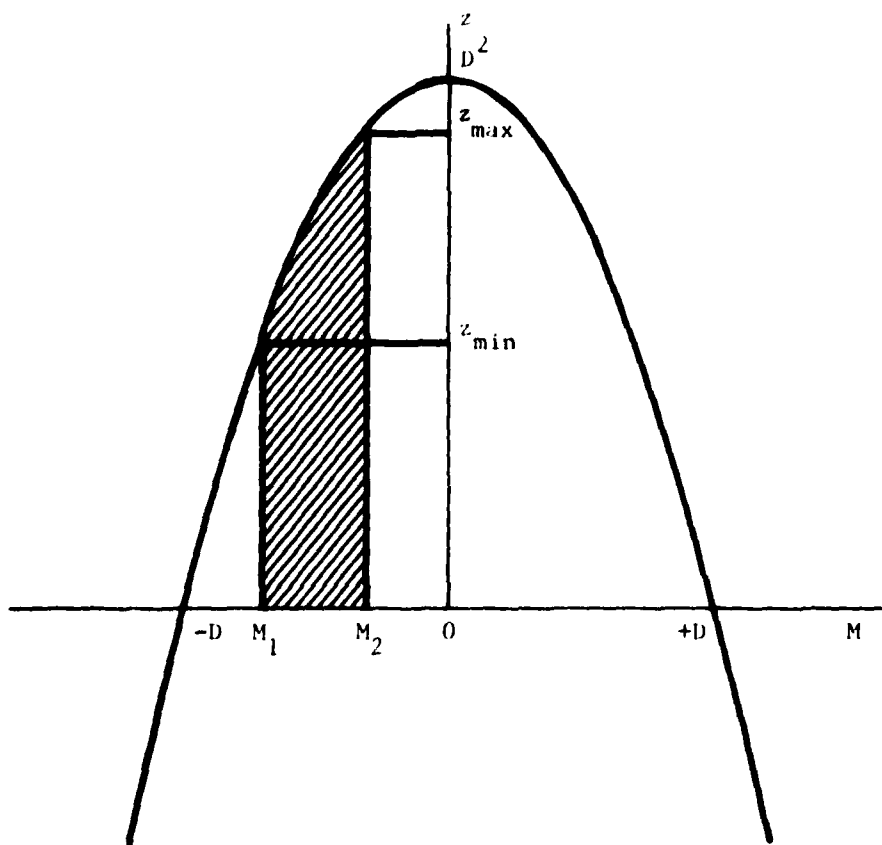


**FIGURE A-3
MAX/MIN REGION FOR
DISCRIMINANT IN EQUATION A-3**

From the above considerations the conflict region boundaries for the range of possible \dot{x} values given in equation (A-7) can be drawn for various values of alongtrack separation (x). Figures A-4 through A-6 show a set of conflict region boundary envelopes for $x = 0.0$ nmi, $x = +3.0$ nmi, and $x = +5.0$ nmi. If a truly conservative risk estimate were to be made, then the left-most conflict region boundary should be used. This boundary would allow the aircraft pair to be closer together before the resolution maneuver is executed and thus increase the risk of collision.

To get an appreciation of the quality of the use of $x = 0$ in equation (A-3) it is instructive to look at the distributions of early and late detections which would result from the use of the $\dot{x} = 0$ conflict region boundary. Such distributions were constructed for a number of values of the crosstrack closing speed (\dot{y}) for several values of x . A set of these distributions are shown in Figures A-7, A-8, and A-9. Each distribution is scaled relative to the frequency with which the particular value of \dot{y} is expected to be observed.

Figure A-7 shows that when $x = 0$, the aircraft are nearly always detected early using the $\dot{x} = 0$ conflict region boundary. However, the maximum time difference is only a few seconds. In Figure A-8, when $\dot{x} = +3$ nmi, the aircraft pairs could be detected early or late. At the lesser values of \dot{y} the distribution is more or less symmetrical, while for greater values of \dot{y} the distribution is skewed toward a later (more conservative) detection. When $x = +5$ nmi (see Figure A-9), one always detects late by using the $\dot{x} = 0$ conflict region boundary. The spike at $\dot{y} = 10$ kts indicates that 20% of the aircraft pairs will be detected more than 200 seconds late. Thus, from the consideration of the early/late detection distributions it appears that the use of the $\dot{x} = 0$ conflict region boundary is prudent if not some what conservative.

Another consequence of not letting $\dot{x} = 0$ is that x would no longer be required to be within the range $-D \leq x \leq D$ to define a conflict region boundary. If $\dot{x} \neq 0$ and $|x|$ is chosen greater than D , there will be a range of conflict region boundaries as depicted in Figure A-10. This figure represents the envelope of conflict region boundaries for $|x| = 6.5$ nmi. For $|x|$ greater than this the aircraft would be too far apart to be in conflict even when $\dot{x} \neq 0$.

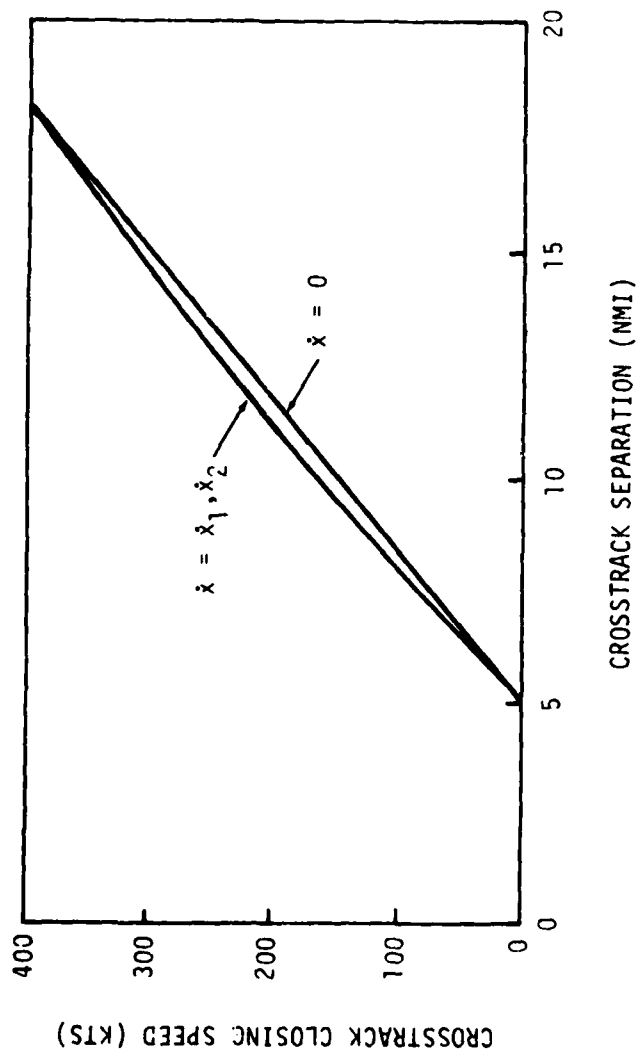


FIGURE A-4
ENVELOPE OF CONFLICT REGION BOUNDARIES
FOR $x = 0.0$ NMI

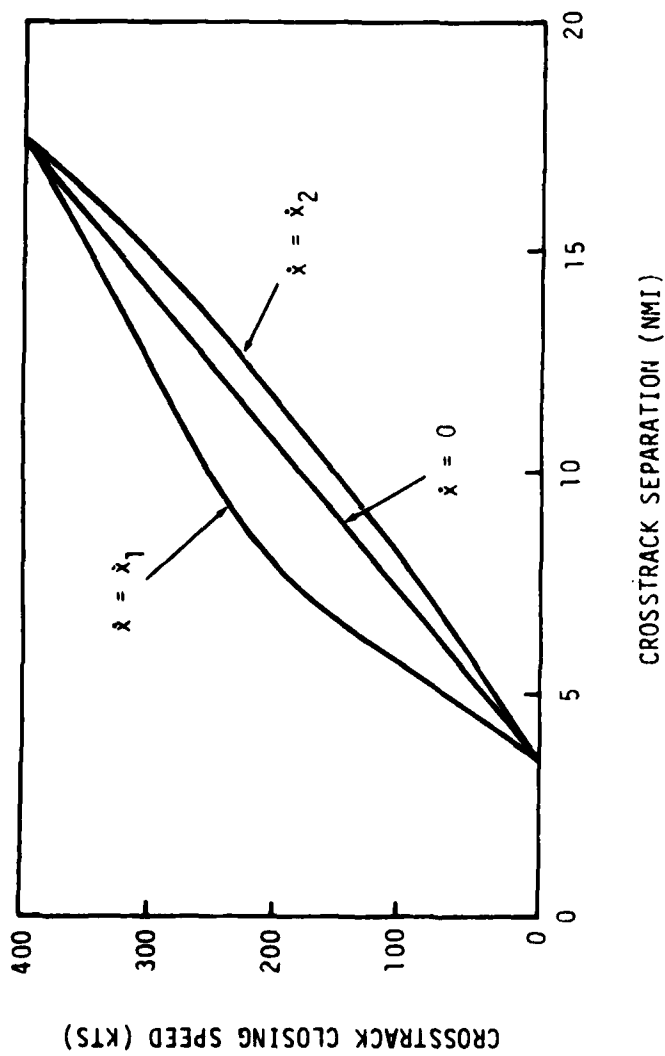


FIGURE A-5
ENVELOPE OF CONFLICT REGION BOUNDARIES
FOR $x = \pm 30$ NMI

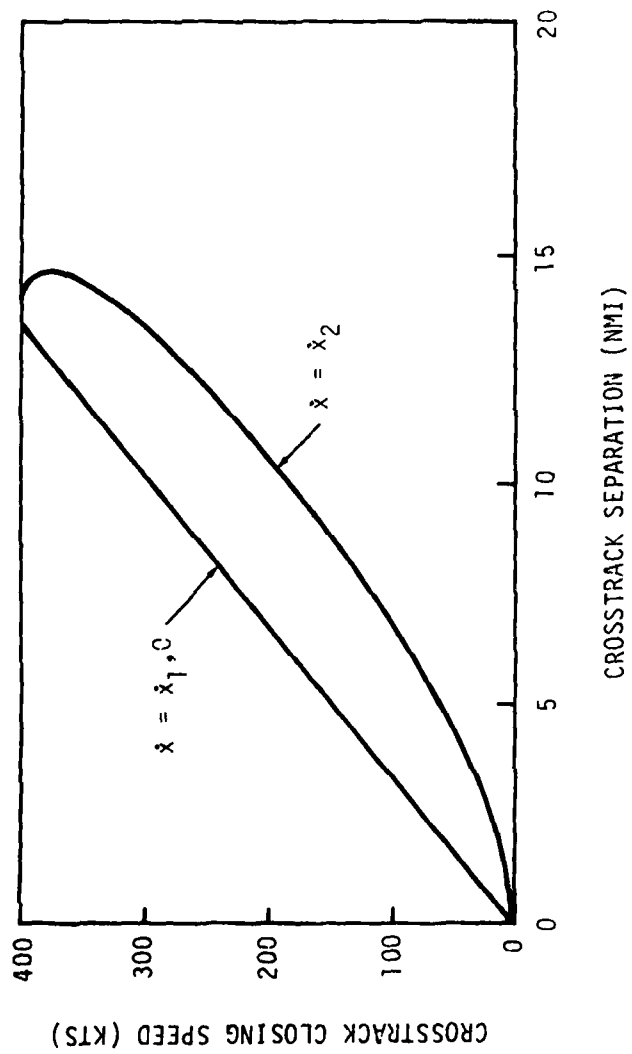


FIGURE A-6
ENVELOPE OF CONFLICT REGION BOUNDARIES
FOR $x = \pm 5.0$ NMI

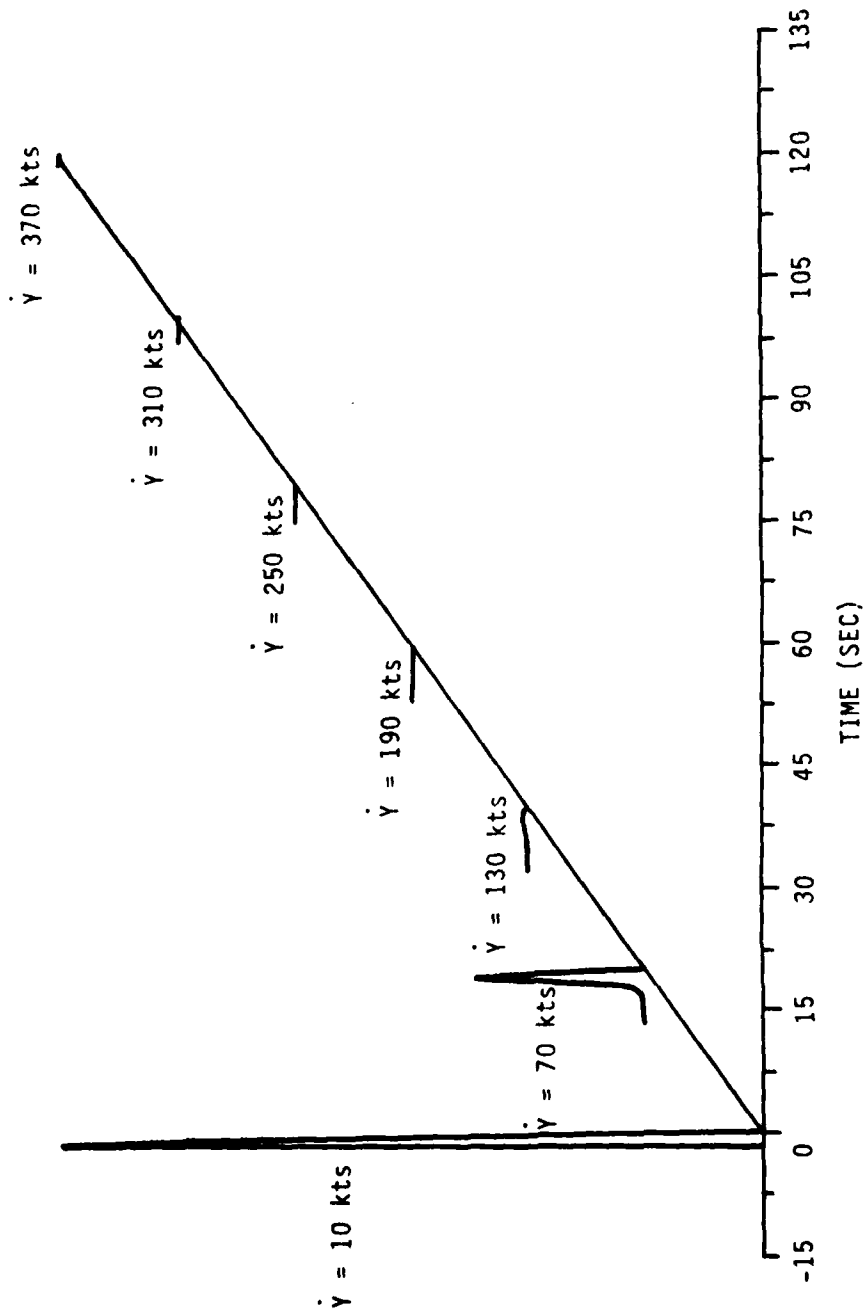


FIGURE A-7
DISTRIBUTION OF EARLY (-) OR LATE (+) DETECTIONS
 (x = 0 NMI)

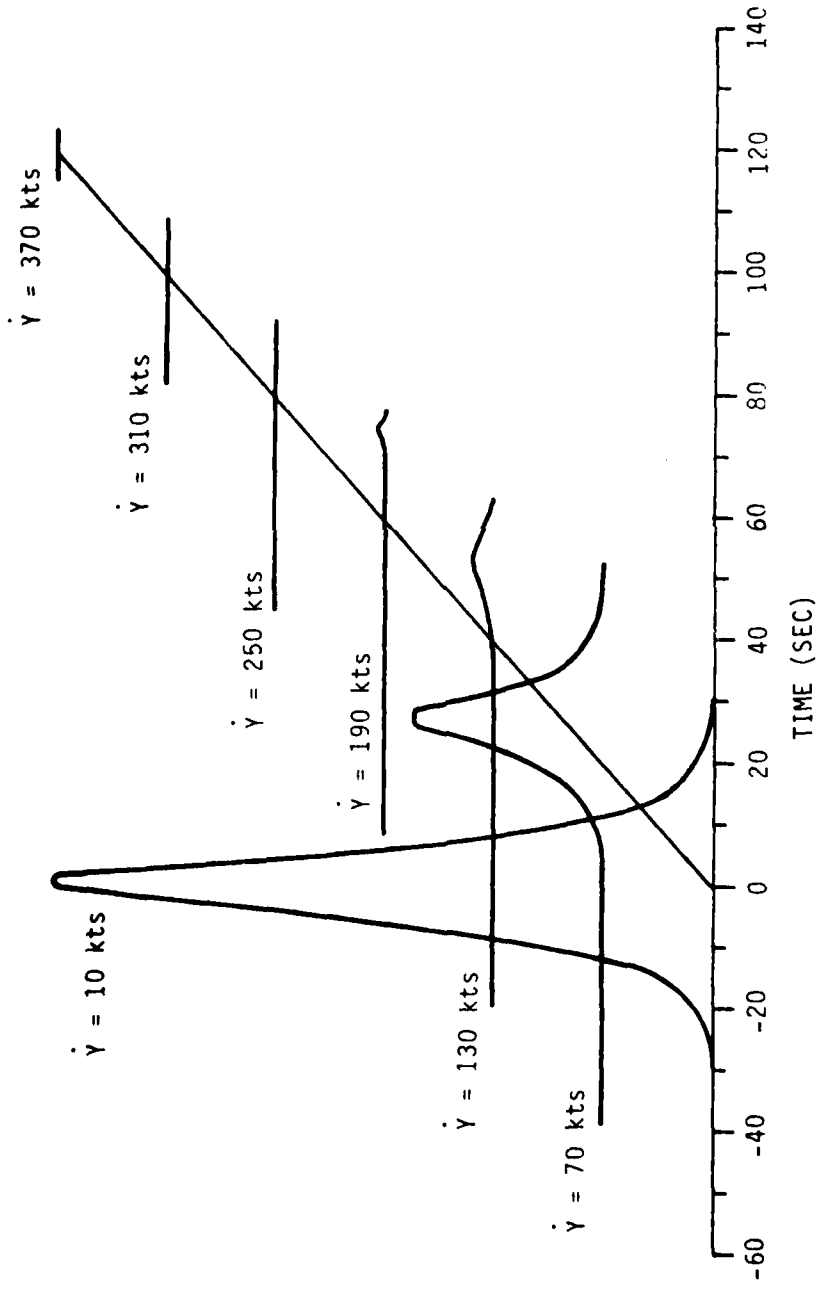


FIGURE A-8
DISTRIBUTION OF EARLY (-) OR LATE (+) DETECTIONS
 ($x = \pm 3$ NMI)

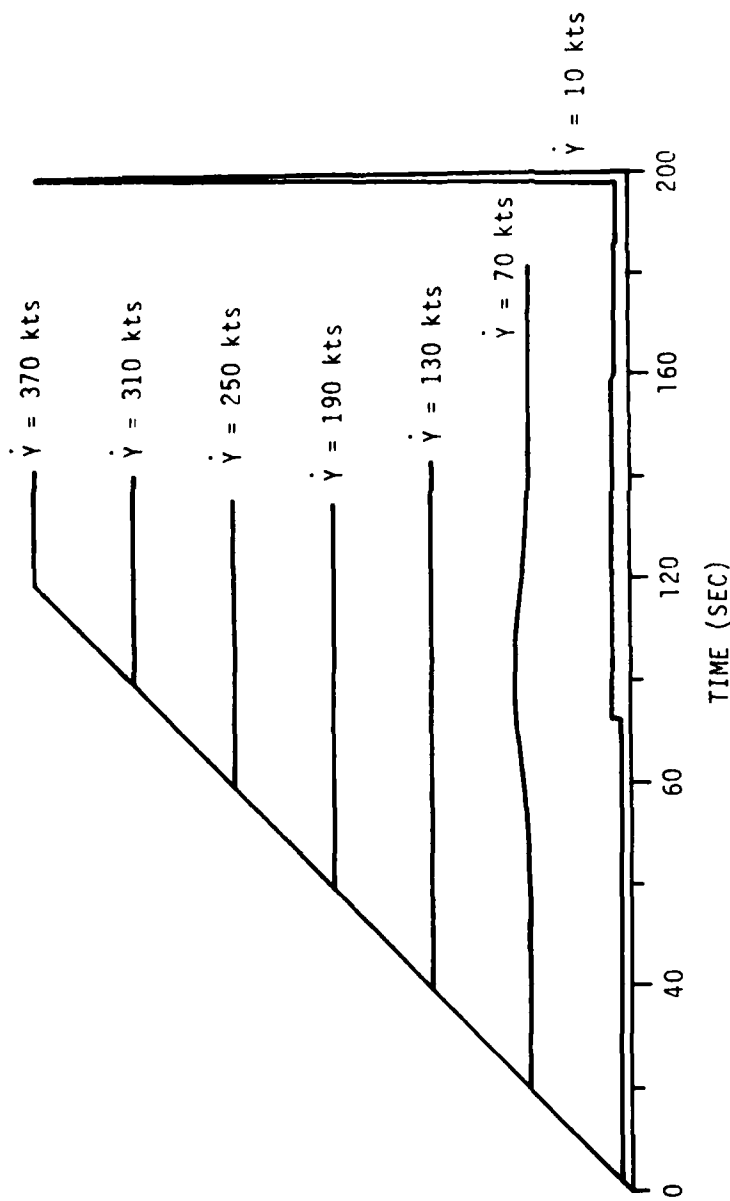


FIGURE A-9
 DISTRIBUTION OF EARLY (-) OR LATE (+) DETECTIONS
 (x = ±5 NMI)

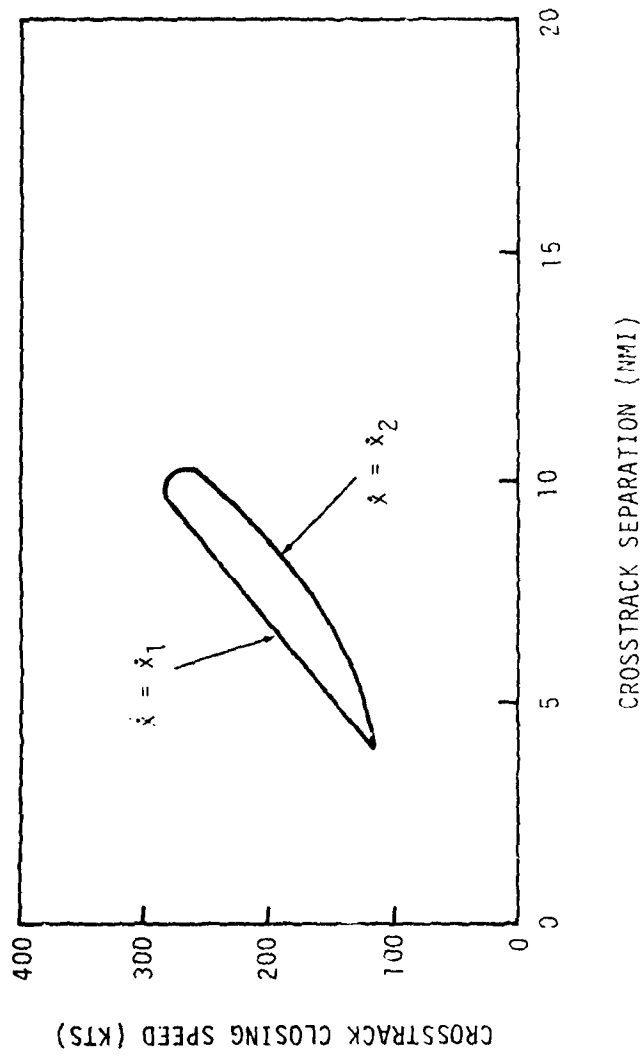


FIGURE A-10
 ENVELOPE OF CONFLICT REGION BOUNDARIES
 FOR $x = \pm 6.5$ NMI

One assumption made in this analysis should be highlighted. For this analysis the forward speeds of both aircraft were assumed to be the same. For the high altitude CONUS airspace with many aircraft with the same performance capabilities flying at the same altitude this assumption should be a reasonable. However, there are some slower aircraft in the high altitude airspace. If one wanted to account for these speed differences, the entire analysis could conceivably be done on a pair-by-pair basis with the results properly weighted. For expediency, the different speed case was not considered in this analysis but will be addressed in the future.

APPENDIX B

COMPUTATION OF THE PROBABILITY OF HORIZONTAL OVERLAP

B1. INTRODUCTION

In order for a pair of aircraft to collide, the pair must first penetrate the conflict region boundary described in Appendix A. Therefore, the probability of horizontal overlap can be calculated as the product of the probability that the aircraft pair is on the conflict region boundary and the conditional probability that the pair has a delay time and an avoidance maneuver turn rate which would result in horizontal overlap given that the pair is on the conflict region boundary.

First, this appendix will discuss the distributions of the time delay and the turn rate which were used for this analysis. Second, the appendix will describe using these distributions to calculate the conditional probability that an aircraft pair has a delay time and a turn rate which would result in horizontal overlap given that the pair is on the conflict region boundary. Finally this appendix will illustrate the calculation of the probability that an aircraft pair is on the conflict region boundary. This then provides all the information necessary to estimate the probability of horizontal overlap.

B2. DELAY TIME

The delay time in the model is defined to be that time when both aircraft are in the conflict region and are flying straight. This includes the time between the actual penetration of the conflict region boundary and the detection of the potential conflict. The delay time will also include the time taken for the controller to recognize the conflict, to decide, and to communicate instructions to the pilot, and for the pilot to start to take action on the instructions. The total delay time will be the sum of the above listed delays. We will first examine the delay due to the detection process and then address the remainder of the delay.

B2.1 Delay Due to Detection

Consider a pair of aircraft transgressing the conflict region boundary as shown in Figure B-1. At radar update 1 the pair is just outside the conflict region boundary. At update 2 the pair is just inside the boundary. At subsequent updates the pair is further inside the conflict region. As shown in the figure, it

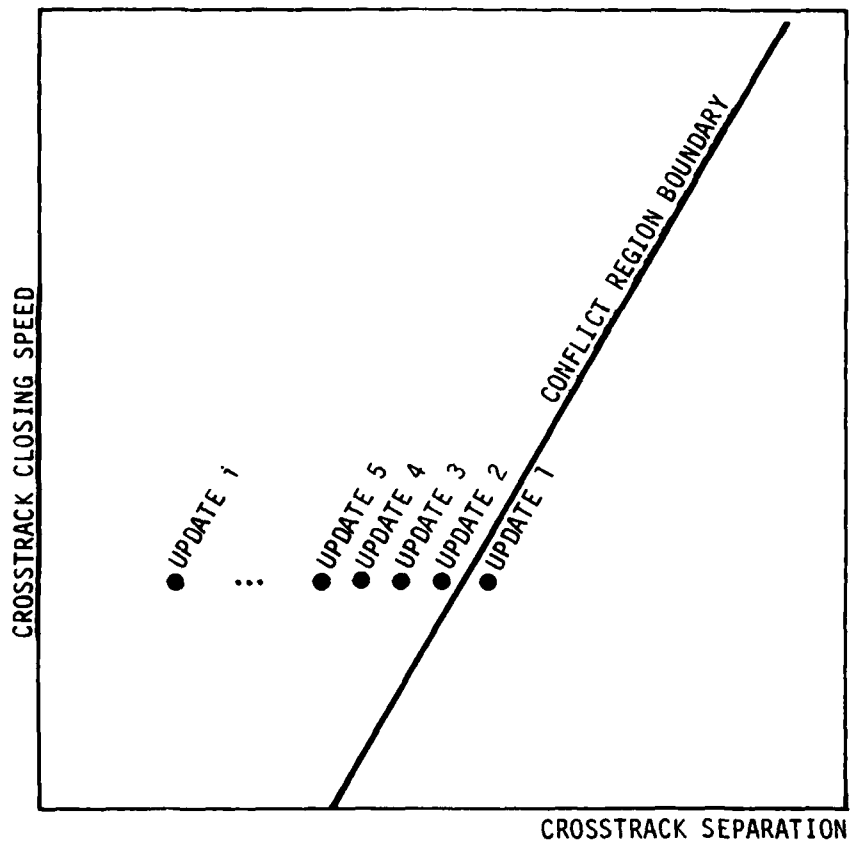


**FIGURE B-1
PROGRESSION OF A PAIR OF AIRCRAFT
ACROSS THE CONFLICT REGION BOUNDARY**

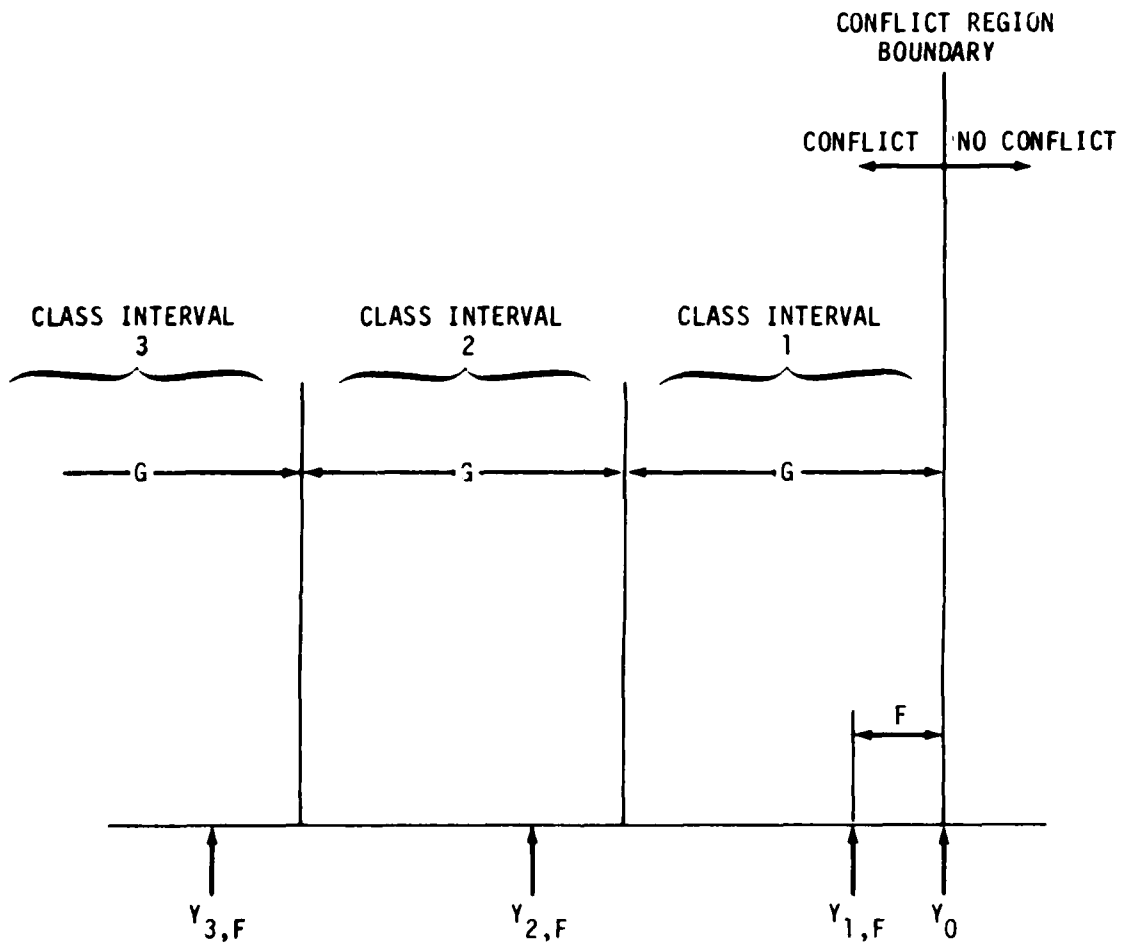
is assumed that the crosstrack closing speed is constant. This assumption is based on the prior assumption that the velocities of the individual aircraft remain constant after the pair crosses the conflict region boundary. As discussed in Appendix A the conflict region boundary is defined under the assumption that $\dot{x}=0$. In terms of Figure B-1 this assumption means that on the average the conflict region boundary is the same for each radar update. Even though the expected value of \dot{x} is zero, \dot{x} can have values in the range given in equation (A-4). For most of the values of \dot{x} in this range the change in the value of x over a update interval of time will be insignificant. The cases of larger changes of x over an update interval will be very infrequent. For a given value of x (alongtrack separation) and \dot{y} (crosstrack closing speed) we want to construct a probability density function of the time interval between the time the aircraft pair enters into the conflict region and the time it is detected as being in potential conflict.

The detection process is based on a set of surveillance returns which have been processed through an alpha-beta tracker. The position and velocity estimates from the tracker are assumed to have normally distributed correlated errors with zero bias. Referring to Figure B-2, one can visualize the detection process. The aircraft pair crosses into the conflict region with a given crosstrack closing speed (\dot{y}) and is a distance F inside the conflict region boundary when the initial radar observation is made. After the next revolution of the radar antenna (after dt hours), the aircraft pair has a crosstrack separation of $Y_{2,F}$. The crosstrack separation lost between $Y_{1,F}$ and $Y_{2,F}$ is $G=\dot{y}dt$.

At each crosstrack separation $Y_{i,F}$, there is a probability $PND_{i,F}$, that the estimates of the crosstrack separation and closing speed will indicate that the aircraft pair is still outside the conflict region. The computation of this probability is discussed in Appendix C.

Since each radar update is assumed to give an independent measurement of the aircraft positions, the probability of not being detected in the conflict region during the first i updates is given as

$$PND^{i,F} = \prod_{k=1}^i PND_{k,F} \quad (B-1)$$



G = CROSSTRACK SEPARATION LOST DURING ONE RADAR UPDATE INTERVAL (CLASS INTERVAL)
 F = CROSSTRACK DISTANCE INSIDE CONFLICT REGION AT INITIAL RADAR OBSERVATION
 Y_0 = CROSSTRACK SEPARATION AT THE CONFLICT REGION BOUNDARY
 $Y_{i,F} = Y_0 - F - (i-1)G$ CROSSTRACK SEPARATION AT RADAR UPDATE i AFTER CROSSING INTO CONFLICT REGION

FIGURE B-2
CROSSTRACK SEPARATIONS DURING THE DETECTION PROCESS

The probability of first detecting an aircraft pair in the conflict region in the class interval i (see Figure B-2) is

$$PFD_{i,F} = PND_{i-1,F} (1 - PND_{i,F}) \quad (B-2)$$

It should be remembered that the initial observation of aircraft pair was made when the aircraft pair was inside the conflict region by a crosstrack separation distance F . The distance F is a random variable with a probability density function $q(F)$. Since the time of entering the conflict region is in no way related to the timing of the radar scans, it is reasonable to assume the F is uniformly distributed between 0 and G . Thus

$$q(F) = 1/G \quad 0 \leq F \leq G \quad (B-3)$$

Therefore, the probability of first detection in class interval i is

$$PFD_i = \frac{1}{G} \int_0^G PFD_{i,F} dF \quad (B-4)$$

In the actual computation a set of N equally spaced initial positions were selected. Thus

$$PFD_i \approx \frac{1}{NG} \sum_{j=1}^n PFD_{i,(j-1)G/N} \quad (B-5)$$

The quantity computed in (B-5) is the probability that an aircraft pair with crosstrack closing speed \dot{y} will be first detected in class interval i . The class interval width is G (see Figure B-2) is the crosstrack separation lost during one radar update.

B2.2 Delay Due to the Controller, the Communication Link, and the Pilot

After the aircraft pair is detected as being within the conflict region there will be an additional delay while the controller decides what to do and the resolution commands are transmitted to the pilot. The pilot then has to decide what to do and start to turn his aircraft.

The various components of this delay are very difficult to model because of the human element. However, there is data available from a simulation done in Great Britain on controller response to threshold transgression.⁽⁷⁾ The histogram of delay times with a computer-assisted system is shown in Figure B-3. These delay times were measured from the time of presentation to the controller to the time the controller communicates with the pilot.

Even though the controllers in the simulation had a workload in addition to their monitoring role, one must still remember that the controllers knew that they were in a simulated environment. For this reason the histogram data in Figure B-3 were fit to a Gamma function to give the delay distribution a long tail. The Gamma function fit is also shown in Figure B-3.

The collision risk will be sensitive to the delay time. This means that the conservativeness of the analysis could be dictated by the chosen delay function. The particular delay function which was fit to the histogram data has a long tail which was truncated at 600 seconds for computational reasons. This length of time is approximately one-half the flying time through a sector. With this length of delay one could argue that possible failure of the controller to notice the potential conflict or short term communication breakdowns or other outages are essentially accounted for.

B2.3 Total Delay

The delay due to the detection process is independent of the delay due to the controller/communication/pilot reactions. Therefore, the total delay is the sum of two independent random variables. The probability density function of the sum of two independent random variables is the convolution of their probability densities. The technique used to convolve the probability density functions is the Fast Finite Fourier Transform. The Fast Finite Fourier Transform technique is discussed in detail in Appendix D.

B3. TURN RATE

In the Conflict Monitoring Analysis the turn rate is specified as a range of bank angles since it is the bank angle that the pilot controls when he makes a turn.

We will assume that the bank angle chosen by the pilot to make his turn back to his assigned route centerline will be in the

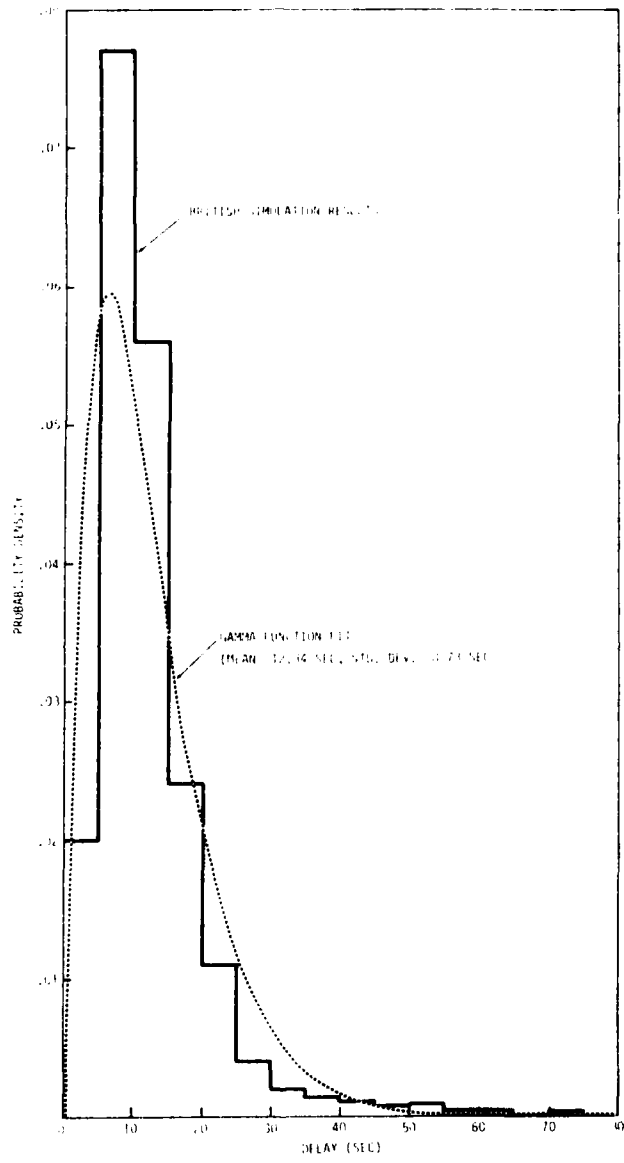


**FIGURE B-3
DELAY DISTRIBUTION**

range of 10 degrees to 30 degrees. The minimum bank angle of 10 degrees means that the pilot will make a definite resolution maneuver. The maximum bank angle of 30 degrees was chosen because it is the angle which usually demonstrates the threshold of passenger discomfort due to g forces. It is also assumed that the choice of each bank angle within this range is equally likely. The probability density function of the bank angle is shown in Figure B-4.

The distribution of bank angles must be related to a distribution of turn rates in order to find the relationship between the turn and the time and distance required for the maneuver. If the pilot makes a coordinated turn then

$$\omega = g (\tan \kappa) / V \quad (B-6)$$

where ω is the turn rate, g is the gravitational constant, V is the forward velocity of the aircraft, and κ is the bank angle.

If the pdf of κ is uniform as shown in Figure B-4, then the pdf of ω , $j(\omega)$, can be shown to be

$$j(\omega) = \frac{V}{(\kappa U - \kappa L) g \left(1 + \frac{V\omega}{g}\right)^2} ; \frac{g}{V} \tan \kappa L \leq \omega \leq \frac{g}{V} \tan \kappa U \quad (B-7)$$

The pdf $j(\omega)$ that corresponds to the bank angle pdf in Figure B-4 is shown in Figure B-5.

B4. HORIZONTAL OVERLAP REGION

Up to this point we have developed the probability density function of the total delay after an aircraft pair penetrates the conflict region and the probability density function of the turn rate used by an aircraft to return toward its route center line. The problem now reduces to finding the probability that the aircraft pair will come into horizontal overlap given that 1) the pair passes into the conflict region, 2) there is a delay, and 3) there is a turn back toward the route centerline by one of the aircraft.

After the aircraft pair passes into the conflict region, the aircraft are assumed to continue flying in a straight line for a delay time t_d . Then one aircraft will make a horizontal turn

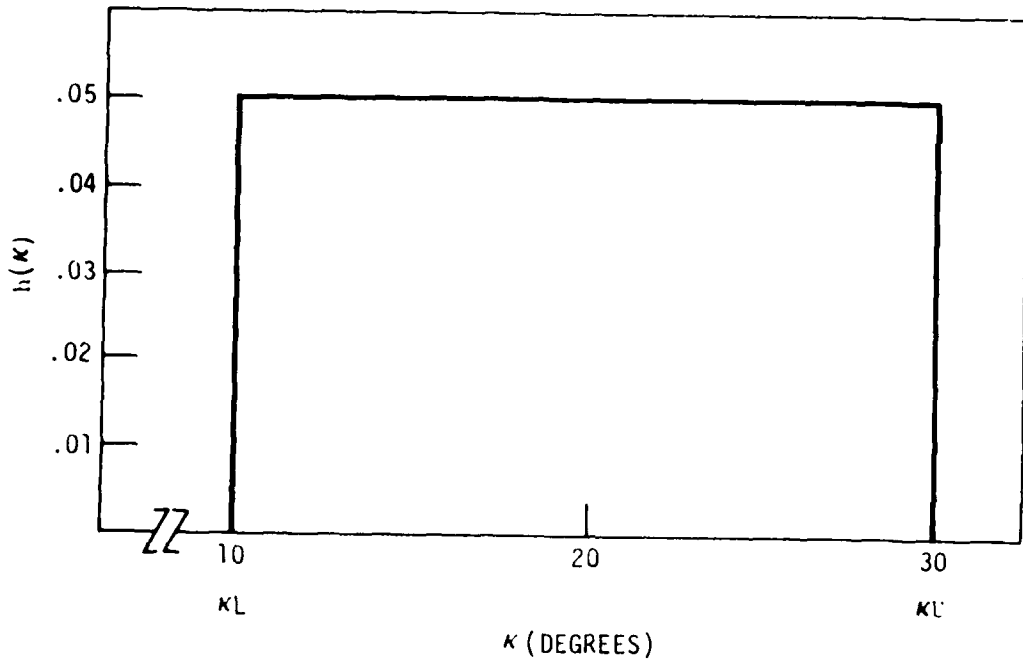
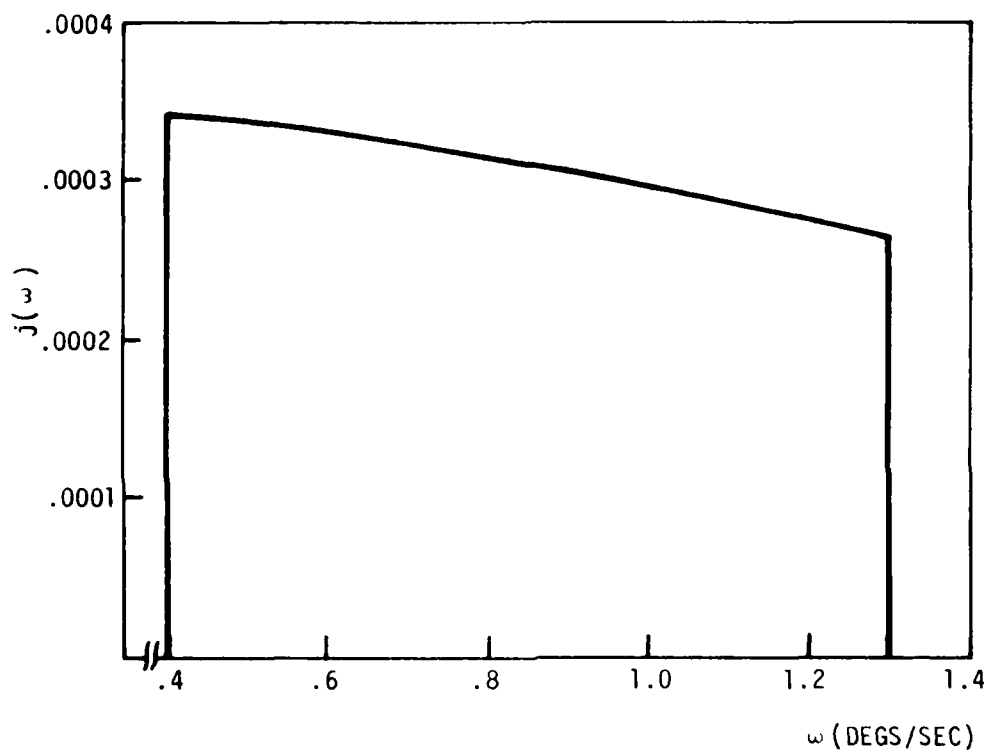


FIGURE B-4
PROBABILITY DENSITY FUNCTION OF THE
BANK ANGLE



**FIGURE B-5
PROBABILITY DENSITY FUNCTION OF THE
TURN RATE**

with a turn rate ω . At some point after the pair enters the conflict region, either a minimum separation between the aircraft will be achieved after which the aircraft will separate, or the aircraft will collide. With a delay and then a turn there are four ways in which minimum separation can occur. First, the minimum separation can occur at that time when the velocities of the two aircraft become parallel. A second way is for the aircraft to reach their minimum separation before one of the aircraft starts to turn. A third way would be for the minimum separation to occur during the turn and before the velocities become parallel. The fourth case is where the absolute minimum separation occurs after the velocities become parallel. Only the first three cases are of interest because the fourth case implies that the paths of the two aircraft cross without a collision and then one of the aircraft turns back into the path of the other aircraft.

To analyze the first three cases we will start the aircraft pair in the condition of horizontal overlap. The aircraft will then be "flown backwards in time". One aircraft will execute a turn at a turn rate ω while the other flies straight. The turning aircraft will then come out of its turn and fly a straight path. Both aircraft fly (backwards) along their respective straight paths until they reach positions which will place them on the boundary of the conflict region. By doing the analysis this way one can identify those combinations of turn rate and delay time which would place an aircraft pair in horizontal overlap given that the pair started from a position on the conflict region boundary.

To find these combinations of delay times and turn rates we consider the scenario shown in Figure B-6. Aircraft 1 is on the conflict region boundary at position X_{10}, Y_{10} with velocity V_{x1}, V_{y1} while aircraft 2 is at position X_{20}, Y_{20} with velocity V_{x2}, V_{y2} .

The velocities are such that

$$v = \sqrt{v_{x1}^2 + v_{y1}^2} = \sqrt{v_{x2}^2 + v_{y2}^2} \quad (B-8)$$

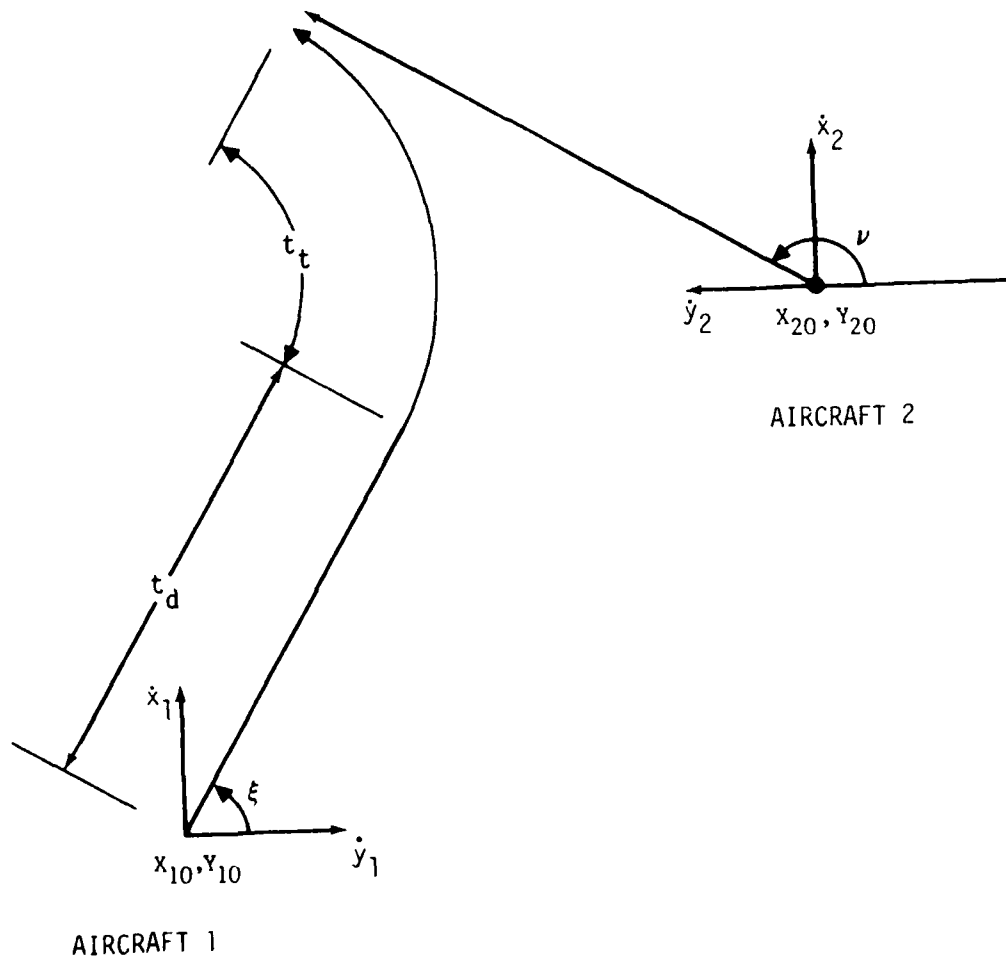


**FIGURE B-6
COLLISION GEOMETRY**

The trajectory of aircraft 2 which flies the straight course is:

$$\begin{aligned} X_2(t) &= X_{20} + v_{x2}t \\ Y_2(t) &= Y_{20} + v_{y2}t \end{aligned} \tag{B-9}$$

The trajectory of aircraft 1 which flies the straight course for a time t_d then a curved course for a time t_c is:

$$\begin{aligned} X_1(t = t_d + t_c) &= X_{10} + v_{x1}t_d + \frac{v}{\omega} (\cos \xi - \cos(\xi + \omega t_c)) \\ Y_1(t = t_d + t_c) &= Y_{10} + v_{y1}t_d + \frac{v}{\omega} (\sin(\xi + \omega t_c) - \sin \xi) \end{aligned} \tag{B-10}$$

where as in Figure B-6

ξ = the initial heading of aircraft 1,

ν = the initial heading of aircraft 2

such that

$$v_{x1} = v \sin \xi$$

$$v_{x2} = v \sin \nu$$

$$v_{y1} = v \cos \xi$$

$$v_{y2} = v \cos \nu.$$

The time that aircraft 1 is in the turn, t_c , is given by

$$t_c = P \frac{\nu - \xi}{\omega}; \quad 0 \leq P \leq 1 \tag{B-11}$$

where P is a factor which delineates the three cases discussed above. If $P=0$ then there is no turn and the minimum separation will be when both aircraft are flying straight. If $P=1$ then aircraft 1 will have made its turn to come parallel to aircraft

2 at the point of minimum separation. If $0 < P < 1$ then the separation at time t will be during the turn of aircraft 1 before the velocities of the two aircraft become parallel.

There are two conditions that are imposed on this scenario:

1. The aircraft pair starts on the conflict region boundary
2. The aircraft pair ends up in a horizontal overlap situation.

The first condition is specified by the expression

$$Y_{20} - Y_{10} = (v_{y1} - v_{y2})TL + \sqrt{D^2 - (X_{20} - X_{10})^2} \quad (B-12)$$

where TL is the look-ahead time and D is the threshold separation which is tested for in the conflict alert function. The second condition is that the aircraft pair end up in horizontal overlap. If we assume that the aircraft are represented as right cylinders with radius R , this means that the aircraft will be in overlap if their centers are separated by less than a distance $2R$. Therefore, if

$$\{X_2(t) - X_1(t)\}^2 + \{Y_2(t) - Y_1(t)\}^2 \leq (2R)^2 \quad (B-13)$$

then the aircraft will be in a condition of horizontal overlap at time t .

Substituting (B-9) and (B-10) into (B-13) and using (B-8), (B-11), and (B-12) we can rearrange terms to arrive at

$$t_d^2 (I^2 + K^2) + t_d (2Ix + 2IJH + 2KLH + 2 KM) + (x^2 + J^2 H^2 + 2JHx + L^2 H^2 + M^2 + 2LMH - 4R^2) \leq 0 \quad (B-14)$$

where $H=1/\omega$

$$\begin{aligned} I &= V(\sin v - \sin \xi) \\ J &= V [P(v-\xi)\sin v - \cos \xi + \cos(\xi(1-P) + Pv)] \\ K &= V(\cos v - \cos \xi) \\ L &= V[P(v-\xi)\cos v + \sin(\xi(1-P) + Pv) + \sin \xi] \\ M &= (V_{y1} - V_{y2}) TL + \sqrt{D^2 - x^2} = y \end{aligned}$$

One can find the range of values of t_d for which equation (B-14) is true by using the quadratic formula. Equation (B-14) will be true for t_d between the roots of the expression obtained by setting the lefthand side of equation (B-14) equal to zero. However, in order that this expression have real roots the following expression must be true:

$$\begin{aligned} -H^2(IL - JK)^2 + 2H(IL - KJ)(Kx - IM) + 4R^2(I^2 + K^2) \\ + 2IKMx - I^2M^2 - K^2x^2 > 0 \end{aligned} \quad (B-15)$$

Therefore, restricting our attention to the range of values of H for which (B-15) is true will insure that there will be real values of t_d which satisfy (B-14). However, in order that (B-15) be true for real values of H, H must lie between the roots of the expression obtained by setting the lefthand side of (B-15) equal to zero. This expression will have real roots if the following inequality holds:

$$(IL-KJ)^2(Kx-IM)^2 + (IL-JK)^2(4R^2(I^2+K^2) + 2IKMx - I^2M^2 - K^2x^2) > 0 \quad (B-16)$$

But (B-16) reduces to

$$R^2(IL - KJ)^2(I^2 + K^2) > 0 \quad (B-17)$$

which is always true. Therefore, the solution to (B-15) is for H between

$$\frac{(Kx - IM) - 2R \sqrt{I^2 + K^2}}{IL - JK}$$

and

$$\frac{(Kx - IM) + 2R \sqrt{L^2 + K^2}}{IL - JK}$$

The additional stipulation on H is that it be positive. This means that the turning aircraft is turning back towards its assigned route rather than away from it. This is the range of H values for which (B-14) is satisfied by real values of t_d . As an example of three different conditions consider Figure B-7. Given the radius of the aircraft (R), the initial alongtrack spacing (x), and the initial crosstrack closing speed (\dot{y}), a "crescent-shaped" region in t_d - ω space can be constructed. The region inside the crescent are those t_d, ω combinations (given R, x, and \dot{y}) for which the aircraft pair start on the conflict region boundary and end in a horizontal overlap condition.

To compute the probability of being within a crescent shaped region in Figure B-7 one would really have to ask for the probability of also being within Δx of x and $\Delta \dot{y}$ of \dot{y} . To approach this problem numerically we will divide up the range of \dot{y} and the range of x into small cells. For instance, consider Figure B-8. Here we have a cell which is 1 nmi in x and 10 knots in \dot{y} . If we were to select those x, \dot{y} combinations shown by the x's in Figure B-8, we could construct a t_d - ω crescent region for each. The result of doing this for P=1 and $V_{y1}=+200$ kts is shown in Figure B-9. On the scale shown in Figure B-9, the crescent regions are lines.

If other values of P between 0 and 1 and other values of V_{y1} are used, Figure B-9 is expanded to get a region in t_d - ω space such as the one shown in Figure B-10. This figure was calculated for P=0, 1/2, and 1, and for five different values of V_{y1} and V_{y2} which could result in \dot{y} . The dots represent the length and width of each crescent shaped region.

The dots in the upper left hand corner of Figure B-10 are those which correspond to the minimum time delay necessary for the centers of the aircraft to overlap when no turn is executed. One way in which these points can be identified is by performing a grid search over various values of crosstrack closing speed (\dot{y}), alongtrack separation (x), and crosstrack speed partition between the two aircraft (F, to be defined below).

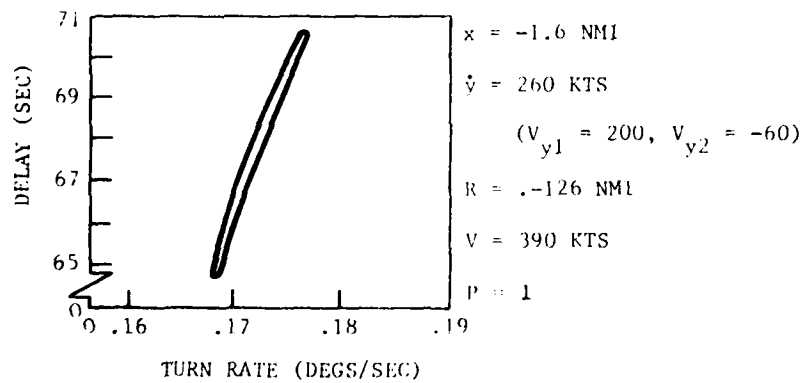
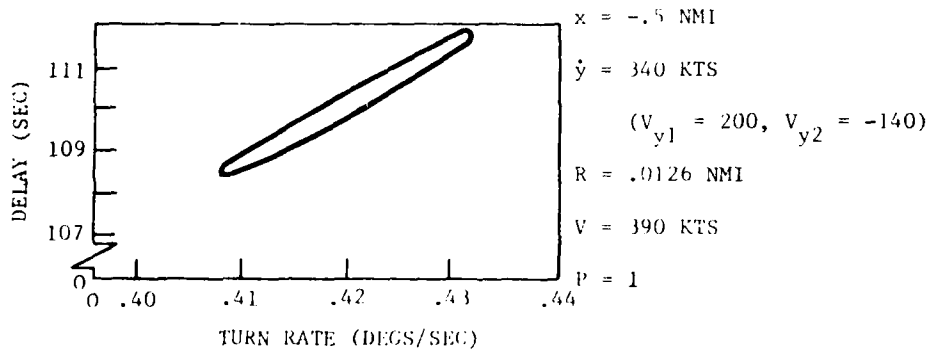
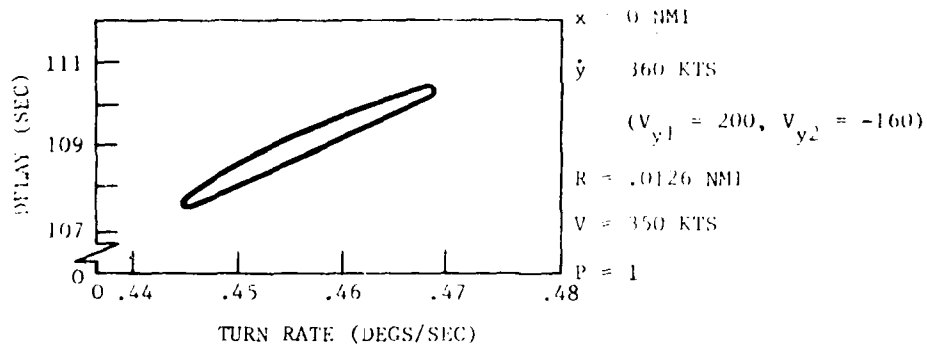


**FIGURE B-7
REGIONS WHERE AIRCRAFT WILL OVERLAP**

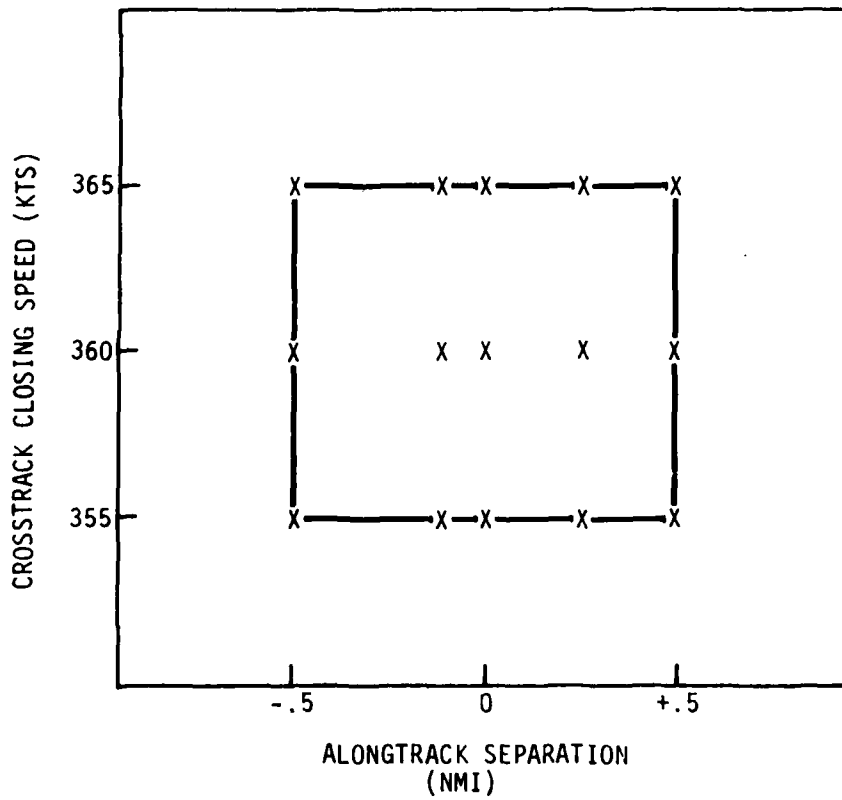


**FIGURE B-8
SELECTED COMBINATIONS OF ALONGTRACK
SEPARATION AND CROSSTRACK CLOSING SPEEDS**

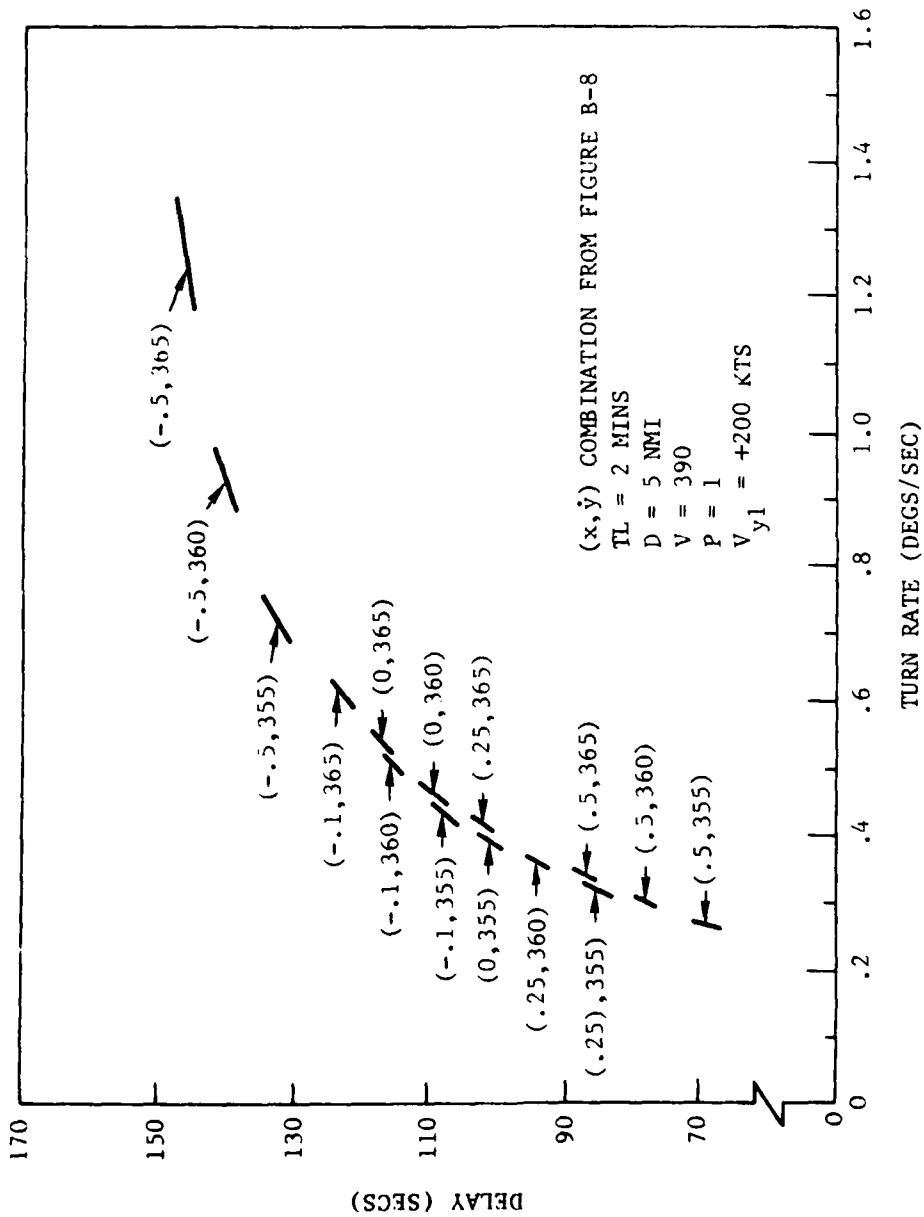


FIGURE B-9
OVERLAP REGIONS FOR VARIOUS COMBINATIONS OF
ALONGTRACK SEPARATION, CROSSTRACK CLOSING SPEED

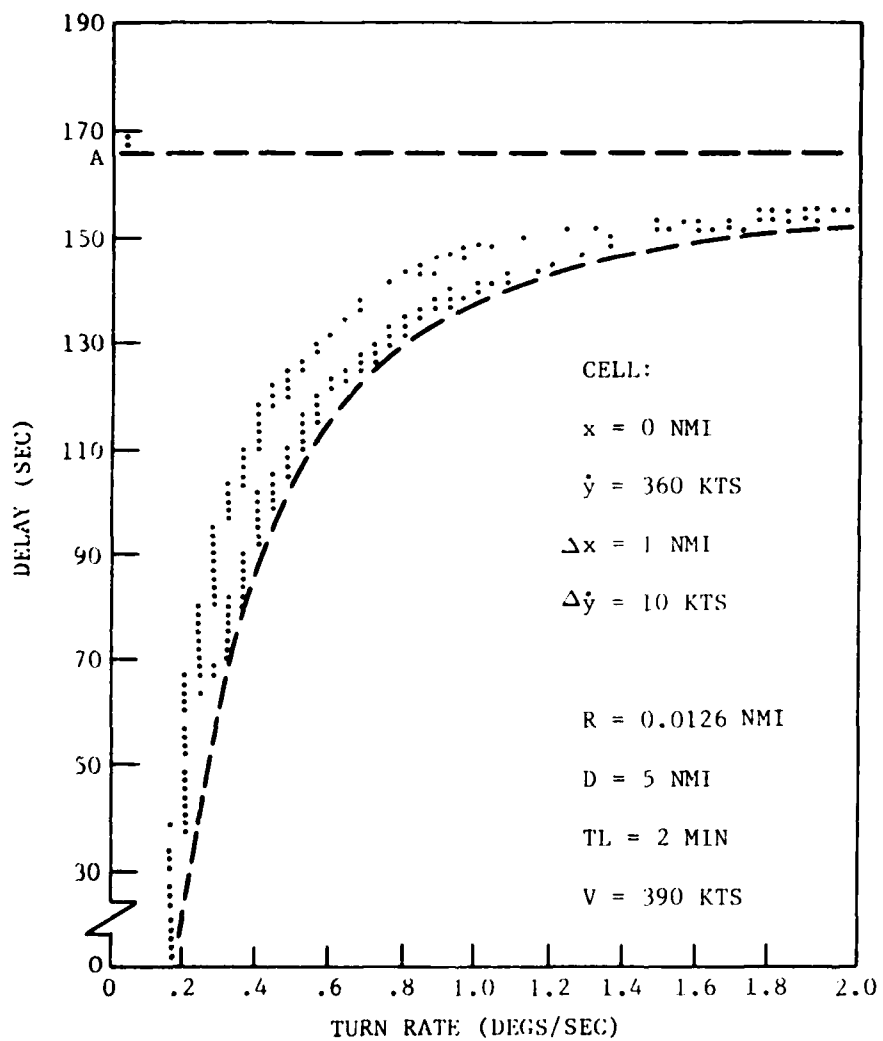


FIGURE B-10
THE ENVELOPE OF HORIZONTAL OVERLAP
REGIONS FOR A GIVEN CELL ON THE
CONFLICT REGION BOUNDARY

It could be that a particular x, \dot{y} cell does not have any "straight line" overlaps. The problem is to determine the existence of such straight line overlaps within an x, \dot{y} cell and if there are such points then find the one with the minimum time delay from the transgression of the conflict region boundary to overlap.

This problem is a nonlinear programming problem with equality and inequality constraints. The problem can be structured as:

$$\text{minimize } t_d = TL + \frac{\sqrt{D^2 - x^2}}{\dot{y}} \quad (\text{B-18})$$

subject to:

$$F-1 \leq 0$$

$$\frac{\dot{y}}{V_m} - 1 - F \leq 0$$

$$\dot{y} - \dot{y}_1 \leq 0$$

$$\dot{y}_2 - \dot{y} \leq 0$$

$$x - x_1 \leq 0$$

$$x_2 - x \leq 0$$

$$(1+B^2)x^2 - 2TL\dot{y}Bx + TL^2\dot{y}^2B^2 - D^2B^2 = 0 \quad (\text{B-19})$$

where

$$B = \frac{\sqrt{v^2 - F^2V_m^2} - \sqrt{v^2 - (FV_m - \dot{y})^2}}{\dot{y}}$$

TL = look ahead time

D = Minimum radar separation

V_m = Maximum observed crosstrack velocity (single aircraft)

x_1, x_2 = limits on x

\dot{y}_1, \dot{y}_2 = limits on \dot{y}

The object is to find x , \dot{y} , and F such that the above conditions are satisfied. Since the general solution is difficult we will investigate the existence of straight line overlaps by considering equation (B-19). This equation sets the condition that the aircraft overlap. Solving this equation for x gives:

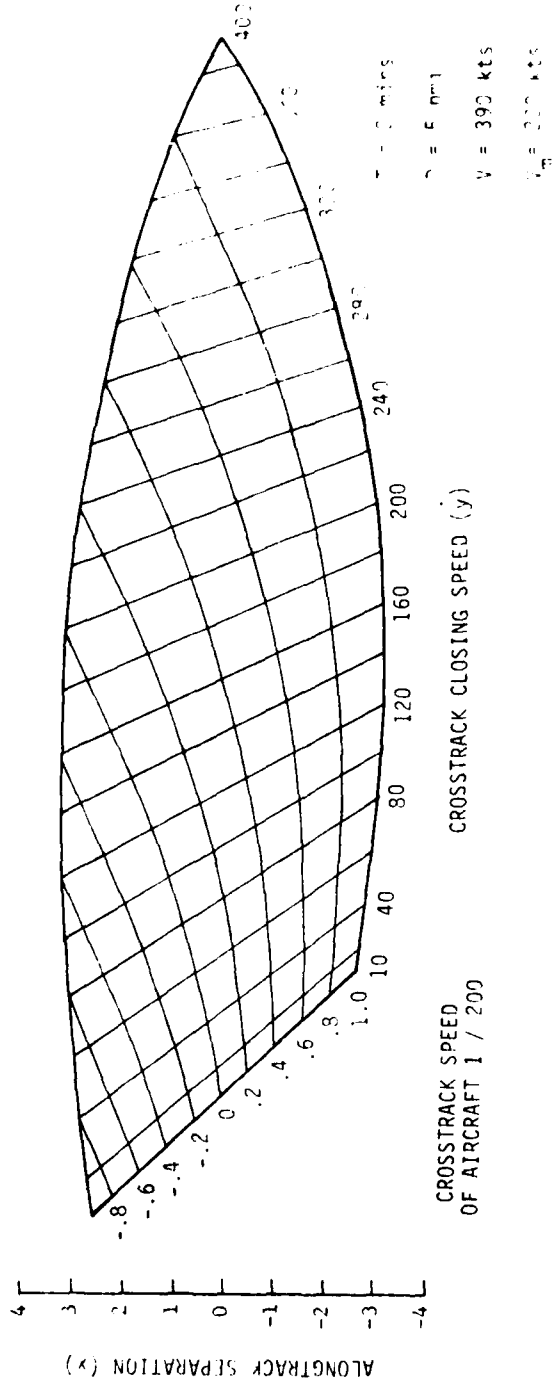
$$x = \frac{TL \dot{y} B + \sqrt{D(1+B)^2 - B^2 TL^2 \dot{y}^2}}{1+B^2} \quad (B-20)$$

If x is substituted back into the expression from which equation (B-19) was derived, it is found that the only applicable root for x is the one with the "+" sign in equation (B-10). The values of x for the spectrum of F and \dot{y} values are shown in Figure B-11. From this figure one can see that for cells with $|x| > 3.5$ nmi there are no straight line overlaps -- aircraft are too far apart from each other in the alongtrack direction for there to be an overlap. Once the existence of a straight line overlap is determined for a particular x , \dot{y} cell, the problem is to find the combination of values of x , \dot{y} , and F which minimize t_d given in equation (B-19). A close approximation to the minimum value of t_d is to choose the maximum value of \dot{y} in the cell and then choose the maximum feasible value of x given that \dot{y} . This then is how the point labeled "A" in Figure B-10 is determined.

For any time delay greater than A for this x , \dot{y} cell, the assumption is made that the aircraft pair will overlap before starting an avoidance maneuver. For time delays from A down to where the pattern of dots ends, one would say that there was horizontal overlap for those time delays at the particular turn rate. To describe this region an envelope of the lower boundary of the pattern of dots was approximated by a function of the form:

$$t_d = A - C/\omega. \quad (B-21)$$

The curved dashed lines in Figure B-10 show the envelope fit to the dots. When the dots in the upper left hand corner (straight line overlaps) are present, the A value in (B-21) (which is the asymptote of equation (B-21)) is set to the minimum upper left hand dot. The envelope curves are then least square fit to the minimum dot at each value of ω .



B-23

FIGURE B-11
STRAIGHT LINE OVERLAP REGION

The meaning of Figure B-10 is depicted in Figure B-12. For any delay time greater than A, the aircraft pair having a cross-track closing speed and an along-track separation which places it in the cell in Figure B-8 is assumed to overlap while still flying straight. For delay times less than A, the turn rate will determine whether the pair will overlap. Therefore, the shaded region in Figure B-12 represents those values of t_d and ω for which aircraft pairs will overlap given that the aircraft pair was initially on the conflict region boundary within the specified ranges of x and \dot{y} .

It should be mentioned at this point that for a given cell in x and \dot{y} , the horizontal overlap region in t_d and ω does not always have the form shown in Figure B-12. Although Figure B-12 is the most common form there are three other forms as shown in Figure B-13. Figure B-13a shows the case where the minimum time delay is for the straight line collision only. Thus, regardless of the value of ω , the aircraft pair will overlap for time delays longer than A. That is, for any turn, as long as the delay is less than A, the horizontal overlap will be avoided.

For a given range of x and \dot{y} values it is easy to check the existence of a straight line overlap. It may turn out that there are no straight line overlaps possible within the given range of x and \dot{y} . In this situation there can be two forms of the t_d , horizontal overlap region as shown in Figures B-13b and B-13c. In Figure B-13b the envelope of the overlap region has the same functional form as the region in Figure B-12, namely that of equation B-21. But since no straight line collisions are possible, equation (B-21) is fit finding the value of A via least squares fitting of (B-21) to the maximum and minimum points (at each ω) in the region.

The second case where no straight line overlaps are possible is shown in Figure B-13c. In this case there is apparently no asymptotic behavior to the horizontal overlap region. Hence, equation (B-21) does not hold. In this case the envelope of the overlap region was fit to the functional form

$$t_d = C \ln \omega + A. \quad (B-22)$$

The lower boundary of the horizontal overlap region was found by least squares fitting the minimum values of t_d for each ω . Using the same value for C, the upper boundary was found by a least square fit on the maximum values at each ω . The same value of C was used for the upper and lower boundaries so that the upper and lower boundaries would not cross.

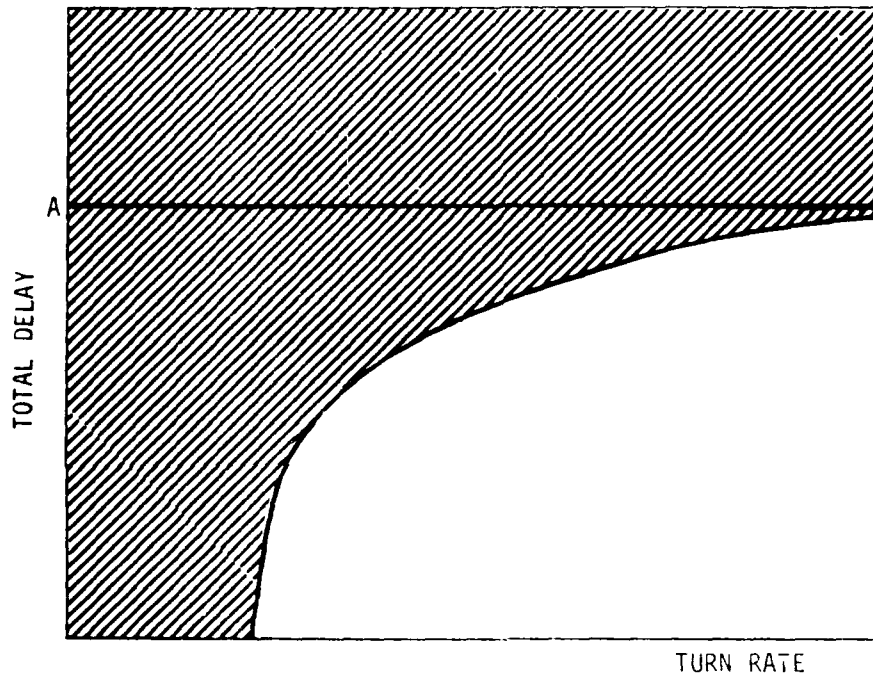
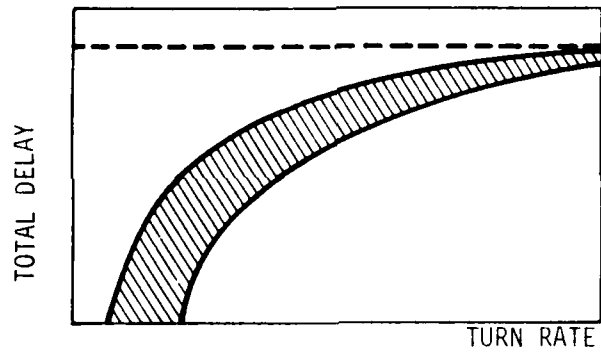


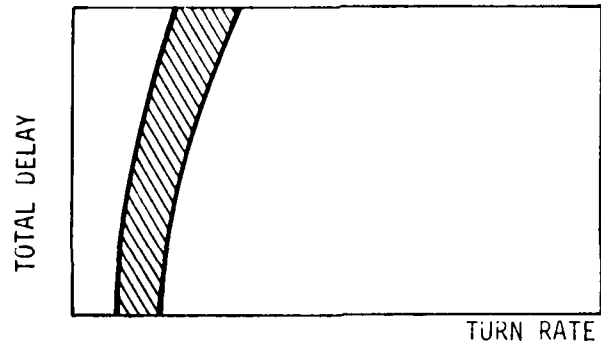
FIGURE B-12
GENERAL FORM OF HORIZONTAL OVERLAP REGION



a



b



c

FIGURE B-13
VARIATIONS ON THE FORM OF THE HORIZONTAL
OVERLAP REGION

B5. COMPUTATION OF THE PROBABILITY OF HORIZONTAL OVERLAP

We now have all the elements necessary to compute the probability of horizontal overlap. If an aircraft pair is initially on the conflict region boundary and has a specific time delay followed by a specific turn rate then there will be overlap in the horizontal plane. If being on the conflict region boundary is independent of the time delay and the choice of the turn rate, and the choice of the turn rate is independent of the time delay, then the probability of horizontal overlap basically will be the probability of being on the conflict region boundary times the probability of having a particular set of delay times and turn rates.

The conflict region boundary discussed in Appendix A is a surface in the three dimensional space x , y , and \dot{y} as shown in Figure B-14. To estimate the probability of being on this surface, the surface is enclosed with I cells of width Δx , $\Delta \dot{y}$ and Δy_i , centered at the points x_i , y_i , and \dot{y}_i for $i=1, \dots, I$. The probability of being on the conflict boundary is given by

$$\begin{aligned} P[\text{CB}] &= \sum_{i=1}^I P[\text{CB}_i] \\ &= \sum_{i=1}^I P\left[|x - x_i| < \Delta x/2, |y - y_i| < \Delta y_i/2, |\dot{y} - \dot{y}_i| < \Delta \dot{y}/2\right] \end{aligned} \quad (\text{B-23})$$

As discussed previously in this appendix, the horizontal overlap regions (associated with the conflict boundary) were defined in terms of cells in the x , \dot{y} plane, centered at the points x_i , and \dot{y}_i , and of fixed width Δx and $\Delta \dot{y}$. Given these fixed values for each i , there is a unique value of y (y_i), and a unique value of Δy (Δy_i) which will enclose the conflict surface. These values are derived from the definition of the conflict region given in equation (A-5).

We now turn over attention to evaluating

$$P[\text{CB}_i] = P\left[|x - x_i| < \Delta x/2, |y - y_i| < \Delta y_i/2, |\dot{y} - \dot{y}_i| < \Delta \dot{y}/2\right] \quad (\text{B-24})$$

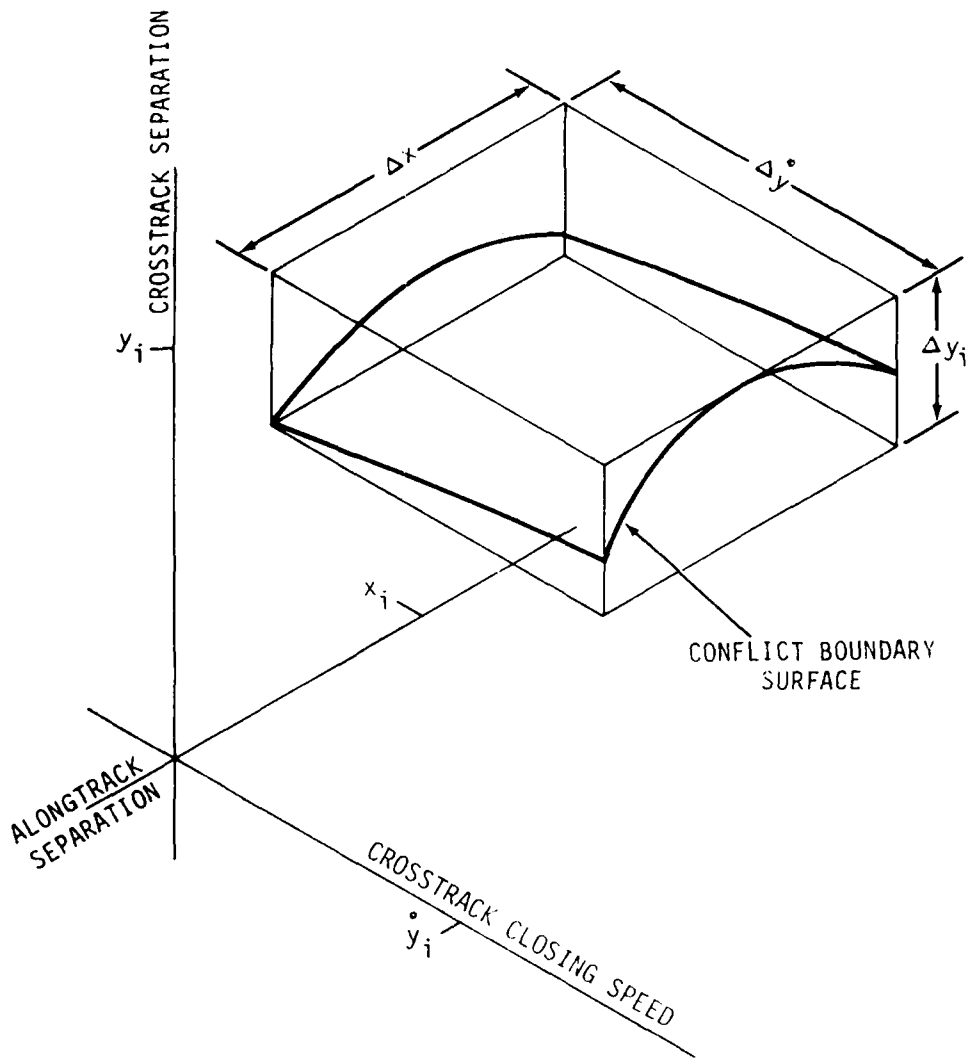


**FIGURE B-14
CONFLICT BOUNDARY SURFACE**

for any i . Now, the aircraft enter their respective routes independently. Therefore, an aircraft pair's alongtrack separation (before a controller intervention) will be independent of the pair's crosstrack separation and crosstrack closing speed. Thus (B-24) can be rewritten as

$$P[CB_i] = P[|x - x_i| < \Delta x / 2] * P[|y - y_i| < \Delta y_i / 2, |\dot{y} - \dot{y}_i| < \Delta \dot{y} / 2] \quad (B-25)$$

The probability of x (the alongtrack separation) being in the range $x_i - \Delta x / 2$ to $x_i + \Delta x / 2$ will depend on the traffic loading on each route. The estimation of this probability is discussed in Appendix E. As shown in that appendix this probability is constant over the ranges of x under consideration (i.e., aircraft pairs separated alongtrack by less than 5 nmi). The probability is denoted as $P_{\Delta x}$ and will depend on the traffic loading and the cell size Δx , but not the position of the cell, x_i . Thus (B-25) can again be rewritten as

$$P[CB_i] = P_{\Delta x} * P(y_i, \Delta y_i, \dot{y}_i, \Delta \dot{y}) \quad (B-26)$$

where

$$P(y_i, \Delta y_i, \dot{y}_i, \Delta \dot{y}) = P[|y - y_i| < \Delta y_i / 2, |\dot{y} - \dot{y}_i| < \Delta \dot{y} / 2]$$

The probability $P(y_i, \Delta y_i, \dot{y}_i, \Delta \dot{y})$ in (B-26) is the joint probability that the aircraft pair has a crosstrack separation in the i th cell and has a crosstrack closing speed in i th cell. This joint probability can be estimated from the data collected by the FAA.⁽⁴⁾ Since the data was gathered on individual aircraft, a convolution of the data is required to generate a bivariate histogram of crosstrack separation and crosstrack closing speed. Appendix F discusses the procedure used to construct the bivariate histogram.

For each cell as shown in Figure B-14 there will be a horizontal overlap region in $t_d - \omega$ space. Such a horizontal overlap region is shown in Figure B-15. From sections B2.3 and B3.0 of this appendix we have a histogram of delay time and a histogram of turn rate. These histograms are shown along their respective axes in Figure B-15. Assume that there are m cells in the delay

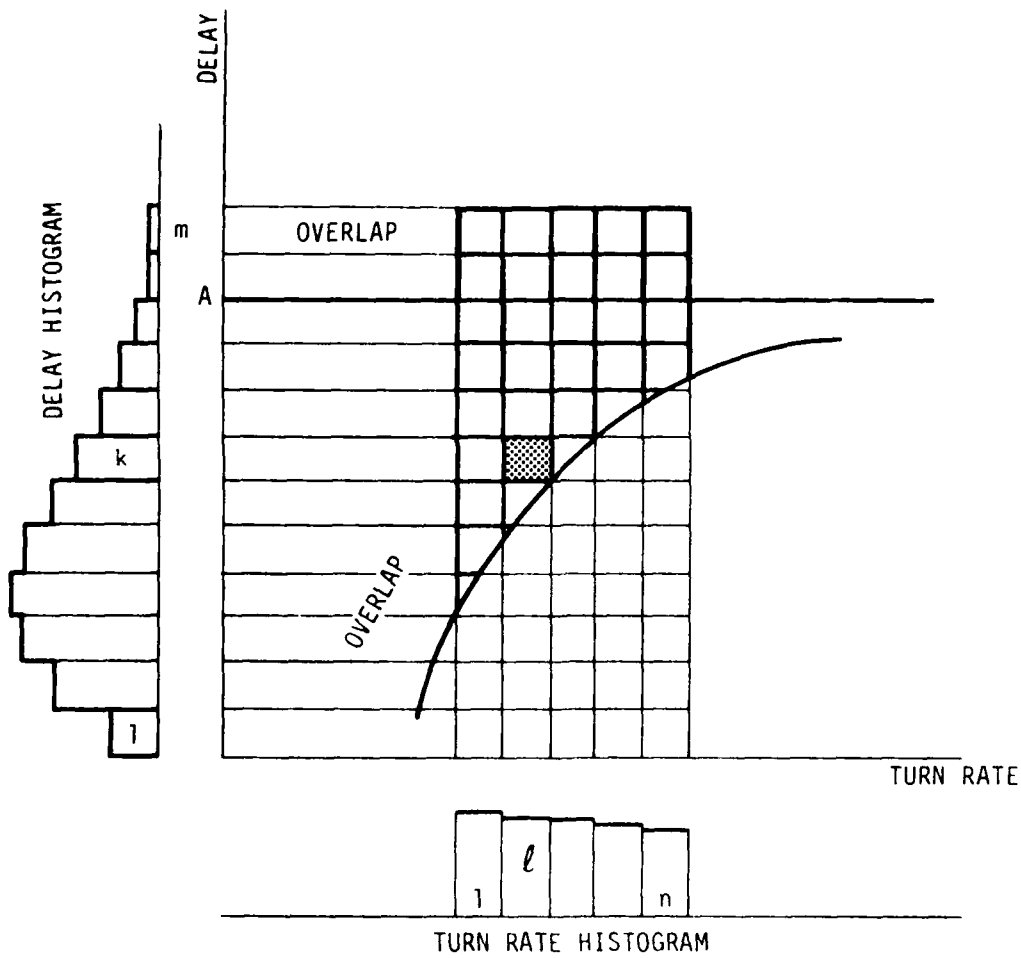


FIGURE B-15
HORIZONTAL OVERLAP REGION
FOR CONFLICT BOUNDARY CELL i

histogram and n cells in the turn rate histogram. Consider the k th cell in the delay histogram and the ℓ th cell in the turn rate histogram. As shown in Figure B-15 this combination of the k th delay and the ℓ th turn rate is in the horizontal overlap region. Let us define the quantity $r_{k\ell i}$ with the following property:

$0 \leq r_{k\ell i} \leq 1$ and is in the same proportion that the k th cell is enclosed within the horizontal overlap region corresponding to the i th conflict region boundary cell.

Let us also define the probability that time delay has a value in the k th cell as P_{ki} and the probability that the turn rate has a value in the ℓ th cell as P_{ℓ} . It should be noted that both $r_{k\ell i}$ and P_{ki} depend on i , the conflict region boundary cell. The values of $r_{k\ell i}$ will obviously depend on the location of the aircraft pair on the conflict region boundary because there is a different horizontal overlap region for each position on the conflict region boundary. The delay time histogram will also depend on the position on the conflict region boundary because the delay due to detection of the potential conflict will depend on the crosstrack closing speed of the aircraft pair.

We can now write down the probability that an aircraft pair will be in horizontal overlap. That probability is

$$P_H = P_{\Delta x} \sum_{i=1}^I P(y_i, \Delta y_i, \dot{y}_i, \Delta \dot{y}) \sum_{\ell=1}^n \sum_{k=1}^m r_{k\ell i} P_{ki} P_{\ell} \quad (B-27)$$

All of the terms in this expression are computable based on the analyses in this appendix and Appendices C, D, E, and F.

APPENDIX C

PROBABILITY OF OBSERVING AN AIRCRAFT PAIR WITHIN THE CONFLICT REGION

C1. INTRODUCTION

This appendix addresses the applicable conflict region, the tracker errors, and the computation of the probability of being detected in the conflict region.

Consider an aircraft pair separated by a crosstrack distance y and closing with a crosstrack speed \dot{y} . What is the probability that the aircraft pair is detected to be in potential conflict based on the information from one radar scan? The probability of observing an aircraft pair as being in potential conflict depends on two factors--the radar/tracker performance and the conflict region. Tracker performance is based on the propagation of the surveillance errors through the tracker. In our model it is assumed that the the crosstrack closing speed and the crosstrack separation error distribution is a bivariate normal with zero mean.

C2. THE CONFLICT REGION

As defined in Appendix A, the conflict region is that region in the crosstrack closing speed - crosstrack separation space where an aircraft pair, if projected ahead along a straight path for 2 minutes, will come within 5 nmi of each other. The shape of that region for the true crosstrack separation and crosstrack closing speed is shown as the solid line in Figure C-1.

In Section C4, we will discuss estimating the probability that an aircraft pair is observed inside the conflict region given that the pair is truly inside the conflict region. In that estimation process we will integrate a bivariate normal distribution over a polygon. Thus, we have limited the extent of the conflict region by considering the maximum crosstrack closing speed to be $10V_{y\max}$. If the maximum crosstrack closing speed based on data is $2V_{y\max}$, then the choice of $10V_{y\max}$ should be ample to include the errors introduced by radar and tracker which would indicate that the aircraft pair is in potential conflict.

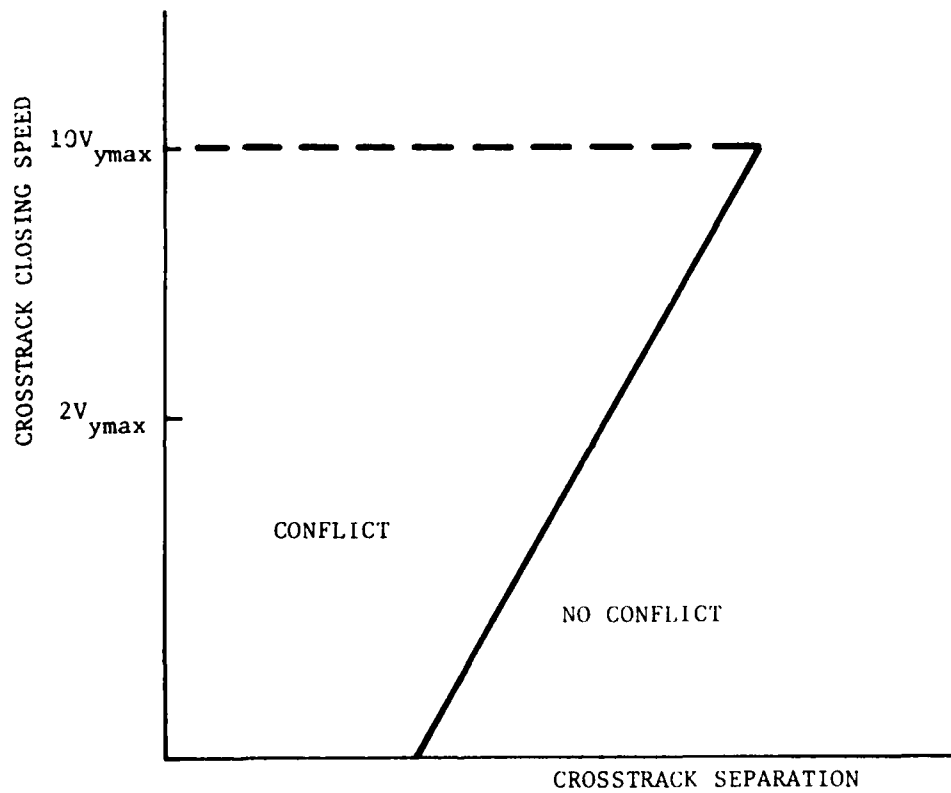


**FIGURE C-1
THE CONFLICT REGION**

C3. THE TRACKER PERFORMANCE

The performance of the tracker is characterized by errors in the crosstrack separation and crosstrack closing speed. These errors are assumed to be correlated and normally distributed. The manner in which the parameters of the bivariate normal were estimated was through a simulation of the NAS tracker.

C3.1 The Tracker Simulation

The simulation was constructed to represent the performance of the NAS tracker for discrete targets from a single radar. The exact scenario which was run was idealized for ease of traffic generation but at the same time would show the performance of the tracker to be worse than one would expect from a typical pair of aircraft flying the routes.

The simulation consisted of flying a pair of aircraft on a set of parallel routes. The radar which observed these aircraft was situated between and at one end of the routes. Since the radar errors in azimuth are greater than the radar errors in distance, this orientation of the radar to the routes is the worst for estimating the crosstrack positions and crosstrack velocities of the aircraft. This is another conservative aspect of this model.

Since the spatial relationship of the aircraft to the radar is important, the aircraft were placed on their respective routes in alongtrack proximity to each other. Alongtrack proximity is defined as being within an alongtrack distance for which a potential conflict is possible. (In the case of the conflict region being used this means that the aircraft has to be separated alongtrack (interoute) by less than 5 nmi.) Thus, once the first aircraft was placed on its route, the second aircraft was placed randomly on its route within alongtrack proximity of the first aircraft.

The tracks of the aircraft were idealized to sinusoids. When an aircraft flies with turns (such as a sinusoidal pattern) the tracker will lag the aircraft through the turns. Therefore, it is important that the sinusoids of the two aircraft not always be in the same synchronization or the results will be biased. The basic assumption is that the navigation on the two routes is independent. A particular synchronization of the sinusoids for each replication of the simulation would definitely invalidate the assumption of independence. Therefore, for each replication the initial heading of each aircraft was randomly chosen from among those headings possible for the specified sinusoid.

C3.2 The NAS Tracker

The NAS tracker is a bimodal alpha-beta tracker. The equations which describe the tracker are as follows:

$$\begin{aligned}X_{sn} &= X_{p(n-1)} + \alpha (X_{rn} - X_{p(n-1)}) \\Y_{sn} &= Y_{p(n-1)} + \alpha (Y_{rn} - Y_{p(n-1)}) \\V_{xn} &= V_{x(n-1)} + \beta (X_{rn} - X_{p(n-1)})/t \\V_{yn} &= V_{y(n-1)} + \beta (Y_{rn} - Y_{p(n-1)})/t \\X_{pn} &= X_{sn} + V_{xn}t \\Y_{rn} &= Y_{sn} + V_{ynt}\end{aligned}\tag{C-1}$$

where

X_{sn}, Y_{sn} = X,Y position estimates for scan n

X_{pn}, Y_{pn} = X,Y predicted position estimates made at scan n for the position at scan n+1

X_{rn}, Y_{rn} = X,Y reported positions from the surveillance system at scan n

V_{xn}, V_{yn} = X,Y velocity estimates for scan n

α = tracker position gain

β = tracker velocity gain

The bimodal aspect of the tracker comes into play through the choice of the parameters α and β . If the predicted position from the previous scan is within a circle of a given radius of the reported position, then it is assumed that the aircraft is flying straight and the appropriate α and β are used. If, however, the predicted position is outside the circle but within a circle of larger radius, then there is a possibility that the aircraft is making a turn and another α and β are chosen. If the predicted position is outside the larger circle, the return is no longer associated with the track and the track goes into the coast mode. In the coast mode the track is extrapolated to the next radar update time using the last predicted position and the last estimated velocity. After the track coasts for several consecutive scans, the track is dropped. The values for α and β are given in Table C-1.

TABLE C-1
NAS TRACKER PARAMETERS

	SMALL SEARCH AREA (1 NMI RADIUS)	LARGE SEARCH AREA (6 NMI RADIUS)
α	.3125	1.0
β	.046875	.15625

C3.3 Simulation Results

The statistics of interest are the mean, standard deviation and correlation coefficient of the crosstrack separation and crosstrack closing speed errors. Since we are interested in the separation/closing speed errors on a per update basis, the averages and standard deviations are taken over all the individual updates for all replications. This procedure will give larger standard deviations than if, for instance, we had taken the mean separation and closing speed errors of each replication and then found the standard deviation of these means. The manner in which the means and standard deviations were computed is, therefore, more appropriate to the use of the statistics.

The beacon radar was assumed to have a range quantization of 0.125 nmi and an avionics bias error of .7 μ sec (.113 nmi). The one sigma azimuthal error of the beacon was assumed to be .26 degrees. If these errors are assumed to have a fixed value, then the important parameters in this simulation are the period and amplitude of the sinusoid pattern that the aircraft fly. Table C-2 shows the variation in the crosstrack separation and crosstrack closing speed errors for three different period/amplitude combinations. The data that was taken in the Cleveland ARTCC has shown that it is not unusual for aircraft to wander 4 nmi off their assigned route centerline. The tracks also oscillated about the route centerline and, while the tracks were not truly sinusoidal, they appear to have periods approaching 100 nmi. A reasonable range of values for the tracker performance would be a crosstrack separation error standard deviation between .45 and .70 nmi, a crosstrack closing speed error standard deviation between 50 and 160 kts, and a correlation coefficient of -0.8. For the risk analysis reported in volume I of this report a value of .7 nmi was used for the one sigma value of the crosstrack separation error, 160 kts was used for the one sigma value of the crosstrack closing speed error, and -.8 was used for the correlation coefficient.

The histograms of the marginal distribution of crosstrack separation and crosstrack closing speed errors are shown in Figures C-2 and C-3, respectively for the case of a period of 60 nmi and an amplitude of 4 nmi, also shown in these figures are the normal distribution fits to the simulation results. As one can see from Figure C-2 the normal assumption is quite good for the crosstrack separation error distribution. The crosstrack closing speed errors are unimodal and symmetrically distributed (see Figure C-3). However, this error distribution is not fit very well by a normal curve. The bulges in the histogram between 150 and 300 kts are probably due to the fact that the aircraft are flying a sinusoidal pattern.

TABLE C-2
 NAS TRACKER SIMULATION RESULTS

PERIOD (NMI)	AMP (NMI)	CROSSTRACK SEPARATION ERRORS		CROSSTRACK CLOSING SPEED ERRORS		CORRELATION COEFFICIENT
		BIAS (NMI)	STD DEV (NMI)	EIAS (KTS)	STD DEV (KTS)	
---	0	-.006	.11	.09	4.5	-.77
120	4	-.009	.45	.3	53.1	-.95
60	4	.010	.70	-1.1	161.5	-.83

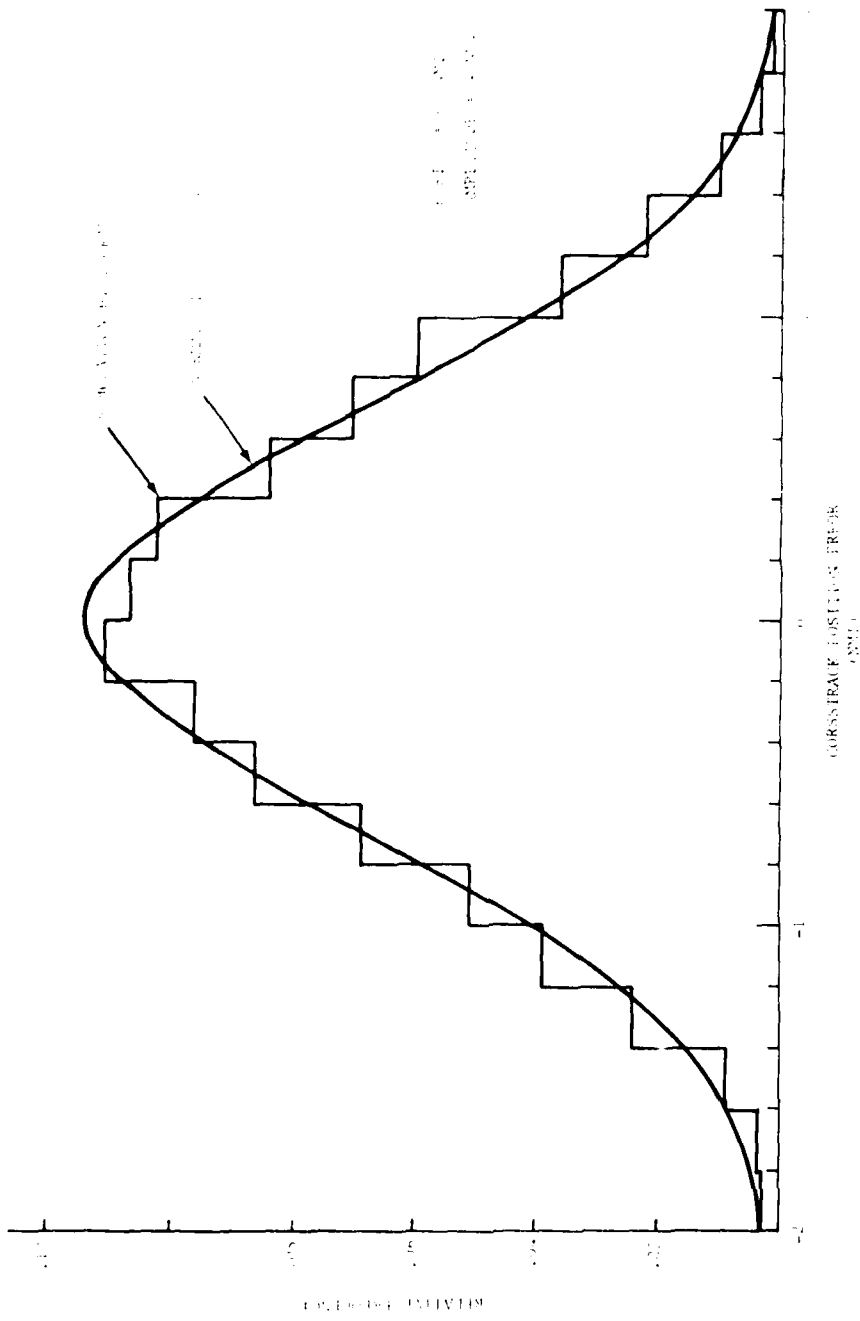


FIGURE C-2
MARGINAL DISTRIBUTION OF POSITION ERROR

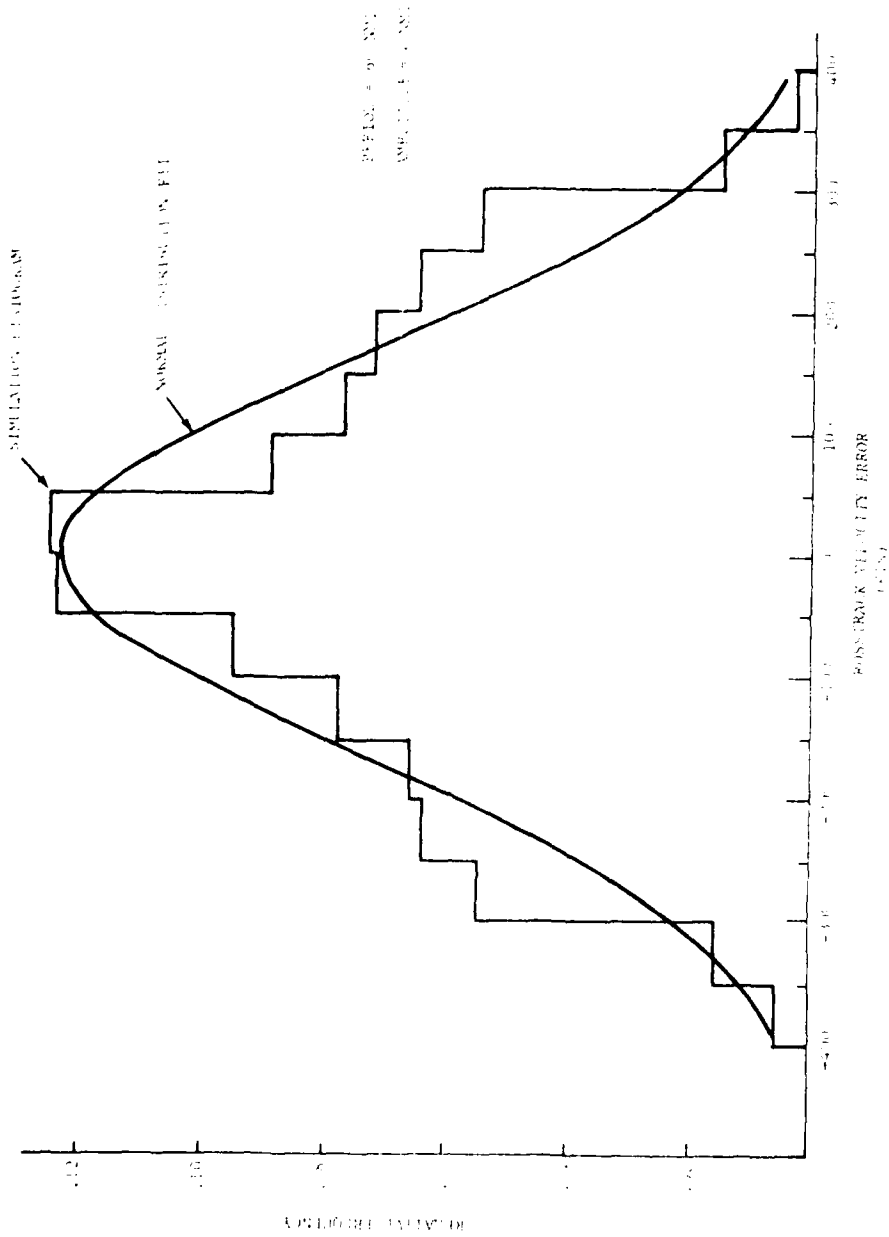


FIGURE C-3
MARGINAL DISTRIBUTION OF VELOCITY ERROR

C4. INTEGRATION OF A BIVARIATE NORMAL DISTRIBUTION OVER A POLYGON

The problem of computing the probability of observing an aircraft pair within the conflict has been reduced to finding the volume under a bivariate normal distribution over a polygon. To illustrate this, consider Figure C-4. The polygon defined by the points A', B', C', and D' is the conflict region discussed above. Let an aircraft pair have a crosstrack separation of μ_y and a crosstrack closing speed of $\mu_{\dot{y}}$ as shown in Figure C-4. The output of the tracker will have errors which are assumed to be distributed normally in crosstrack separation and crosstrack closing speed. The ellipses shown in Figure C-4 represent constant probability lines from the bivariate normal distribution of errors of the tracker.

If the polygon in Figure C-4 is denoted as B, the probability of observing the aircraft pair in that polygon given that the pair is at μ_y and $\mu_{\dot{y}}$ is

$$\frac{1}{2\pi\sigma_y\sigma_{\dot{y}}\sqrt{1-\rho^2}} \iint_B \exp \left[-\frac{1}{2(1-\rho^2)} \left\{ \left(\frac{y-\mu_y}{\sigma_y} \right)^2 - 2\rho \left(\frac{y-\mu_y}{\sigma_y} \right) \left(\frac{\dot{y}-\mu_{\dot{y}}}{\sigma_{\dot{y}}} \right) + \left(\frac{\dot{y}-\mu_{\dot{y}}}{\sigma_{\dot{y}}} \right)^2 \right\} \right] d y d \dot{y} \quad (C-2)$$

where σ_y is the standard deviation of the tracker's crosstrack separation error and $\sigma_{\dot{y}}$ is the standard deviation of the tracker's crosstrack closing speed error. The quantity ρ is the correlation coefficient between the errors in the crosstrack closing speed and the crosstrack separation.

The first step in computing the integral (C-2) is to transform the y and \dot{y} axes using the following transformation:

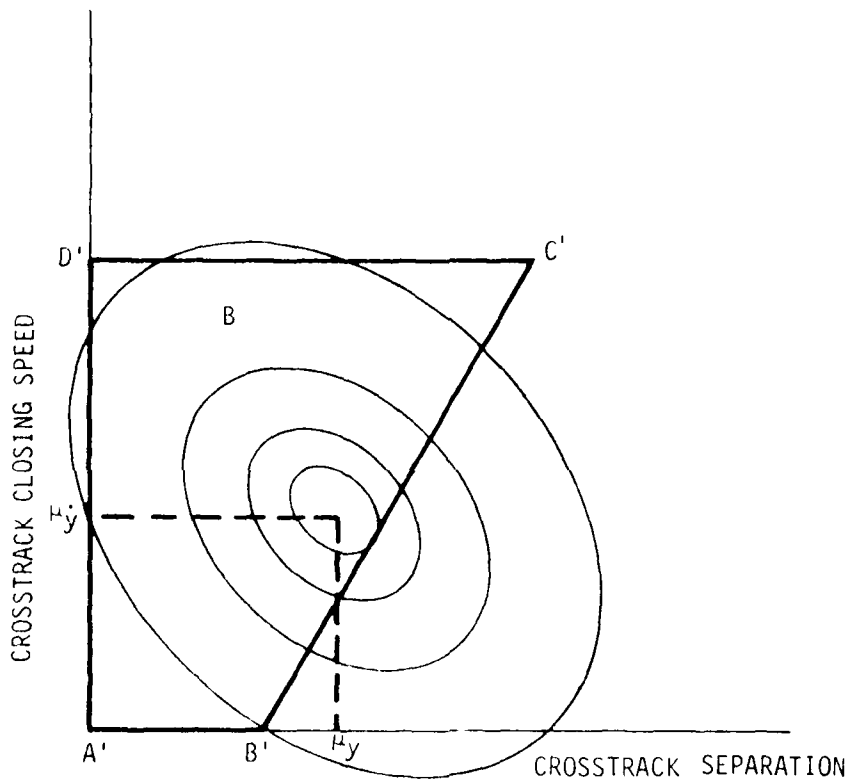


FIGURE C-4
 TRACKER OUTPUT ERRORS SUPERIMPOSED
 ON THE CONFLICT REGION

$$u = \frac{1}{\sqrt{2-2\rho}} \left(\frac{y-\mu_y}{\sigma_y} + \frac{\dot{y}-\mu_{\dot{y}}}{\sigma_{\dot{y}}} \right) \quad (C-3)$$

$$v = \frac{-1}{\sqrt{2-2\rho}} \left(\frac{y-\mu_y}{\sigma_y} - \frac{\dot{y}-\mu_{\dot{y}}}{\sigma_{\dot{y}}} \right)$$

where

$$\rho \neq 1$$

Making this transformation circularizes the bivariate normal probability density function under the integral in (C-2). This makes the correlation between the random variables u and v equal to zero. Another important feature of this transformation is that straight lines are mapped into straight lines and convex polygons are mapped into convex polygons. Schematically, Figure C-5 shows the result of mapping the polygon B in y, \dot{y} space into u, v space.

Since a polygon can always be defined by a set of triangles, we will compute the probability over the polygon by accounting for the probability over a set of triangles that define the polygon. Therefore, consider a triangular area in u, v space as shown by the triangle $OA'B'$ in the Figure C-6a/b. The probability of being within that triangle can be computed by standard methods. Let the point S be on the line connecting A' and B' , such that SO is perpendicular to the line A', B' . If the point S lies between B' and A' , as shown in Figure C-6a then the probability of being within the shaded triangle is

$$V(h, k_1) + V(h, k_2) \quad (C-4)$$

where

h is the distance from the origin to point S ,

k_1 is the distance from point S to point B' ,

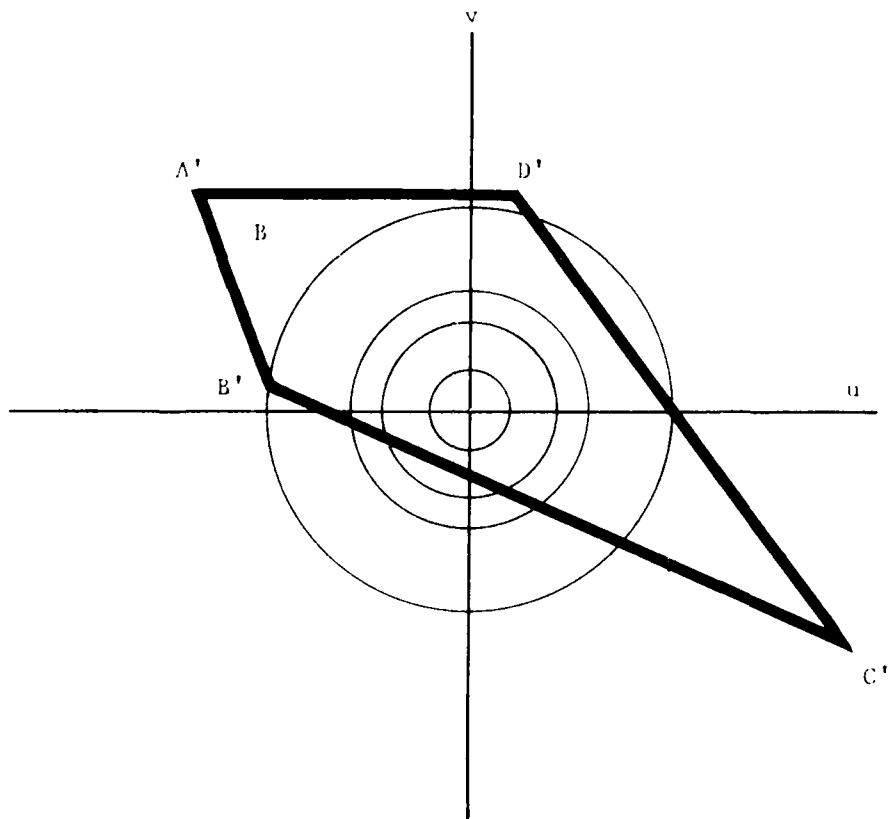
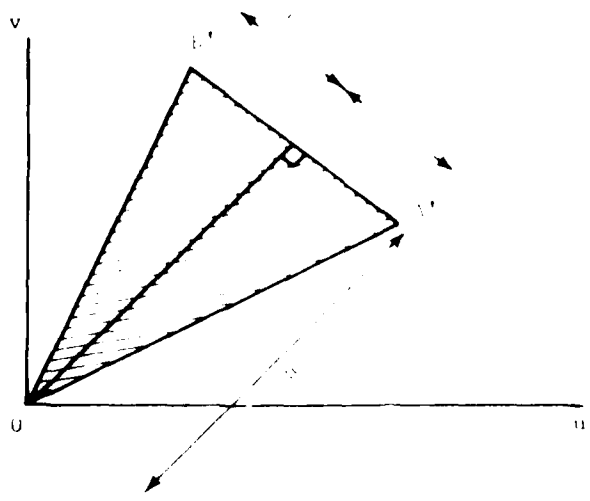
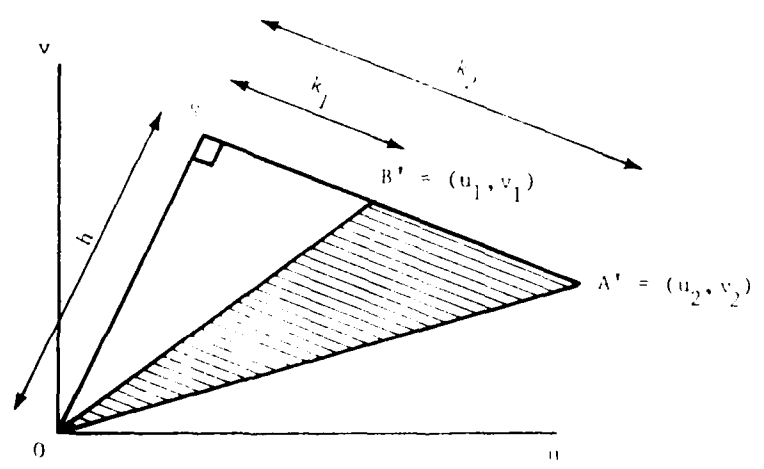


FIGURE C-5
THE TRANSFORMED TRACKER OUTPUT ERRORS AND CONFLICT REGION



a



b

FIGURE C-6
 GEOMETRY FOR INTEGRATION OVER A TRIANGULAR REGION IN $u-v$ SPACE

k_2 is the distance from point S to point A', and the function V will be defined below.

If the point S does not lie between B' and A', as shown in Figure C-6b, then the probability is given by

$$V(h, k_2) - V(h, k_1) \quad (C-5)$$

where $k_2 > k_1$

As derived in Reference (3), the function V can be written in a Taylor expansion:

$$V(h, k) = (\pi)^{-1} \left[\lambda (1 - e^{-a}) - \frac{1}{3} \lambda^3 (1 - e^{-3a} - 3ae^{-a}) + \frac{1}{5} \lambda^5 (1 - e^{-5a} - 5ae^{-a} - \frac{15}{2} a^2 e^{-a}) - \dots \right] \quad (C-6)$$

where $\lambda = k/h < 1$, $a = 1/2h^2$ and $h > 0$ and $k > 0$. If $\lambda > 1$, then equation (C-7) can be used in conjunction with (C-6):

$$V(h, k) + V(k, h) = (\Phi(h) - 1/2) (\Phi(k) - 1/2) \quad (C-7)$$

where

$$\Phi(h) = (\sqrt{2\pi})^{-1} \int_{-\infty}^h \exp(-t^2/2) dt \quad (C-8)$$

Returning to Figure C-6, we can see that the values of h , k_1 , and k_2 can be determined from the following expressions:

$$h = \frac{|u_2 v_1 - u_1 v_2|}{\sqrt{(u_2 - u_1)^2 + (v_2 - v_1)^2}} \quad (C-9)$$

$$k_1 = \frac{|u_1 (u_2 - u_1) + v_1 (v_2 - v_1)|}{\sqrt{(u_2 - u_1)^2 + (v_2 - v_1)^2}}$$

$$k_2 = \frac{|u_2 (u_2 - u_1) + v_2 (v_2 - v_1)|}{\sqrt{(u_2 - u_1)^2 + (v_2 - v_1)^2}}$$

where $B' = (u_1, v_1)$, $A' = (u_2, v_2)$.

To compute the probability over the polygon shown in Figure C-5, we could divide the polygon into triangles as shown in Figure C-7. In this particular example the aircraft pair is within the conflict boundary so that the origin in u,v space will be within the transformed conflict region polygon. This means that the probabilities of being within triangles I, II, III, and IV in Figure C-7 are added. If the aircraft pair were not within the conflict region then the u,v origin would not be within the transformed conflict region polygon. Figure C-8 shows such a configuration. To compute the probability of being within polygon A'B'C'D' one would find the probabilities of being within triangles I, II, III, and IV and then compute the probability as

$$P(A'B'C'D')=P(I)+P(II)-P(III)-P(IV). \quad (C-10)$$

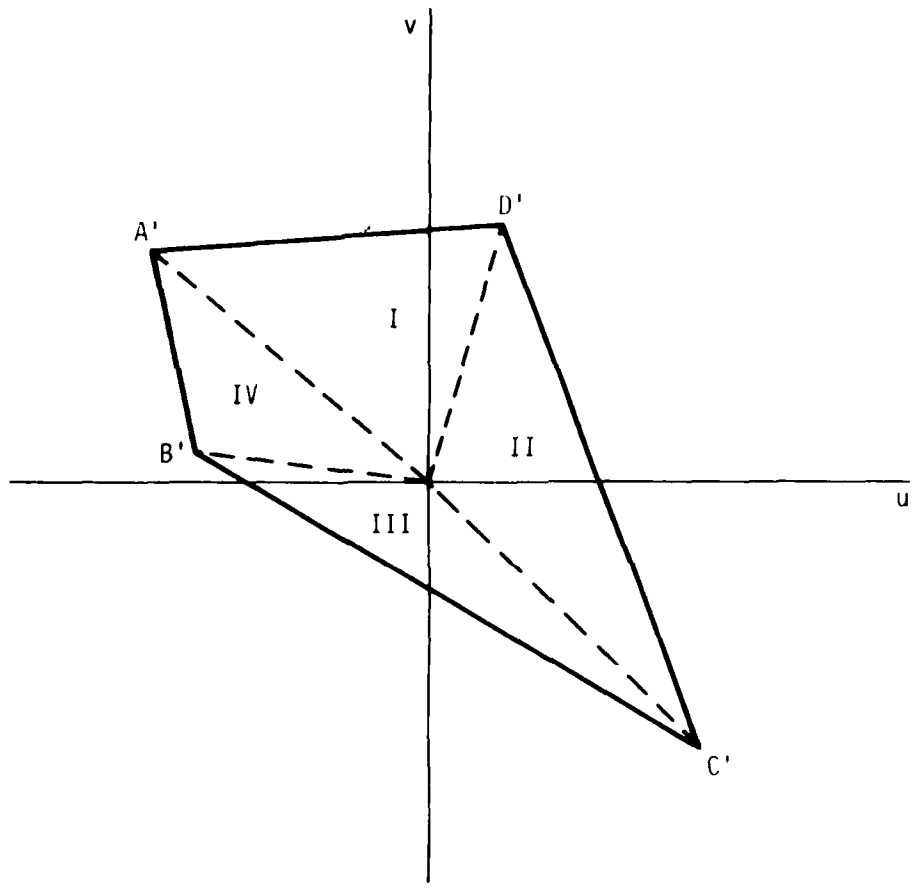


FIGURE C-7
THE PARTITIONED TRANSFORMED CONFLICT
REGION (ORIGIN INCLUDED)

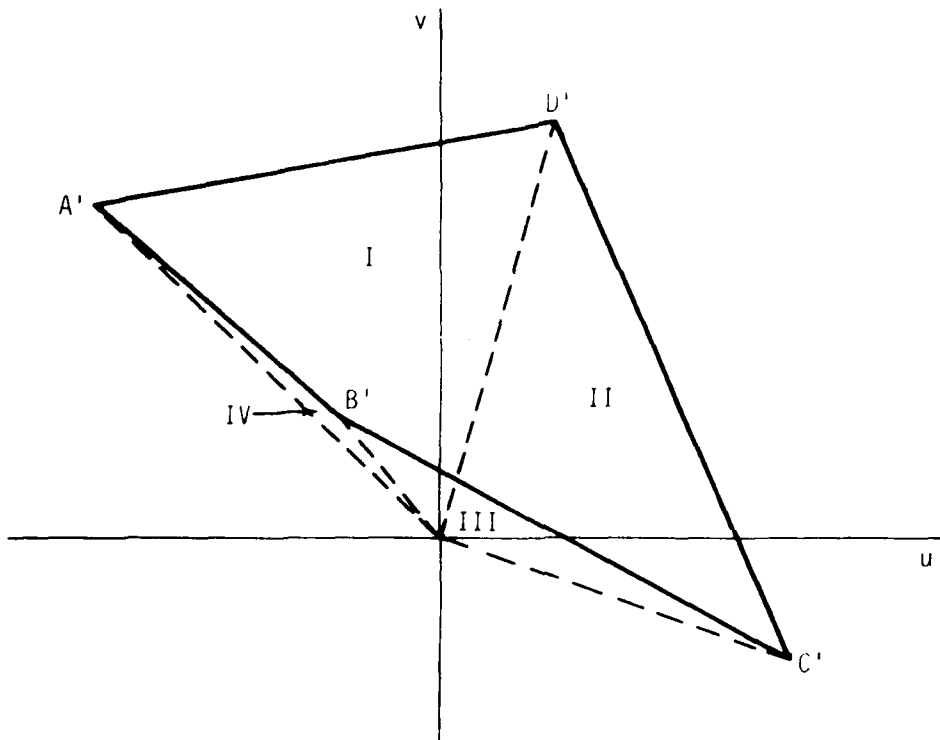


FIGURE C-8
THE PARTITIONED TRANSFORMED CONFLICT REGION
(ORIGIN EXCLUDED)

APPENDIX D

THE FAST FINITE FOURIER TRANSFORM

D1. INTRODUCTION

The purpose of this appendix is: 1) to give a general description of some of the properties of the finite Fourier transform, including the properties which enable the "fast" calculation of the transform; 2) to describe the use of a fast Fourier transform computer program for computing convolutions and 3) to present a fast finite Fourier transform computer program. There are many applications for the fast finite Fourier transform which are not treated here, such as for the estimation of spectral density functions and Fourier series. Articles in Reference 9 include a discussion of the fast Fourier transform algorithm and its history, as well as a treatment of some applications.

The finite Fourier transform, $F(n)$, of a finite, complex series, $f(t)$ where $t=0, \dots, T-1$ is given by the series

$$F(n) = \frac{1}{\sqrt{T}} \sum_{t=0}^{T-1} f(t) e^{\frac{2\pi i n t}{T}} \quad \text{for } n=0, \dots, T-1. \quad (D-1)$$

The finite Fourier transform is the finite analogue of the usual discrete Fourier transform and enjoys many of the properties associated with the infinite dimensional version. The properties of the finite Fourier transform are discussed in Section 2 of this Appendix. The fast Fourier transform is a computational procedure used for efficiently calculating the finite Fourier transform. It is not an estimation procedure, but simply an efficient calculation procedure. The fast Fourier transform algorithm permits calculation of (D-1) in approximately $T \log_2 T$ operations instead of the T^2 operations required for its direct calculation. The properties of (D-1) which lead to this efficient calculation procedure are outlined in Section 3 of this appendix. Section 4 of this appendix discusses certain features of the finite transform which are necessary for the correct use of the fast Fourier transform computer program and for the correct interpretation of the results when it is used to calculate convolutions. Finally one computer program which can be used for calculating the fast Fourier transform is presented in Section 5.

D2. PROPERTIES OF THE FINITE TRANSFORM

First, since the finite Fourier transform defined by (D-1)

is a finite sum of finite valued functions, it always exists and is finite. The properties presented in this section do not require any assumptions (other than finiteness) concerning the function $f(t)$. However, restrictions on $f(t)$ are frequently required for estimation procedures based on the finite transform.

If the finite Fourier transform of a function $f(t)$ is defined by equation (D-1), then using the fact that

$$\sum_{t=0}^{T-1} e^{\frac{2\pi i n t}{T}} e^{-\frac{2\pi i m t}{T}} = \begin{cases} T & \text{if } n = m \text{ mod } T \\ 0 & \text{otherwise,} \end{cases} \quad (D-2)$$

it is possible to show that the inverse relationship

$$f(t) = \frac{1}{T} \sum_{n=0}^{T-1} F(n) e^{-\frac{2\pi i n t}{T}} \quad \text{for } t=0, \dots, T-1 \quad (D-3)$$

also holds. Thus, the finite Fourier transform satisfies conditions which are similar to the infinite dimensional discrete Fourier transform. Functions such as $f(t)$ and $F(n)$ which satisfy (D-1) and (D-3) are referred to as finite transform pairs.

By definition of the finite transform in (D-1), it is easy to see that $F(n)$ is periodic with period T . Since $e^{2\pi i k} = 1$ for any integer k , we have that

$$\begin{aligned} F(n+kT) &= \frac{1}{T} \sum_{t=0}^{T-1} f(t) e^{\frac{2\pi i (n+kT)t}{T}} \\ &= \frac{1}{T} \sum_{t=0}^{T-1} f(t) e^{-\frac{2\pi i n t}{T}} e^{2\pi i k t} \\ &= \frac{1}{T} \sum_{t=0}^{T-1} f(t) e^{-\frac{2\pi i n t}{T}} = F(n), \end{aligned}$$

for any integer k and $n=0, \dots, T-1$.

By the same argument, equation (D-3) implies that $f(t) = f(kT+t)$ for any integer k and $t=0, \dots, T-1$. Thus, the finite transforms are computed under the assumption that $f(t)$ is periodic with period T .

A useful property of the finite transform is that if $f(t)$ is a real valued function, then

$$F(n) = F^*(T - n) \quad (D-4)$$

for $n=0, \dots, T/2$, where $*$ denotes complex conjugate. Thus, $F(n)$ is uniquely determined by its values at the points $n = 0, 1, \dots, T/2$.

Finally, the most important property for the analysis presented in this paper is that convolution and point by point multiplication are dual operations in time and frequency, i.e., if $f(t)$ and $F(n)$ are finite transform pairs and $g(t)$ and $G(n)$ are finite transform pairs with the same domain $n, t = 0, \dots, T-1$, then

$$\sum_{u=0}^{T-1} f(t-u) g(u) = \sum_{n=0}^{T-1} F(n) G(n) e^{-\frac{2\pi i n t}{T}} \quad (D-5)$$

Because of the operational efficiency of the fast Fourier transform algorithm, the calculation of the left hand side of (D-5) proceeds most efficiently by calculating $F(n)$ and $G(n)$ via (D-1) and then using (D-3) to obtain the inverse transform of $F(n) G(n)$. This method will be most efficient as long as the total number of operations* required to calculate the left hand side of (D-5) directly (T^2) is greater than the number required to calculate $F(n)$, $G(n)$ and the inverse transform of $F(n) G(n)$ ($3T \log_2 T$). Thus if T is a power of 2, using the fast Fourier transform as described above to calculate the left hand side of (D-5) is more efficient than direct calculation as long as $T \geq 16$.

D3. THE DOUBLING ALGORITHM

Consider a series $f(t)$ of length $T = 2N$. Then the finite transform of $f(t)$ is given by (D-1) to be

* Complex multiplications and adds

$$F(n) = \frac{1}{\sqrt{2N}} \sum_{t=0}^{2N-1} f(t) e^{-\frac{2\pi i n t}{2N}} \quad \text{for } n = 0, \dots, 2N-1. \quad (D-6)$$

Let

$$f_o(t) = f(2t+1) \quad \text{for } t=0, \dots, N-1$$

be the series of odd numbered elements of $f(t)$ and

$$f_e(t) = f(2t) \quad \text{for } t=0, \dots, N-1$$

be the series of even numbered elements of $f(t)$. Then the finite transforms of $f_o(t)$ and $f_e(t)$ are given by (D-1) to be

$$F_o(n) = \frac{1}{\sqrt{N}} \sum_{t=0}^{N-1} f_o(t) e^{-\frac{2\pi i n t}{N}}$$

and

$$F_e(n) = \frac{1}{\sqrt{N}} \sum_{t=0}^{N-1} f_e(t) e^{-\frac{2\pi i n t}{N}}.$$

Now, from (D-6) we can write $F(n)$ in terms of $F_o(n)$ and $F_e(n)$ as follows

$$\sqrt{2N} F(n) = \sum_{t=0}^{N-1} f(2t+1) e^{-\frac{2\pi i n(2t+1)}{2N}} + \sum_{t=0}^{N-1} f(2t) e^{-\frac{2\pi i n(2t)}{2N}},$$

or

$$\begin{aligned} \sqrt{2N} F(n) &= e^{-\frac{2\pi i n}{2N}} \frac{1}{\sqrt{N}} \sum_{t=0}^{N-1} f_o(t) e^{-\frac{2\pi i n t}{N}} \\ &+ \frac{1}{\sqrt{N}} \sum_{t=0}^{N-1} f_e(t) e^{-\frac{2\pi i n t}{N}} \quad \text{for } n=0, \dots, 2N. \end{aligned}$$

Thus, since

$$e^{-\frac{2\pi i(n+N)}{2N}} = -e^{-\frac{2\pi i n}{2N}} \quad \text{for } n=0, \dots, N-1,$$

we have

$$\left. \begin{aligned} x_{2N} F(n) &= e^{-\frac{2\pi i n}{2N}} F_o(n) + F_e(n) \quad \text{for } n=0, \dots, N-1 \\ x_{2N} F(n) &= -e^{-\frac{2\pi i n}{2N}} F_o(n) + F_e(n) \quad \text{for } n=N, \dots, 2N-1 \end{aligned} \right\} \text{(D-7)}$$

The equations (D-7) are the so-called doubling algorithm. Given the finite transforms of the two series consisting of the odd and even numbered elements of a series of length $T=2N$, (D-7) enables calculation of the transform of the total series by N complex multiplications. Thus, if we denote by Q_N the number of multiplications required for calculating the transform of an N point array, using (D-7) to calculate the transform of a $2N$ point array we have that

$$Q_{2N} = 2Q_N + N.$$

Since $Q_2 = 1$, this implies that

$$Q_N = \frac{1}{2} N \log_2 N.$$

Thus, the fast Fourier transform algorithm reduces the number of complex multiplications from the T^2 required by the direct calculation to $\frac{1}{2} T \log_2 T$.*

If the length of the data, T , is a power of two, the fast Fourier transform proceeds as follows:

1. The series of data is split into T subseries of length 1. Thus, the Fourier transform for each series is the series itself. These T transforms are called the first level transforms.

*The figure $T \log_2 T$ given on page D-1 is obtained by doubling $\frac{1}{2} T \log_2 T$ in order to include the number of complex additions.

2. The doubling algorithm (D-7) is applied to the k^{th} and $T/2+k^{\text{th}}$ first level transforms to compute the finite transforms for the second level subseries k , where $k=0, \dots, T/2$. These are the finite transforms of the $T/2$ subseries of length 2.

3. Doubling continues in this way until finally the transforms of the two subseries of length $T/2$ are combined via the doubling algorithm to give the finite transform of the entire series.

The fast Fourier transform program presented in Section 5 operates solely on data arrays of length a power of two. Other computer programs (using similar algorithms) can handle series of any length. In general, the restriction to a length of a power of two has not been too restrictive. The series is simply filled with zeros to give it the proper length.

D.4. FEATURES

This section will discuss several features of the use of the fast Fourier transform. These include features relating to the input of data for transformation, the required length of the input, and the interpretation of the output when the fast Fourier transform is used to perform convolutions. Knowledge of these features was necessary for correct use of the fast Fourier transform in the analysis presented in this paper. A more complete description of the fast Fourier transform and features applicable in other types of analysis may be found in Reference 9.

As mentioned previously, the finite Fourier transform operates under the assumption that the function to be transformed is periodic with period T . Thus, the algorithm calculates the finite transform of a periodic extension of the data observed between $t=0$ and $t=T-1$. If the data $x(t)$ represents observations which are symmetric about zero, i.e., if actual observations were taken at $t=-T/2+1, \dots, T/2$ then the data should be shifted in the following way before its finite transform is calculated. Define

$$y(t) = \begin{cases} x(t) & \text{for } t=0, \dots, T/2 \\ x(t-T) & \text{for } t=T/2+1, \dots, T-1. \end{cases} \quad (\text{D-8})$$

Then the desired transform of $x(t)$ is obtained by transforming $v(t)$. It would also be possible to transform the function $v(t) = x(t - T/2 + 1)$ for $t=0, \dots, T-1$ instead. This represents a shifted version of the periodic extension of (D-8) and its transform would just be a shifted version of the transform of (D-8). (D-8), however, directly represents the function which is symmetric about zero.

There are several features of the finite Fourier transform which must be considered when it is used to calculate convolutions. First, let us consider the convolution of two functions: $f(t)$ and $g(t)$. Let us assume that $f(t)$ was observed for $t=0, \dots, L-1$ and $g(t)$ was observed for $t=0, \dots, N-1$. Let T be a power of two, with the property that

$$T \geq L + N - 1 \quad (D-9)$$

Then define $f(t) = 0$ for $t = L, \dots, T-1$ and $g(t) = 0$ for $t = N, \dots, T-1$. The convolution of $f(t)$ and $g(t)$ can then be computed via (D-5). One way to justify the constraint (D-9) is to view the convolution in (D-5) as the probability function of the sum of two independent random variables with density functions $f(t)$ and $g(t)$ respectively. Then if $f(t)$ is defined for L data points and $g(t)$ is defined for N data points, the sum of the two random variables will have a domain of definition of $N+L-1$ data points.

The finite Fourier transform presented above is defined for a function $f(t)$ observed at values of $t=0, \dots, T-1$. In practice, observations are frequently taken at a fixed sampling interval, say Δ , which is not necessarily unity. In addition, the first observation of real data may not correspond to an observation at zero. For example, in the analysis presented in this paper it was desired to compute the convolution of two probability functions, symmetric about zero, observed in $1/2$ mi intervals. There was no zero observation; instead, observations within $1/2$ mi of zero fell into one of the intervals $[-.5, 0)$ or $[0, .5)$. The finite transform can still be used to calculate the convolution of such functions. The following analysis provides the key to interpretation of the results.

Let us assume that we have two sets of T data points $x(s)$ and $y(s)$ (including the necessary number of zeroes to satisfy (D-9)) observed in time intervals of Δ starting at time a . Thus $x(s)$ and $y(s)$ are defined for $s = \Delta t + a$ where $t=0, \dots, T-1$. In order to calculate the convolution of x

and y , we set

$$\begin{aligned} f(t) &= x(\Delta t + a) \\ \text{and} \\ g(t) &= y(\Delta t + a) \quad \text{for } t = 0, \dots, T-1. \end{aligned} \quad (D-10)$$

The functions $f(t)$ and $g(t)$ are now in a form to use the fast Fourier transform methodology to calculate the convolution. We have from (D-5), that the output of the fast Fourier transform convolution computation would be given by $h(t)$, where,

$$h(t) = \sum_{u=0}^{T-1} f(t-u) g(u) \quad t=0, \dots, T-1.$$

Substituting for f and g from (D-10), we have

$$h(t) = \sum_{u=0}^{T-1} x(\Delta(t-u) + a) y(\Delta u + a).$$

This can be written as

$$h(t) = \sum_{u=0}^{T-1} x(\Delta t + 2a - \Delta u + a) y(\Delta u + a).$$

Since the expressions involving u in the above equation are the same, this can be written as

$$h(t) = z(\Delta t + 2a) \quad \text{for } t=0, \dots, T-1. \quad (D-11)$$

In (D-11), $z(\Delta t + 2a)$ represents the desired convolution of $x(s)$ and $y(s)$. (D-11) implies that the series of points representing the convolution of two functions are observed at the same time interval as the original series, namely Δ . However the fact that the first observations in the initial series were offset from zero by "a" units, implies that the first point in the convolved series will be offset from zero by "2a" units.

For the example mentioned above, the observation intervals were $1/2$ nmi, so that $\Delta = 1/2$. The first observation intervals were centered at $1/4$, so that $a = 1/4$. Thus, the convolution of $x(s)$ with $y(s)$ has the interpretation (D-11), or

$$h(t) = z(t/2 + .5) \quad \text{for } t=0, \dots, T-1.$$

Thus, the first item in the array returned by the program, namely $h(0)$, represents the desired convolved density function, z , evaluated at $1/2$ nmi. Because of the periodicity of the finite Fourier transform, we have that the last item in the data array $h(t)$, namely $h(T-1)$ is equal to $h(-1)$. Thus, we have that $z(T/2) = z(0)$, so that the last item in the array returned by the finite transform computer program represents the desired convolved density function evaluated at zero.

The same characteristic applies when (D-5) is used to determine the convolution of three shifted functions as was done in the analysis discussed in this paper to include distributional characteristics of delay, bank angle, and detection (Appendix C). In this case, it can easily be verified that

$$h(t) = z(\Delta t + 3a) \quad \text{for } t=0, \dots, T-1. \quad (D-12)$$

Let us assume that $\Delta = 1/2$ and $a = 1/4$ as before. Thus, the first cell of the array $h(t)$, (corresponding to $t = 0$), actually represents the convolved density data z centered at $.75$ nmi. The last item in the array $h(t)$ (corresponding to $t = T-1$) represents the convolved density data centered at $.25$ nmi.

D5. THE COMPUTER PROGRAM

The fast Fourier transform program used in this analysis is a FORTRAN IV program which was obtained from Dr. Robert Shumway of George Washington University and is attributed to Norman Brenner of MIT Lincoln Lab. It is listed in Table D-1. The call statement to the subroutine is:

```
CALL FFT (NN, DATA, SIGNI)
```

where,

DATA is a complex double precision array of length 2^{NN} . It contains the data to be transformed on the call and the transformed data on return.

TABLE D-1
THE FAST FINITE FOURIER TRANSFORM
COMPUTER PROGRAM

```

SUBROUTINE FFT(NN,DATA,SIGNI)
IMPLICIT REAL*8 (A-H,O-Z)
DIMENSION DATA (1)
DATA TWOPI/6.2831853072D0/
C
C THIS SUBROUTINE COMPUTES THE FAST FINITE FOURITE TRANSFORM OF A
C L=2**NN POINT COMPLEX DOUBLE PRECISION ARRAY.
C
C INPUTS: DATA(.) COMPLEX L=2**NN POINT ARRAY
C NN POWER OF 2 CORRESPONDING TO THE LENGTH OF
C DATA(.)
C SIGNI 1. OR -1. (DOUBLE PRECISION) DEPENDING ON
C WHETHER THE DIRECT OR INDIRECT TRANSFORM IS
C DESIRED
C
C OUTPUTS: DATA(.) COMPLEX DOUBLE PRECISION L POINT ARRAY OF
C TRANSFORMATIONS.
C
C DATA(N) = SUM FROM T = 0 TO T = L-1 OF
C DATA(T) * EXP(SIGNI*2*PI*I*N*T/L)
C WHERE N = 0,1,...,L-1 AND I = SQRT(-1.)
C
N=2**(NN+1)
J=1
DO 5 I=1,N,2
IF(I-J)1,2,2
1 TEMPR=DATA(J)
TEMPI=DATA(J+1)
DATA(J)=DATA(I)
DATA(J+1)=DATA(I+1)
DATA(I)=TEMPR
DATA(I+1)=TEMPI
2 M=N/2
3 IF(J-M)5,5,4
4 J=J-M
M=M/2
IF(M-2)5,3,3
5 J=J+M
MMAX=2
6 IF(MMAX-N)7,10,10
7 ISTEP=2**MMAX
THETA=SIGNI*TWOPI/FLOAT(MMAX)
SINTH=DSIN(THETA/2.D0)
WSTPR=-2.D0*SINTH*SINTH
WSTPI=DSIN(THETA)
WR=1.D0
WI=0.D0
DO 9 M=1,MMAX,2
DO 8 I=M,N,ISTEP
J=I+MMAX
TEMPR=WR*DATA(J)-WI*DATA(J+1)
TEMPI=WR*DATA(J+1)+DATA(J)*WI
DATA(J)=DATA(I)-TEMPR
DATA(J+1)=DATA(I+1)-TEMPI
DATA(I)=DATA(I)+TEMPR
2 DATA(I+1)=DATA(I+1)+TEMPI
TEMPR=WR
WR=WR*WSTPR-WI*WSTPI+WR
9 WI=WI*WSTPR+TEMPR*WSTPI+WI
MMAX=ISTEP
GO TO 6
10 RETURN
END

```

NN is the power of two corresponding to the length of the data series.

SIGNI is double precision $\pm 1.$, depending on whether a direct or inverse transform is desired.

...

APPENDIX E

PROBABILITY OF ALONGTRACK SEPARATION

E1. INTRODUCTION

In Appendix B there is a term $P_{\Delta x}$ which is the probability of that two aircraft, cleared on adjacent parallel routes, have an alongtrack separation of $x \pm \Delta x/2$. This appendix will show that $P_{\Delta x}$ is constant over the range of alongtrack separations being considered. This will be followed by a discussion of the relationship between $P_{\Delta x}$ and P_x , the probability of alongtrack overlap. The estimation of P_x using an analytical model will then be addressed.

E2. DISTRIBUTION OF ALONGTRACK SEPARATION

To show that $P_{\Delta x}$ is constant for $|x \pm \Delta x/2| < D$ we first investigate the distribution of alongtrack separation between aircraft that are assigned to adjacent parallel routes. Consider the situation depicted in Figure E-1. The aircraft on the same route are separated by a distance W . The air traffic control rules state that W has to be greater than some minimum distance D (the radar separation). Since W is a random variable it has a probability density function which can be written as

$$f(W) = \begin{cases} 0 & 0 < W < D \\ g(W) & D < W \end{cases} \quad (E-1)$$

where $g(W)$ is an arbitrary probability density function.

Now, the aircraft on route 2 are assumed to operate independently from the aircraft on route 1. Thus, if we have aircraft A_1 and B_1 on route 1, then an aircraft A_2 on route 2 would in general be positioned between the two aircraft on route 1 as shown in Figure E-1. The alongtrack distance from A_2 to A_1 is denoted as x_1 while the alongtrack distance from A_2 to B_1 is denoted as x_2 . Since the position of A_2 with respect to A_1 and B_1 is randomly chosen, the distances x_1 and x_2 are random variables.

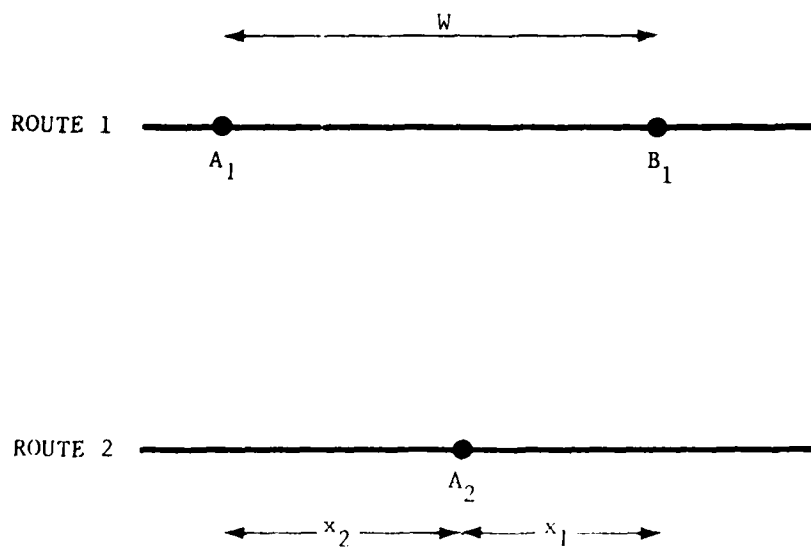


FIGURE E-1
INTERAIRCRAFT SPACING GEOMETRY

From renewal theory (Reference 10) we have two results. The first result is that the random variables x_1 and x_2 are identically distributed. The second result is that this probability density function is given as

$$h(x) = \frac{1 - \int_0^x f(W) dW}{\int_0^{\infty} W f(W) dW} \quad (E-2)$$

But, we are only interested in the probability density function of x (i.e., x_1 and x_2 in Figure E-1) in the range of 0 to D . One recalls that this is our definition of proximity from Appendix A. Thus, if we are considering $0 < x < D$, then equation (E-2) becomes

$$h(x) = \frac{1 - \int_0^{x < D} f(W) dW}{E(W)} = \frac{1 - \int_0^{x < D} 0 dW}{E(W)} = \frac{1}{E(W)} \quad (E-3)$$

where $E(W)$ is the expected value of the variable W . Equation (E-3) tells us that the probability density function of x is constant over the range $0 < x < D$. This means that it is equally likely to find adjacent route aircraft separated between 0 and D nmi.

E3. RELATIONSHIP BETWEEN $P_{\Delta x}$ AND P_x

In the notation of Appendix B

$$P_{\Delta x} = P[|x - x_1| < \Delta x / 2]. \quad (E-4)$$

For $|x_1 + \Delta x / 2| < D$, the results of renewal theory (equation (E-3)) tell us that

$$P_{\Delta x} = \Delta x / E(W). \quad (E-5)$$

From the procedural collision risk model we have

$$P_x = P[x < 2\lambda_x] \quad (E-6)$$

Since $2\lambda_x < D$, and the distribution of alongtrack separation between aircraft on adjacent routes is uniform within the range 0 to D, we can write

$$\frac{2\lambda_x}{P_x} = \frac{\Delta x}{P_{\Delta x}} \quad (E-7)$$

Rearranging terms one arrives at

$$P_{\Delta x} = \frac{P_x \Delta x}{2\lambda_x} \quad (E-8)$$

for $|x_i + \Delta x/2| < D$.

Therefore, we have determined that $P_{\Delta x}$ is a constant that is related to P_x as shown in equation (E-8). The next section will discuss how one can estimate P_x .

E4. ESTIMATING P_x

An analytical model to estimate P_x was developed by the ICAO Review of the General Concept of Separation Panel (RGCSPP) (Reference 11). For aircraft that are coalitute, in level flight, and flying the same direction, the analytical model gives a value of P_x as

$$P_x = \frac{4\lambda_x N_1 N_2}{V(N_1 + N_2)} \quad (E-9)$$

where λ_x is the length of the aircraft,

V is the average velocity of the aircraft, the average velocity being the same on both routes, and

N_i is the flow rate on route i .

The validity of this analytical model was tested by comparing the results from (E-9) with data on observed aircraft passings in an operational environment. This comparison was made using data from a two week period in the FAA's large scale data collection in the Cleveland ARTCC (Reference 12).

Since equation (E-9) was developed under the assumption that the flow rates N_i are constant during a steady-state period, it was necessary in Reference 12 to determine the flow rates over a set of assumed steady-state periods. Time periods for 1/2 hour to 6 1/2 hours were investigated. The ratio of the total flying time in passing to the total flying time was computed for each day. These values were compared to the P_x values calculated from the model under the various steady state assumptions for each day and for the entire time period.

The results from the investigation of the data showed that the interarrival spacings are consistent with a Poisson process. Also, there was a diurnal pattern observed in the data. From day to day there was some variation in the arrival rates for a particular "steady-state" time period but not more than one would expect from a Poisson process. This result allowed the combination of the data in the same "steady-state" period across all days. It was concluded in Reference 16 that the 1/2 hour "steady-state" time period gave the best approximation to steady-state. For this steady-state time period, the data derived values of P_x and the analytical model derived values of P_x were comparable over a long time period for same direction flight on both routes. Therefore, for properly interpreted data, the analytical model provides a vehicle for estimating the fraction of the flying time spent in passing.

APPENDIX F

CALCULATION OF THE JOINT CLOSING SPEED-SEPARATION
HISTOGRAM FROM SINGLE AIRCRAFT DATA

The Conflict Monitoring Model requires the probability that an aircraft pair has a crosstrack closing speed and a crosstrack separation within a given range. Since the FAA's data collection could not take this data on aircraft pairs, single aircraft data on crosstrack deviations and crosstrack speed that was taken was used. This appendix will outline the procedure to convert a joint histogram of crosstrack deviation and crosstrack speed to a joint histogram of crosstrack separation and crosstrack closing speed.

First let us assume that we have the bivariate probability density function of the crosstrack deviation and crosstrack speed from single aircraft observations. We will call this probability density function for aircraft on route i $f_i(Y_i, V_{yi})$. We could then compute another probability density function, g , a function of $y = Y_2 - Y_1$, V_{y1} , and V_{y2} as

$$g(y, V_{y1}, V_{y2}) = \int_{-\infty}^{\infty} f_1(Y_1, V_{y1}) f_2(y - Y_1, V_{y2}) dY_1 \quad (F-1)$$

But we really have histogram data rather than a probability density function so that we will denote $f_i(Y_i, V_{yi})$ as the estimate for $f_i(Y_i, V_{yi})$ based on the histogram data $\hat{f}_i(Y_i, V_{yi})$. The quantities \hat{f} and \tilde{f} are related by the following expression:

$$\hat{f}_i(Y_i, V_{yi}) = \frac{\tilde{f}_i(Y_i, V_{yi})}{\Delta Y \Delta V_y} \quad (F-2)$$

where ΔY is the histogram cell size for crosstrack deviations and ΔV_y is the histogram cell size for the crosstrack speed. We can then write the estimate for the function g as

$$\begin{aligned} \hat{g}(y, v_{y1}, v_{y2}) &= \sum_{Y_1=-\infty}^{\infty} \hat{f}_1(Y_1, v_{y1}) \hat{f}_2(y - Y_1, v_{y2}) \Delta Y \\ &= \sum_{Y_1=-\infty}^{\infty} \frac{\tilde{f}_1(Y_1, v_{y1})}{\Delta Y \Delta v_y} \frac{\tilde{f}_2(y - Y_1, v_{y2})}{\Delta Y \Delta v_y} \Delta Y \end{aligned}$$

(F-3)

$$= \sum_{Y_1=-\infty}^{\infty} \frac{\tilde{f}_1(Y_1, v_{y1}) \tilde{f}_2(y - Y_1, v_{y2})}{\Delta Y (\Delta v_y)^2}$$

But

$$\tilde{g}(y, v_{y1}, v_{y2}) = \hat{g}(y, v_{y1}, v_{y2}) \Delta Y (\Delta v_y)^2 \quad (F-4)$$

Therefore

$$\tilde{g}(y, v_{y1}, v_{y2}) = \sum_{Y_1=-\infty}^{\infty} \tilde{f}_1(Y_1, v_{y1}) \tilde{f}_2(y - Y_1, v_{y2}) \quad (F-5)$$

The expression in (F-5) is the histogram convolution of the crosstrack deviations. The result, \tilde{g} , is a histogram in terms of the spacing between the aircraft and their individual crosstrack velocities. By letting $\hat{y} = v_{y2} - v_{y1}$, we can change the variables in the function \tilde{g} . Thus

$$\tilde{g}(y, v_{y1}, v_{y2}) = \tilde{g}(v, v_{y2} - \hat{y}, v_{y2}) \quad (F-6)$$

By summing over V_{y2} we arrive at

$$g(y, \hat{y}) = \sum_{V_{y2}=-\infty}^{\infty} g(y, V_{y2}-\hat{y}, V_{y2}) \quad (F-7)$$

The histogram $g(y, \hat{y})$ is the desired histogram. The histogram is centered on a crosstrack closing speed of zero and a crosstrack separation of zero. To use the histogram it has to be shifted so that its center corresponds to the spacing between the routes to which the aircraft have been assigned. Once the histogram $g(y, \hat{y})$ has been computed, the probability that an aircraft pair has a given range of crosstrack closing speed and crosstrack separation can be estimated by adding up the appropriate cells of the histogram.

APPENDIX G

INTERVENTION RATE SIMULATION

G1. INTRODUCTION

This appendix will discuss the estimation of the controller intervention rate. The estimate of this system performance measure was obtained through a simulation. The input data to the simulation will be described followed by an outline of the steps the simulation performs to arrive at the intervention rate estimates. The analysis of the output from the simulation is dealt with at the end of the appendix.

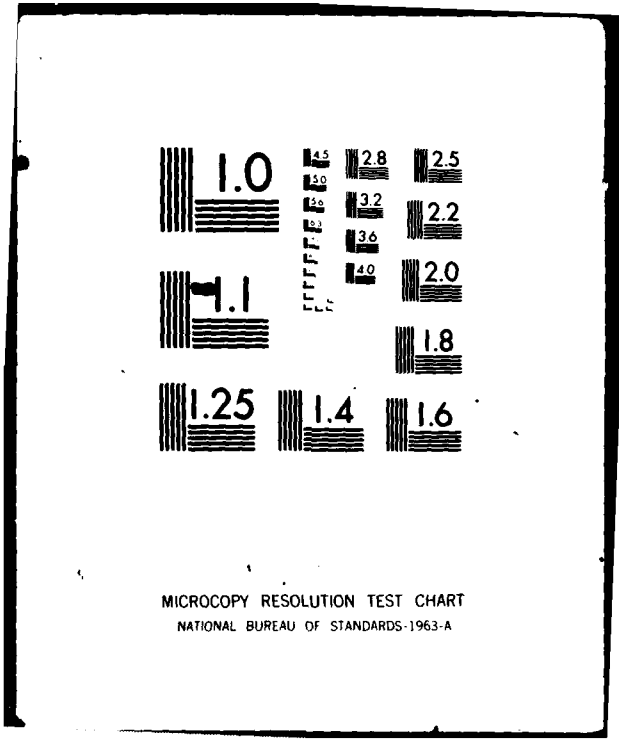
G2. THE INPUT

The data which were used in the simulation were smoothed aircraft tracks which are part of the FAA's VOR navigation data collection. About 100 aircraft on each of two selected routes in the Cleveland ARTCC were randomly chosen over the time period of the data collection. The only requirement on these aircraft were that they had actually flown the entire route segments of interest. The other data used in the simulation are shown in Figure G-1. These data include the radar noise and the location of the radar, the route coordinates, the sector boundaries, a random number seed, the number of route spacings and replications for the simulation to consider, and the requested flow rates of the traffic on the routes. The time duration of the simulation is also specified.

G3. THE SIMULATION FLOW

The object of the simulation is to estimate the controller intervention rate at several route spacings for several flow rates along the routes. Since this is a simulation "experiment," several replications should be made so that meaningful statements can be made concerning the results.

To minimize the cost of these numerous runs, a definite simulation run strategy was employed. The strategy depends on the use of the same traffic for each different route spacing during the same replication of the simulation. The minimum route separation to be considered (8 nmi) was run first. Of the traffic run on the routes spaced a minimum distance apart, only a subset of the traffic would form the set of potential conflicts for the next set of wider spaced routes. In other words, with the same traffic, aircraft which are not projected to get near to other aircraft at the narrower route spacing will



MICROCOPY RESOLUTION TEST CHART
NATIONAL BUREAU OF STANDARDS-1963-A

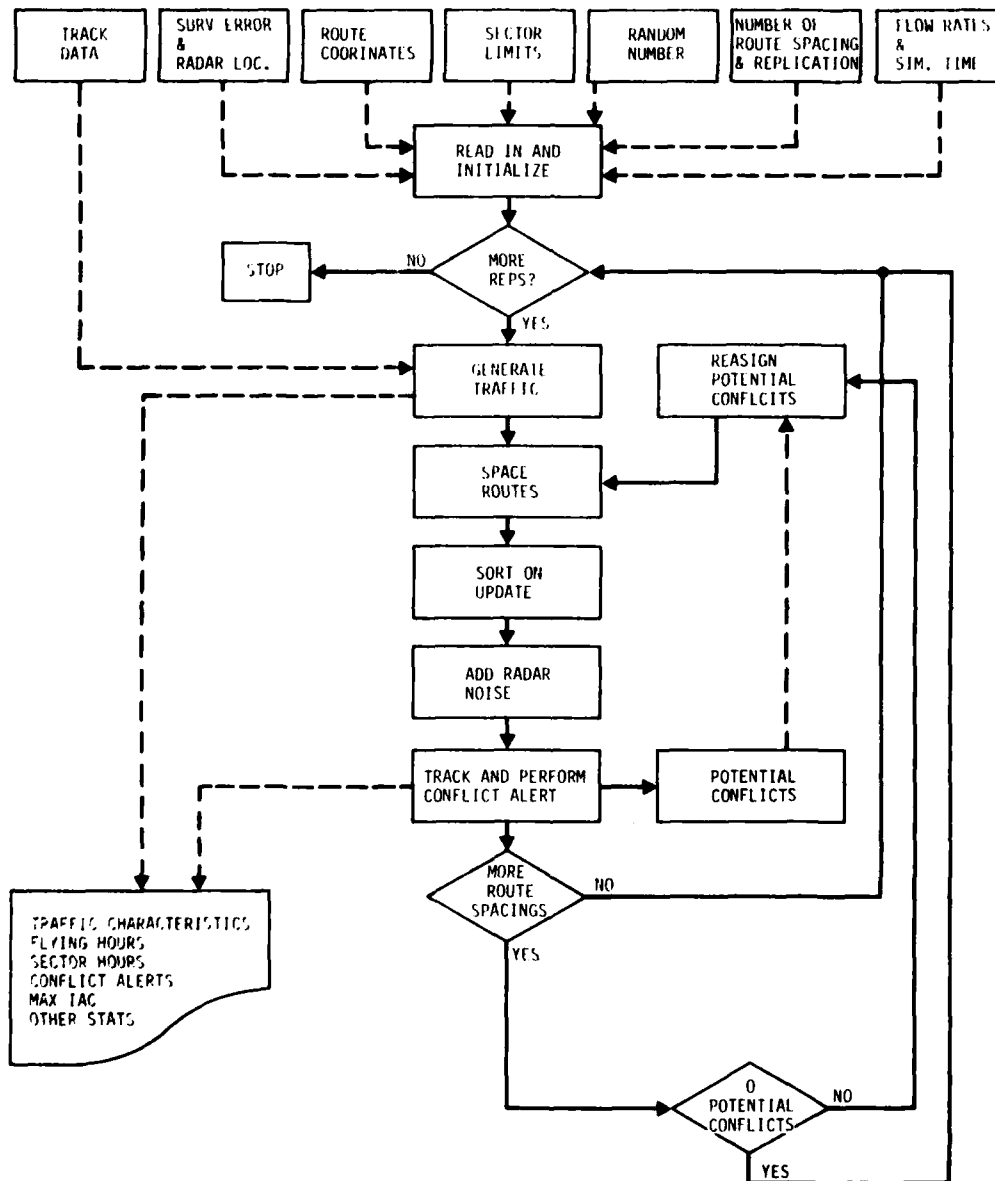


FIGURE G-1
INTERVENTION RATE SIMULATION FLOW

not be projected to get near to other aircraft when the routes are farther apart. Of course some care must be taken in choosing the definition of what it means to be projected to get near to another aircraft for the purposes of carrying the aircraft along to the next route spacing. The reason for this care is that an aircraft pair may barely not be detected in conflict at one route spacing but might be detected in conflict at a wider route spacing. For instance, at the narrow route spacing, a deviating aircraft might be projected to pass in front of an aircraft on the adjacent route but with enough separation not to cause an alarm. However, with the aircraft in exactly the same positions except on routes that are spaced farther apart, the projected minimum separation might be small enough to trigger an alarm. To guard against not including such aircraft in the wider route spacing sample an additional "window" which is larger than the conflict alert criteria was employed.

The flow of the simulation itself is rather straightforward as shown in Figure G-1. First, the traffic is generated. This is done by randomly selecting a track from the track data. This data consists of the best estimate of an aircraft's position every 12 seconds during the time the aircraft was observed in the FAA's data collection. Next an entry time is chosen for that aircraft. The entry time is chosen such that the interaircraft entry times are exponentially distributed corresponding to the desired average flow rate on the route. Since exponentially distributed interaircraft entry times could allow two aircraft to be very closely separated in time along the same route, a check is made to insure that the radar separation is not violated between aircraft on the same route. If an aircraft pair is detected to violate the separation standard, the second aircraft is delayed at the route entry point to insure the minimum separation, plus a buffer, between the two aircraft.

After the traffic is generated, the coordinates of the aircraft positions are transformed to correspond to two routes that are spaced at the minimum spacing. At this point the simulation has a string of positions and times that is organized by aircraft. To simulate radar returns, the aircraft positions must be organized by time. This is achieved by sorting the aircraft position records by time (radar update).

The simulation can now track and perform conflict alert on the aircraft positions. But before the simulation can perform either of these functions on a particular set of aircraft,

certain conditions must prevail. The first condition is that the time of the radar update must be between the starting and ending time values of the simulation. These values are set when the traffic is generated to account for the "end effects" of the simulation. The simulation does not start until the latter of the first aircraft on each route exits the sector. The simulation ends when the earlier of the last aircraft on each route enters the sector. After the starting update, the tracker will maintain a track on all the aircraft.

The positions of the aircraft from the "track data" have been smoothed as part of the FAA's data collection program. Therefore, radar noise (azimuth and range) is added to the position reports prior to going into the NAS tracker in the simulation. The tracked aircraft are then subjected to the conflict alert function if two further conditions are met. One condition is that both aircraft have to be within the sector of interest. The other condition is that there has not been a previous conflict alert declared on this aircraft pair.

An aircraft pair which satisfies the above conditions are then passed to the conflict alert function where the pair is subjected to a set of coarse geographic and velocity filters. Passing these coarse filters indicates that the pair is near and generally closing on each other. The aircraft pairs that pass the coarse filtering are then subjected to a set of fine filters. These fine filters project the positions of the pair ahead in time. If, within a given look-ahead time, the pair is projected to be separated by less than a certain distance, then the pair is called a conflict pair. If the pair passes the fine filtering in two out of the last three passes through the filters then the pair is in potential conflict. In the NAS, the controller is alerted to this conflict pair by the NAS automation blinking the aircraft symbology on his screen. In the simulation, the potential conflict is tallied as part of the simulation statistics. The current conflict and predicted conflict parameters are the same ones used in NAS. In addition other parameters are used by the simulation to identify those aircraft pairs which should be included in the next wider route spacing run. The definitive formulation of the NAS Conflict Alert function can be found in Reference (13). Appendix H gives a detailed description of the horizontal components of the NAS Conflict Alert.

Referring back to Figure G-1, we can see that after the conflict alert has been performed, we have a list of nearly conflicting pairs of aircraft to be used in the simulation of the next wider

route spacing. If there are no more nearly conflicting pairs or there are no more route spacings to consider, we go back to do another replication of the simulation. If there are nearly conflicting pairs and more route spacings then the simulation reassigns, the nearly conflicting pairs to the routes. The same entry times that they had originally are maintained. The newly assigned aircraft's positions are then transformed to correspond to the new route spacing. The loop is thus closed and the processing continues until all the route spacings and replications are done.

G4. THE OUTPUT

The output from the simulation consists of several statistics. First, the traffic generator lists the traffic characteristics: the particular aircraft chosen, their entry times onto the routes, the delays that were incurred, and the realized average traffic flow rates. The tracking and conflict alert part of the simulation records another set of statistics. These include the number of flying hours in the sector, the number of aircraft generating those flying hours, the maximum instantaneous aircraft count (IAC), the number of hours the conflict alert function was "watching" the sector, and the number of conflict alerts declared. Other miscellaneous statistics concerning the detailed workings of conflict alert are also taken.

G5. THE ANALYSIS OF THE OUTPUT

As Reference (14) points out, there are basically two types of simulations as far as the analysis of the simulation output is concerned -- terminating and steady-state. The difference between these is the desired result. In all cases a simulation has to be terminated after some finite time interval. In some cases, one wishes to evaluate steady state property of the system as if the time interval goes to an infinite length. In other cases, the behavior of the system over a defined (terminated) length of time is desired such as the peak of the traffic demand. The simulation of conflict alerts belongs to the terminating type of simulation. One of the results of Reference (14) is that for a terminating simulation the usual statistical tests and procedures can be applied to the output from the simulation.

In the particular simulation described above, the event of a conflict alert occurs over a period of time. It is also as likely that this event will occur in one interval as in any other and that the occurrence of the event has no effect on

whether or not another occurs. The number of events in a fixed time with the above attributes is often assumed to have a Poisson distribution. In fact in the results section (Section 5 in Volume I of this report) it is shown that the number of conflict alerts per hour from the simulation does look as if it were Poisson distributed.

The result we are looking for is the expected value of the Poisson distribution. The unbiased and maximum likelihood estimator is the sample mean. This is the number of conflict alerts divided by the number of hours which were simulated. We can also construct a confidence interval for the expected value of a Poisson distribution (Reference (15)). If

$$f(n) = \frac{e^{-\lambda} \lambda^n}{n!} \quad n = 0, 1, 2, \dots \quad (G-1)$$

then for any value n' and $\alpha < .5$, lower and upper limits of may be determined such that

$$\sum_{n=n'}^{\infty} \frac{e^{-\lambda_a} \lambda_a^n}{n!} = \alpha$$

and

(G-2)

$$\sum_{n=0}^{n'} \frac{e^{-\lambda_b} \lambda_b^n}{n!} = \alpha$$

such that $\lambda_a < \lambda_b$. The values of λ_a and λ_b are tabulated for $100(1-2\alpha)\%$ = 95% and 99% significance levels in Reference (15). These tables are applied to the simulation output to construct 95% confidence intervals for the expected rate of conflict alerts. The results are shown in Section 5 of Volume I of this report.

APPENDIX H

THE NAS CONFLICT ALERT

In Section 3.1.1 of Volume I of this report it was stated that the conflict alert function in the NAS computer was not modelled precisely in the Conflict Monitoring Analysis. The NAS Conflict Alert function uses both horizontal and vertical filters when determining the condition of conflict between a pair of aircraft. Since we have assumed the aircraft to be in straight and level flight at the same altitude, this appendix will discuss only the horizontal filters used by the NAS Conflict Alert function.

In the NAS computer the Conflict Alert performs a series of tests to determine the conflict status of a pair of aircraft. The tests are structured in such a way as to minimize false alarms, maximize the chance of an alarm on a true conflict while at the same time minimizing the computational complexity of the tests.

After the tracks are geographically sorted and tested for being near in altitude, a series of horizontal filters are applied. The filters are diagrammed in Figure H-1. The Conflict Alert has two types of horizontal filters, coarse and fine. For each type there may be two levels designated as A and B. The type and level of the filter will depend on the previous history of the aircraft pair with respect to the Conflict Alert function. The values of the Conflict Alert parameters are summarized on Table H-1.

The process starts with position estimates (X_i, X_j, Y_i, Y_j) and velocity component estimates $(\dot{X}_i, \dot{X}_j, \dot{Y}_i, \dot{Y}_j)$ of aircraft i and j . It is first determined what type and level of filter should be used. The choice will depend on whether the aircraft pair has been observed previously and, if so, what the result of the previous Conflict Alert tests were. If the aircraft pair has not passed any filters successfully in the past two applications of the filters, a level A filter is used. If a level A filter is required then a coarse horizontal filter is performed on the position estimates:

$$(X_i - X_j)^2 + (Y_i - Y_j)^2 \leq \text{MAXR}^2 \quad (\text{H-1})$$

where $\text{MAXR}=55$ nmi. If the aircraft are separated by more than 55 nmi they are no longer considered by Conflict Alert.

TABLE H-1
HORIZONTAL CONFLICT ALERT PARAMETERS

FILTER TYPE	PARAMETER	LEVEL A	LEVEL B
COARSE	MAXR	55.0 nmi	
FINE	CURRENT CONFLICT	5.0 nmi	4.2 nmi
	PREDICTED CONFLICT	8.0 nmi ² /hr 0.7 nmi/min 6.0 nmi 2.5 min 6.0 nmi	8.0 nmi ² /hr 0.7 nmi/min 4.8 nmi 2.0 min 4.8 nmi
	NEAR CONFLICT	MIN SEPARATION DISTANCE AT WRNT	8.0 nmi 8.0 nmi

If the coarse filter is passed the positions and velocities of the aircraft pair are subjected to the fine filter of level A.

The fine filter first checks if the aircraft pair is in current lateral conflict. If

$$R_0^2 = (X_i - X_j)^2 + (Y_i - Y_j)^2 \quad (H-2)$$

is less than $SEPR^2$, a current horizontal conflict exists. For level A $SEPR = 5$ nmi and for level B $SEPR = 4.2$ nmi.

If the aircraft pair is not in current conflict, it could be in predicted conflict. This part of the fine filter projects an aircraft pair ahead in a straight line for a certain period in time and tests to see if the aircraft come within a given distance of each other during that time interval. This check is done in several steps to reduce computation time. The first step is to determine whether the tracks are generally converging toward each other. If we let

$$V_c = (X_i - X_j)(\dot{X}_i - \dot{X}_j) + (Y_i - Y_j)(\dot{Y}_i - \dot{Y}_j) \quad (H-3)$$

then the inequality $V_c < VELC$ must be satisfied to continue testing. For both level A and level B, $VELC = 8$ nmi²/hr. The sign of quantity V_c indicates a closing condition in the X and Y directions. If the aircraft were closing in both X and Y simultaneously then V_c would be less than zero. If the aircraft were opening in both X and Y simultaneously, then V_c would be positive. If the aircraft were closing in one direction and opening in the other direction, the value of V_c may be positive or negative. Even if V_c is positive the miss distance might be small enough to qualify as a potential conflict. Thus V_c is tested against a positive number.

If the aircraft are closing, they may be doing so very slowly. If the closure is too slow there cannot be a conflict within the prescribed time interval. If we let

$$v^2 = (\dot{X}_i - \dot{X}_j)^2 + (\dot{Y}_i - \dot{Y}_j)^2 \quad (H-4)$$

then the inequality $v^2 > CLOS^2$ must be satisfied to continue testing. $CLOS$ is equal to .7 nmi/min for both level A and level B.

The predicted minimum separation is tested next. The time to minimum separation, T_m , is $-V_c/v^2$. If $v^2 = 0$, then $T_m = 0$. The square of the predicted minimum separation is

$$R_m^2 = R_0^2 - V_c T_m \quad (H-5)$$

If $R_m^2 \leq \text{SEPM}^2$ then the checking can continue. For level A SEPM is set to 6 nmi. For level B SEPM is set to 4.8 nmi. The window is opened wider on level A to allow for a turning aircraft to be detected at the earliest moment.

After it is determined that the aircraft are predicted to close to less than the preset minimum, a test is performed to determine if the minimum separation is violated within the look-ahead time (WRNT). For level A WRNT = 2.5 min. For level B, WRNT = 2.0 min. The minimum separation is violated within the look-ahead time if one of the following conditions holds:

- The time to minimum separation, T_m , is less than or equal to WRNT or
- The square of the separation predicted at WRNT violates the separation limits.

The square of the separation predicted at WRNT is given by

$$R_p^2(\text{WRNT}) = R_0^2 + (2V_c * \text{WRNT}) + V^2 * \text{WRNT}^2 \quad (\text{H-6})$$

Violation of the separation limits occurs when

$$R_p^2(\text{WRNT}) \leq \text{SEPP}^2.$$

The value of SEPP for level A is 6 nmi. For level B the value is 4.8 nmi. Here again, the longer time window on level A is designed to allow more efficient detection of accelerating aircraft.

If an aircraft pair passes both the fine horizontal filter and the fine altitude filter (which is not being considered here) at level A then it is placed in a conflict pairs table. On the next tracking cycle this conflict pair will be tested against the level B set of filters. An aircraft pair is eligible for controller alert generation if it has been determined to be in a condition of conflict at least twice in the past three successive applications of the filters. This procedure reduces the rate of false alarms due to noise in the surveillance system. Once an aircraft pair has been in a condition of conflict for the requisite number of successful tests, the pair will be identified to the controller by flashing data blocks and list displays at the controller's position. This flashing will continue as long as the aircraft pair continues to meet the Conflict Alert criteria or the controller manually turns off the alarm.

The parameters in Table H-1 labeled as Near Conflict parameters are those used by the intervention rate simulation described in Appendix G. These parameters are used to identify those pairs of aircraft that might be potential conflict pairs in the simulation run at a wider route spacing.

APPENDIX I

GLOSSARY

A	The total delay time at which the aircraft pair will come into horizontal overlap before there is an avoidance turn. (Figure 3-5, Volume I).
A'	One corner of the polygon B (Figure C-4, Volume II).
A ₁ , A ₂	The alongtrack positions of two aircraft on their respective routes (Figure E-1, Volume II).
ACP	Azimuth Count Pulse. A unit of angular measure equal to 1/4096 of a circle (.0879 degrees) (Table 5-1, Volume I).
a	A parameter of the integral of the circular normal probability function (Equation C-6, Volume II).
B	The polygonal area over which one computes the probability of observing an aircraft pair (Figure C-4, Volume II).
B'	One corner of the polygon B (Figure C-4, Volume II).
B ₁	The alongtrack position of an aircraft on a route (Figure E-1, Volume II).
b	The starting time of the periodic observations (Section D-4, Volume II).
C	A parameter used to fit the envelope for the horizontal overlap region (Equation B-21, Volume II)
CLOS	Closing Speed Threshold parameter (Equation H-4, Volume II).
C'	One corner of the polygon B (Figure C-4, Volume II).

D	The minimum projected separation between an aircraft pair used by the conflict alert function (Equation 3-4, Volume I).
D'	One corner of the polygon B (Figure C-4, Volume II).
d	The separation between two aircraft (Equation A-1, Volume II).
D _{MIN}	The minimum separation between a pair of aircraft (Figure 3-3, Volume I).
E(W)	The expected value of the separation between aircraft on the same route (Equation E-3, Volume II).
F	The crosstrack distance inside the conflict region at the initial radar observation (Figure B-2, Volume II). The partitioning parameter for the crosstrack closing speed (Equation B-18, Volume II).
FFT	The Fast Fourier Transform (Appendix D, Volume II).
f(n)	The Poisson probability density function (Equation G-1, Volume II).
F(n)	A finite Fourier transform (Equation (D-1), Volume II).
f(t)	A finite, complex series (Equation D-1, Volume II).
f(W)	The probability density function of the separation between two aircraft on the same route (Equation E-1, Volume II).
$\tilde{f}(Y_i, V_{yi})$	The histogram data corresponding to \hat{f}_i . (Equation F-2, Volume II).
F _e (n)	The even elements of the transformed series, F(n) (Equation D-6, Volume II).
f _e (t)	The even elements of the series f(t) (Equation D-6, Volume II).

$f_i(Y_i, V_{yi})$	The joint probability density function of crosstrack deviation and crosstrack speed from single aircraft observations from aircraft on route i (Equation F-1, Volume II).
$\hat{f}_i(Y_i, V_{yi})$	The estimate for $f_i(Y_i, V_{yi})$ (Equation F-2, Volume II).
$\tilde{f}_i(Y_i, V_{yi})$	The histogram data associated with the probability density function $f_i(Y_i, V_{yi})$ (Equation F-2, Volume II).
$F_o(n)$	The odd elements of the transformed series, $F(n)$ (Equation D-6, Volume II).
$f_o(t)$	The odd elements of the series $f(t)$ (Equation D-6, Volume II).
G	The crosstrack separation lost during one radar update time interval (Figure B-2, Volume II).
g	The gravitational constant (Equation B-6, Volume II).
$G(n)$	A finite Fourier Transform (Equation D-5, Volume II).
$g(t)$	A finite, complex series (Equation D-5, Volume II).
$\bar{g}(y, \dot{y})$	The derived histogram of crosstrack separation and crosstrack closing speed. (Equation F-7, Volume II).
$g(y, V_{y1}, V_{y2})$	The joint probability density function of the crosstrack separation and the two crosstrack speeds (Equation F-1, Volume II).
$\hat{g}(y, V_{y1}, V_{y2})$	The estimate for $g(y, V_{y1}, V_{y2})$ (Equation F-3, Volume II).
$\tilde{g}(y, V_{y1}, V_{y2})$	The histogram data corresponding to \hat{g} . (Equation F-4, Volume II).
H	Dummy Variable (Equation B-14, Volume II).

h	A distance defined in Figure C-6, Volume II
$h(t)$	The convolved density function (Equation D-11, Volume II).
$h(\kappa)$	The probability density function of the bank angle κ (Figure B-4, Volume II).
$h(x)$	The probability density function of the alongtrack distance between aircraft on one route and an aircraft on an adjacent route (Equation E-2, Volume II).
I	Dummy Variable (Equation B-14, Volume II).
IAC	Instantaneous aircraft count (Appendix G, Volume II).
J	Dummy Variable (Equation B-14, Volume II).
$j(\omega)$	The probability density function of the turn rate ω (Equation B-7, Volume II).
K	Dummy Variable (Equation B-14, Volume II).
k_1, k_2	Distances defined in Figure C-6, Volume II.
L	Dummy Variable (Equation B-14, Volume II).
M	Dummy Variable (Equation B-14, Volume II), (Appendix A, Volume II).
MAXR	The maximum separation at which Conflict Alert will continue to consider a pair of aircraft (Equation H-1, Volume II).
N	The half series length (Equation D-6, Volume II), also the number of equally spaced initial positions in the Conflict Region Boundary (Equation B-5, Volume II).
n	Index of the FFT (Equation D-1, Volume II).
N_1, N_2	The average flow rate of aircraft on routes 1 and 2 (Equation 3-7, Volume I).
P	The factor which delineates the three cases of overlap (Equation B-11, Volume II).

PFD_i	The probability of first detecting an aircraft pair on update i . (Equation B-4, Volume II).
$PFD_{i,F}$	The probability of first detecting an aircraft pair on update i given the first observation was at F . (Equation B-2, Volume II).
P_H	The proportion of time that the horizontal separation is lost (Section 2.2, Volume I).
P_{ki}	The probability that the time delay has a value in the k th cell. This probability will also depend on the conflict region boundary cell, i . (Equation B-27, Volume II).
P_l	The probability that the turn rate has a value in the l th cell (Equation B-27, Volume II).
$PND_{i,F}$	The probability that the aircraft pair will not be detected in the conflict region on radar update i given the first observation was at F (Equation B-1, Volume II).
PND^i,F	The probability of not being detected in the conflict region during the first i updates given the first observation was at F . (Equation B-1, Volume II).
P_x	The proportion of time that the alongtrack separation is lost (Section 2.1, Volume I).
P_y	The proportion of time that the crosstrack separation is lost (Section 2.1, Volume I).
$P(CB)$	The probability of an aircraft pair being on the conflict region boundary (Equation B-23, Volume II).
$P(CB_i)$	The probability of an aircraft pair being on the conflict region boundary in integration cell i . (Equation 3-2, Volume I).
$P(HO CB_i)$	The probability of an aircraft pair coming into horizontal overlap given that the pair started on the conflict region boundary in integration cell i (Equation 3-2, Volume I).

$P(y_i, \Delta y_i, \dot{y}_i, \Delta \phi)$	The joint probability that the aircraft pair has a crosstrack separation y_i in the i th cell and has a crosstrack closing speed \dot{y}_i in the i th cell (Equation B-26, Volume II).
$P_{\Delta x}$	The probability that an aircraft pair has an interroute alongtrack separation Δx (Equation 3-4, Volume I).
Q_n	The number of multiplications required for calculating the transform of air N point array. (Equation D-7, Volume II).
$q(F)$	The probability density function of the distance inside the conflict region boundary at which the first observation is made (Equation B-3, Volume II).
R	The radius of the right cylindrical collision shape (Section 3.2, Volume I).
R_m	The predicted minimum Separation (Equation H-5, Volume II).
R_o	The lateral separation between tracks (Equation H-2, Volume II).
R_p	Predicted separation at the warning time (Equation H-6, Volume II).
$r_{k \& i}$	The proportion of the k th cell in the overlap space is enclosed within the horizontal overlap region corresponding to the i th conflict region boundary cell (Equation B-27, Volume II).
SEPM	Minimum Separation Parameter (Equation H-5, Volume II).
SEPP	The separation at the warning time parameter (Equation H-6, Volume II).
SEPR	The current lateral conflict threshold (Equation H-2, Volume II).
T	The number of elements in the series on which the FFT operates (Equation D-1, Volume II).

t	The time variable, also a summation index
t_d	The total delay time from the time the aircraft pair enters the conflict region to the time one aircraft starts its avoidance maneuver. (Equation B-10, Volume II).
T_L	The look-ahead time in the conflict alert function (Equation A-3, Volume II).
T_m	Time to minimum separation (Equation H-5, Volume II).
t_c	The time the aircraft is in the turn to the point of closest approach (Equation B-10, Volume II).
T_1	The time the aircraft pair is at the conflict region boundary (Figure 3-3, Volume I).
T_2	The time at which the system has cognizance that the aircraft pair is within the conflict region (Figure 3-3, Volume I).
T_3	The time at which the aircraft start its avoidance maneuver (Figure 3-3, Volume I).
u	A coordinate axis used to circularize the bivariate normal distribution (Equation C-3, Volume II).
u_1	The u coordinate value of point A' (Equation C-9, Volume II).
u_2	The u coordinate value of point B' (Equation C-9, Volume II).
V	The forward velocity of the aircraft (Equation 3-7, Volume I).
v	A coordinate axis used to circularize the bivariate normal distribution (Equation C-3, Volume II).
V_c	Converging speed indicator (Equation H-3, Volume II).
VELC	Converging speed threshold parameter (Equation H-3, Volume II).

v^2	Closing speed indicator (Equation H-4, Volume II).
v_{xn}	The tracker x velocity estimate for scan n (Equation C-1, Volume II).
v_{x1}, v_{x2}	The alongtrack speeds of aircraft on routes 1 and 2 (Figure A-1, Volume II).
v_{ymax}	The maximum crosstrack speed observed in the data (Equation A-4, Volume II).
v_{yn}	The tracker Y velocity estimate for scan n (Equation C-1, Volume II).
v_{y1}, v_{y2}	The crosstrack speeds of aircraft on routes 1 and 2 (Figure A-1, Volume II).
$v(h,k)$	The integral of the circular normal probability function (Equation C-6, Volume II).
v_1	The v coordinate value of point A' (Equation C-9, Volume II).
v_2	The v coordinate value of point B' (Equation C-9, Volume II).
W	The separation between two aircraft on the same route (Figure E-1, Volume II).
WRNT	Warning Time (Look-ahead time) (Equation H-6, Volume II).
x	The alongtrack, interroute, separation between a pair of aircraft (Section 3.2, Volume I).
\dot{x}	The alongtrack, interroute, closing speed between a pair of aircraft (Equation A-1, Volume II).
\dot{x}_1, \dot{x}_2	The bounds on the value \dot{x} (Equation A-7, Volume II).
x_i	The alongtrack position of an aircraft on route i (Figure A-1, Volume II).

\dot{x}_i	The alongtrack component speed of an aircraft on route i (Equation H-3, Volume II).
$x_i(t)$	The alongtrack trajectory of the aircraft on route i (Equation B-9, Volume II).
x_i	The alongtrack, interroute, separation of an aircraft pair in the i th integration cell (Figure 3-4, Volume I).
x_{pn}	The tracker predicted X position estimate made at scan n for the position at scan $n+1$ (Equation C-1, Volume II).
x_{rn}	The reported X position to the tracker from the surveillance system at scan n (Equation C-1, Volume II).
x_{sn}	The tracker X position estimate for scan n (Equation C-1, Volume II).
x_{io}, y_{io}	The X and Y positions of an aircraft on route i when it is on the conflict region boundary in conjunction with another aircraft on the other route. (Equation B-9, Volume II).
$x(t)$	A series of data points (Equation D-8, Volume II).
y	The crosstrack separation between a pair of aircraft (Section 3.2, Volume I).
\dot{y}	The crosstrack closing speed between a pair of aircraft (Section 3.2, Volume I).
y_i	The crosstrack deviation of an aircraft from the centerline of route i (Figure A-1, Volume II). Also the Y component (crosstrack) position of an aircraft on route i (Equation H-1, Volume II).
\dot{y}_i	The crosstrack component speed of an aircraft on route i (Equation H-3, Volume II).

$Y_i(t)$	The crosstrack trajectory of the aircraft on route i (Equation B-9, Volume II).
y_i	The crosstrack separation of an aircraft pair in the i th integration cell (Figure 3-4, Volume I).
\dot{y}_i	The crosstrack closing speed of an aircraft pair in the i th integration cell (Figure 3-4, Volume I).
$Y_{i,F}$	The crosstrack separation at radar update i after crossing into conflict region and being initially observed at F (Figure B-2, Volume II).
Y_{pn}	The tracker predicted Y position estimate made t scan n for the position at scan $n+1$ (Equation C-1, Volume II).
Y_{rn}	The reported Y position to the tracker from the surveillance system at scan n (Equation C-1, Volume II).
Y_{sn}	The tracker Y position estimate from scan n (Equation C-1, Volume II).
Y_0	The crosstrack separation at the conflict region boundary (Figure B-2, Volume II).
$y(t)$	A shifted series of data points (Equation D-8, Volume II).
z	A variable which is minimized and maximized in Appendix A. (Equation A-6, Volume II).
$z(t)$	The convolved density function (Equation D-11, Volume II).
α	The NAS tracker position gain (Equation C-1, Volume II), and the significance level for the confidence interval of the expected value of the Poisson distribution (Equation G-2, Volume II).
β	The NAS tracker velocity gain (Equation C-1, Volume II).
Δ	A fixed sampling interval (Section D-4, Volume II).

ΔV_y	The histogram cell size for crosstrack speed (Equation F-2, Volume II).
Δx	The integration interval in the alongtrack dimension (Figure 3-4, Volume I).
Δy_i	The integration interval in the crosstrack dimension (Figure 3-4, Volume I).
$\Delta \dot{y}$	The integration interval in the crosstrack closing speed dimension (Figure 3-4, Volume I).
ΔY	The histogram cell size for crosstrack deviations (Equation F-2, Volume II).
κ	The bank angle of the aircraft making the avoidance maneuver (Equation B-6, Volume II).
κ_L/κ_U	The lower, κ_L , and upper, κ_U , bounds on the bank angle distribution (Equation B-7, Volume II).
λ	A parameter of the integral of the circular normal probability function (Equation C-6, Volume II), and the parameter of the Poisson distribution (Equation G-1, Volume II).
λ_a, λ_b	The lower and upper confidence limits on the expected value of a Poisson distribution (Equation G-2, Volume II).
λ_x	The length of the rectangular collision shape which represents the aircraft (Table 5-1, Volume I).
λ_y	The width of the rectangular collision shape which represents the aircraft (Table 5-1, Volume I).
μ_y	The expected value of the crosstrack separation of an aircraft pair (Equation C-2, Volume II).
$\mu_{\dot{y}}$	The expected value of the crosstrack closing speed of an aircraft pair (Equation C-2, Volume II).

- ν The angle the velocity vector of the aircraft on route 2 makes with the crosstrack axis (Figure B-6, Volume II).
- ξ The angle the velocity vector of the aircraft on route 1 makes with the crosstrack axis (Figure B-6, Volume II).
- ρ The correlation coefficient between the errors in the crosstrack closing speed and separation (Equation C-2, Volume II).
- $\phi(h)$ The normal probability integral (Equation C-8, Volume II).
- ω The turn rate of the aircraft making the avoidance turn (Equation B-6, Volume II).

APPENDIX J

REFERENCES

1. Flener, William M., "Request for E&D Effort," Letter from the FAA Associate Administrator for Air Traffic and Airway Facilities to the FAA Associate Administrator for Engineering and Development, November 9, 1976.
2. Kirkendall, N.J., "A Specification for a Data Collection to Determine Lateral Pathkeeping of Aircraft Flying VOR Defined Routes in High Altitude En Route Areas," The MITRE Corporation, MTR-7430, Washington, D.C., June 1977.
3. Kirkendall, N.J., and Smith, A.P., "An Extension to the Data Specification for the High Altitude Lateral Pathkeeping Study," The MITRE Corporation, MTR-7638, Washington, D.C., December 1977.
4. Colamosca, B.F., Arch, H.L., Parkins, K.D., "Data Collection for Study of Lateral Separation of Aircraft Flying CONUS High Altitude VOR-Defined Air Routes," NAFEC Technical Letter Report NA-78-24-LR, RTCA Paper No. 69-78/SSRG-18, May 1978.
5. Busch, A.C. and Colamosca, B.F., "Modeling Safety in a Procedural Air Traffic Control Environment," Draft NAFEC Letter Report NA-77-57-LR, RTCA Paper No. 155-77/SSRG-11, October 1977.
6. Polhemus, N.W., "Introduction to a General Collision Risk Model for Intersecting and Nonparallel Routes," RTCA Paper No. 9-79/SSRG-27, January 1979.
7. George, P.H., Johnson, A.E., and Hopkin, V.D., "Radar Monitoring of Parallel Tracks -- Automatic Warning to Controllers of Track Deviations in a Parallel Track System," Eurocontrol Experimental Center Report No.67 (Task C21/1), September 1973.
8. Johnson, N.L., and Kotz, S., "Distributions in Statistics: Continuous Multivariate Distributions," New York: John Wiley & Sons, Inc., 1972.
9. IEEE Transactions on Audio and Electroacoustics, Vol. AU-15, No. 2., June 1967.
10. Kleinrock, L., "Queueing Systems, Volume 1: Theory," New York: John Wiley & Sons, Inc., 1976.

11. "Methodology for the Derivation of Separation Minima Applied to the Spacing Between Parallel Tracks in ATS Route Structures," ICAO Circular 120-AN/89/2, 1976.
12. Kirkendall, N.J., "Probability of Passings Between Aircraft on Adjacent Parallel Routes: Observed Data vs Model Estimates," The MITRE Corporation, WP-79W00397 Washington, D.C., June 1979.
13. Hauser, S.J., Dodge, P.O. and Steinbacher, J.G., "Computer Program Functional Specifications for Conflict Alert," The MITRE Corporation, MTR-7311, Washington, D.C., September 1976.
14. Law, A.M., "Statistical Analysis of the Output Data from Terminating Simulations," Unpublished and Undated Report supported by the Office of Naval Research and the Army Research Office.
15. Handbook of Tables for Probability and Statistics. The Chemical Rubber Co., Cleveland, Ohio, 1968.